Nuclear SphK2 and S1P Signaling Epigenetically Regulates *Pseudomonas aeruginosa* Induced Lung Inflammation

BY

DAVID L. EBENEZER
M. Sc Madurai Kamaraj University, 2003

DISSERTATION

Submitted as partial fulfillment of the requirements for the degree of Doctor of Philosophy in Biochemistry and Molecular Genetics in the Graduate College of the University of Illinois at Chicago, 2017, Chicago, Illinois

Defense Committee:

Dr. Viswanathan Natarajan, Advisor and Chair
Dr. Steven Ackerman
Dr. Sojin Shikano
Dr. Steven Dudek, Medicine
Dr. Nadim Mahmud, Medicine

TABLE OF CONTENTS

CHAPTER		PAGE
I.	LITERATURE REVIEW	
	1.1 Sphingolipids	1
	1.2.1. Sphingolipid Metabolism	1
	1.2.2. Sphingosine-1-Phosphate Signaling	3
	1.3 Respiratory Epithelium	9
	1.3.1 Barrier Functions of Lung Epithelial Cells	9
	1.4 *Pseudomonas aeruginosa*	10
	1.4.1 Recognition of *P. aeruginosa* by Toll Receptors	10
	1.4.2 Cytokine and Inflammatory Mediators of Pseudomonas Infection	11
	1.5 Epigenetic Regulation of Lung Inflammation and Repair	12
	1.5.1. Histone Modifications	14
	1.5.2. Histone Modifications in Inflammation	14
	1.6 HDAC Family	16
	1.6.1. Class I HDAC Complexes	16
	1.6.2. Sin3 Complex	19
	1.6.3. NuRD Complex	19
	1.6.4. CoREST	19
	1.7 Reactive Oxygen Species	19
	1.8 Protein Kinase C	20
	1.9 NADPH-Oxidases (NOXs)	23
II.	OBJECTIVES	25
	2.1 To Determine the Role of Sphingolipid Metabolism in *Pseudomonas aeruginosa* Induced Lung Inflammation	
	2.2 To Elucidate the Role of Sphingosine Kinase-2 Mediated Nuclear Sphingosine-1-phosphate Signaling in Epigenetic Regulation of Pro-Inflammatory Cytokine Secretion	
III.	METHODS AND MATERIALS	
	3.1 Reagents	26
	3.2 Inhibitors	27
	3.3 Antibodies	28
	3.4 Assay Kit	28
	3.5 Enzymes	29
	3.6 Quantitative Real-Time PCR	29
	3.7 Sphingosine Kinase Activity Assay using [γ-^{32}P] ATP	29

3.8 Analysis of Sphingoid Base-1-Phosphates, Ceramides and Sphingoid Bases by Mass Spectrometry 30
3.9 ChIP Assay 31
3.10 Exposure of Epithelial Cells to Heat-Inactivated *Pseudomonas aeruginosa* 32
3.11 HDAC Activity Assay 33
3.12 Human Cystic Fibrosis Lung Specimens 33
3.13 IL-6 Gene Expression 33
3.14 Immunoblotting 34
3.15 Immunofluorescence Microscopy 34
3.16 Immunoprecipitation 35
3.17 Isolation of Alveolar Type II Epithelial Cells from Mouse Lung 35
3.18 Isolation of Epithelial Cell Nuclear Fraction 37
3.19 Lipid Extraction 37
3.20 Measurement of H_2O_2 38
3.21 Measurement of IL-6 and TNF-α 38
3.22 *Pseudomonas aeruginosa* Infection on Mouse Lungs 38
3.23 PKC Activity 38
3.24 Preparation of *Pseudomonas aeruginosa* Culture 39
3.25 RNA-Seq Analysis 39
3.26 Transfection of MLE-12 or HBEpCs with Small Interfering RNA 40
3.27 Data Analysis 40

IV. RESULTS I
4.1 Hypothesis: Sphingosine-1-phosphate Generation in Response to *PA*-induced Lung Inflammation Modulate Host Defense Response 41
4.1.1 *Pseudomonas aeruginosa* Infections Alter Sphingolipid Levels in Mouse Lungs and Bronchoalveolar Lavage Fluids 41
4.1.2 SphK2, but not SphK1, Deficient Mice are Protected from *PA*-mediated Lung Inflammation 45
4.1.3 SphK2 Genetic Deletion Affect *PA*-induced Gene Expression in Mouse Lung 51
4.1.4 Inhibition of SphK2 Ameliorates *PA*-induced Lung Inflammation in Mice 53
4.1.5 *PA* induced Post-Translational Modification of SphK2 and Nuclear Localization in Mouse Lung and *In vitro* in Mouse Lung Epithelial Cells 58

V. RESULTS II
5.1 Hypothesis: Sphingosine Kinase 2 Generated Nuclear S1P Epigenetically Regulates Pro-Inflammatory Cytokine Secretion 68

5.1.1 Deletion or Inhibition of SphK2 reduces *PA*-mediated H3 and H4 Histone Acetylation and IL-6 Secretion 68
5.1.2 Activation of PKC δ is Essential for *PA*-induced SphK2 Phosphorylation, H3 and H4 Histone Acetylation and IL-6 Secretion 74
5.1.3 *PA* Enhances Association of SphK2 and HDAC1/2 and S1P Generation in the Nucleus 83
5.1.4 *PA*-mediated Nuclear SphK2/S1P Signaling Stimulates Nuclear ROS Production and Oxidation of HDACs 87
5.1.5 *PA*-mediated Nuclear ROS Production and Oxidation of HDACs by Stimulating NOX4 in The Nucleus 90
5.1.6 Nuclear Co-localization of SphK2 in Cystic Fibrosis Lung Specimens 97

VI. DISCUSSION 99

VII. LITERATURE CITED 109

VIII. VITAE 135

ACKNOWLEDGMENTS

I would like to extend my profound gratitude to my advisor, Dr. Viswanathan Natarajan, for his excellent mentorship, the unlimited opportunities that he provided me to grow as a researcher, for being a wonderful human being and an excellent role model to emulate.

Special thanks to my thesis committee members: Dr. Steven Ackerman, Dr. Steven Dudek, Dr. Sojin Shikano, and Dr. Nadim Mahmud, for their positive criticism, insights and suggestions throughout my thesis work.

I would like to thank, Dr. Michael Caffrey and Dr. Alisa Katzen, Directors of Graduate Studies, and Dr. Jack Kaplan, the department head of Biochemistry and Molecular Genetics, for the constant support and encouragement they gave me during my program of study.

My special thanks goes to Dr. Panfeng Fu for his immense contribution to this research work and for being an amazing research partner. My special appreciation to Ms. Alison Ha for her invaluable assistance and its been a pleasure working with her throughout my thesis research work. I wouldn't have completed my thesis research work without their support.

I would also like to thank my other lab members, Dr. Anantha Harijith, Dr. Fernando Testai, Dr. Longshuang Huang, Dr. Peter Usatyuk, Donghong He and my wonderful peers, Mark Shaaya, and Vidyani Suryadevara. Thanks to all the student volunteers who worked with me for their wonderful camaraderie-Hamed Shafiuddin, Lizar Ace Mangio, Mahathi

Challapalli, Alex Heinz, Rachana Reddy, Sriramya Vemulakonda, Kavya Chowdary, Rajan Jayasankar and Mounica Bandela.

On the same note, I would like to convey my gratitude to the members from Dr. Steve Dudek, Dr. Jeff Jacobson, and Dr. Robert Machado's labs. Special thanks to Mrs. Lakshmi Natarajan, Dr. Lucille Meliton, Dr. Yulia Epstein, Dr. Justin Sysol, and Karen Gordon for their moral support and help at all times.

I would like to thank my collaborators Drs. Evgeny Berdyshev, Rubin Tudor, and Yulia Komarova without whose help my research would not have been successful. I would also like to thank Peter Toth and Ke Ma, RRC microscopy facility for their expertise.

I would like to thank the office members Abdul Khan, Rekha Pandya, and Sun Fangmin in the Department of Biochemistry Molecular Genetics and Aileen Baker, Jeanne Chang, Laura Devaney Foote, Yi Dong, Amina Chavero, Chunfang Dai in the Department of Pharmacology for their invaluable help. Special thanks also to Dr. Asrar Malik, Head, Pharmacology department for his financial support through the NIH T32 fellowship. I would also like to thank Dr. Prasad Kanteti for his tutoring and assistance in editing articles and manuscripts. I would also like to extend my gratitude to UIC-CCTS PECTS program for their financial support.

Thank you to my friends Abraham & Jamie, Saravanan & Lekha, Bala & Aarthy, Drs. Ram Ramachandran, Indira Elangovan, Gaurang Bhide and Uma Harijith, for providing the requisite breaks from scientific research.

My Parents- Rev. Doss Ebenezer & Vimala, Brothers-Goel, James & Solomon, Aunt and Uncle-Elizabeth & Rajakumar Rhenius and my in-laws-Michael and Mary deserve special thanks for their love and constant encouragement. I would like to express my deepest gratitude to wife Alexis for the countless sacrifices and constant support throughout the entire process. Stephen and Eleora- my wonderful kids, for being mature way beyond their age when it came to understanding my working in the lab for long hours. My endeavor would not have been complete without their love and support.

DE

LIST OF FIGURES

FIGURE **PAGE**

1. **Fig 1:** *De novo* Sphingolipid Metabolic Pathway 2

2. **Fig 2:** Sphingosine-1-phosphate Signaling 4

3. **Fig 3:** Sphingosine Kinase isoforms 6

4. **Fig 4:** Domain Structure of PKC Isoenzymes 21

5. **Fig 5A, B, C:** *Pseudomonas aeruginosa* (*PA*) Infection Alters Sphingolipid Levels in Mouse Lungs 42
   a. **Fig 5D, E, F:** *Pseudomonas aeruginosa* (*PA*) Infection Alters Sphingolipid Levels in Mouse Bronchoalveolar Lavage Fluids 43

6. **Fig 6:** Schematic diagram depicting *PA*-induced Sphingoid base Levels in lungs and BAL 44

7. **Fig 7A:** Deletion of SphK2 Prevents *PA*-Induced Alveolar Infiltration of Neutrophils 46
   a. **Fig 7B, C:** *PA*-induced Neutrophil Influx in Alveolar Space is Attenuated by SphK2 Deficiency 47
   b. **Fig 7D, E:** Deletion of SphK2 Prevents *PA*-induced Pulmonary Leak 48
   c. **Fig 7F, G, H, I:** Deletion of Sphk2 Prevents *PA*-induced Lung Inflammatory Cytokine Secretion 49
   d. **Fig 7J, K, L:** Deletion of SphK2 Blocks ROS and Increases Survival of Mice After *PA* Challenge 50

8. **Fig 8:** Differential Expression of 35 Genes 24 h After *PA* Challenge of Wild Type and SphK2 KO Mouse Lung 52

9. **Fig 9:** Administration of SphK2 Inhibitor ABC294640 at the Time of *PA* Infection Ameliorates Lung Inflammation and Injury 54

10. **Fig 10A, B, C, D:** Inhibition of SphK2 with ABC294640 Post-Infection Ameliorates *PA*-induced Inflammatory Lung Injury 55
    a. **Fig 10E, F:** Inhibition of Sphk2 with ABC294640 Blocks *PA*-induced Cytokines Secretion 56

11. **Fig. 11:** Schematic diagram showing blocking SphK2 with SphK2 inhibitor ABC294640 attenuates *PA*-induced lung inflammation 57

12. **Fig 12A, B:** *PA* Stimulates SphK2 Phosphorylation and Nuclear Localization in Lung Epithelium 60
    a. **Fig 12C, D:** *PA* Stimulates SphK2 Phosphorylation and Nuclear Localization in Lung Alveolar Epithelium 61
    b. **Fig 12E, F:** *PA* Stimulates SphK2 Phosphorylation and Nuclear Localization in Alveolar Epithelial Cells 62
    c. **Fig 12G, H:** *PA* Infection Stimulates Nuclear SphK2 Phosphorylation in Primary Human Bronchial Epithelial Cells 63
    d. **Fig 12I, J:** *PA* Infection Stimulates Nuclear SphK2 Phosphorylation in MLE-12 Cells 64
    e. **Fig 12K, L:** *PA* Infection Stimulates Nuclear SphK2 Phosphorylation And Activation in MLE-12 Nuclei 65
13. **Fig 13:** Sphingoid Bases Levels in Cytoplasm and Nuclear Fractions of Alveolar Epithelial Cells 66

14. **Fig. 14:** Schematic diagram showing the role of *PA*-induced phosphorylation of SphK2 in lung inflammation**.** 67

15. **Fig 15A, B, C:** SphK2 is Essential for *PA*-Induced H3 and H4 Histone Acetylation and IL-6 Secretion 70
    a. **Fig 15D, E, F:** *PA*-induced HDAC Activity Reduction is Modulated by SphK2 Inhibition 71
    b. **Fig 15G, H:** SphK2 Inhibition Blocks IL-6 Secretion and Acetylated Histone H3K9 Enrichment on IL-6 Promoter 72

16. **Fig 16:** Schematic Diagram Showing *PA*-induced Histone Acetylation and IL-6 Secretion was Blocked by Inhibiting Sphk2 73

17. **Fig 17A, B:** *PA*-induced SphK2 Phosphorylation and IL-6 Secretion is Not Mediated by ERK1/2 76
    a. **Fig 17C, D:** PKC δ Activation Regulates *PA*-induced SphK2 Phosphorylation, Histone Acetylation and IL-6 Secretion in MLE-12 cells 77
    b. **Fig 17E, F:** Inhibition of PKC δ Reduces Secretion of IL-6 78
    c. **Fig 17G, H:** Inhibition of PKC δ Reduces mRNA Expression of IL-6 and TNF-α 79
    d. **Fig 17I, J, K:** PKC δ Activation Regulates *PA*-induced SphK2 Phosphorylation In MLE-12 cells and Histone Acetylation in HBEpCs 80

e. **Fig 17L, M:** PKC δ Activation Enriches Histone H3K9 Acetylation on IL-6 Promoter and Nuclear S1P Production in MLE-12 cells 81

18. **Fig. 18:** Schematic diagram showing blocking PKC δ, attenuates *PA*-induced SphK2 phosphorylation and downstream signaling 82

19. **Fig 19A, B, C:** *PA* Enhances Association of SphK2 with HDAC1/2 in the Nucleus 84
    a. **Fig 19 D, E:** *PA* Enhances Association of SphK2 with HDAC 2 85

20. **Fig 20:** Schematic Diagram Showing SphK2-mediated S1P blocks HDAC Activity in the Nucleus After *PA*-Infection 86

21. ***Fig 21A, B, C:*** *PA*-mediated Nuclear SphK2/S1P Signaling Stimulates ROS Production in the Nucleus 88
    a. **Fig 21D, E, F:** *PA*-Mediated Nuclear SphK2/S1P Signaling Stimulates Oxidation of HDACs 89

22. **Fig 22A-H:** SphK2, but Not SphK1, Deletion Modulates NOX4 Expression and NOX4-Dependent Nuclear ROS Generation 91

23. **Fig 23A-C:** Inhibition of SphK2 with ABC294640 or PKC δ with DN PKC δ Attenuated *PA*-Induced Nuclear ROS Production 93

24. **Fig 24A-E:** Downregulation of NOX4, but not NOX2, with siRNA Attenuated *PA*-induced H3 and H4 Histone Acetylation *In Vivo* and *In Vitro* as well as Oxidation of HDAC2 95

25. **Fig 25:** Schematic diagram showing PA-induced histone acetylation is regulated by SphK2/S1P signaling to stimulate NOX4 dependent ROS generation in the nucleus 96

26. **Fig 26:** Nuclear Localization of p-SphK2 in Cystic Fibrosis Lung Specimens 98

27. **Fig 27:** Proposed Model for the Role of Nuclear SphK2/S1P Signaling Axis in the Epigenetic Regulation of *PA*-Induced lung inflammation 108

LIST OF TABLES

TABLE		PAGE
I.	Sphingosine Kinase Isoforms in Lung Diseases	8
II.	Inflammatory Mediators of Lung Inflammation	13
III.	Classes of HDAC	18
IV.	Classes of PKC	22
V.	NOX Family Proteins	24

LIST OF ABBREVIATIONS

ABC	ATP-Binding Cassette
ANOVA	Analysis of Variance
AT-I	Alveolar Type I Cells
AT-II	Alveolar Type II Cells
ATF	Activating Transcription Factor
BALF	Broncho-Alveolar Lavage Fluid
CBP	CREB-Binding Protein
CF	Cystic Fibrosis
CFU	Colony Forming Unit
CYS	Cysteine
DAG	Diacylglycerol
DHS	Dihydrosphingosine
ELISA	Enzyme-Linked Immunosorbent Assay
ER	Endoplasmic Reticulum
ESI	Electrospray Ionization
FACS	Fluorescence Activated Cell Sorting
FOXP3	Forkhead Box Protein 3
HAT	Histone Acetyl Transferases
HBEpCs	Human Bronchial Epithelial Cells
HDACs	Histone Deacetylases
HDMs	Histone Demethylases
HMT	Histone Methyl Transferases
hTERT	Human Telomerase Reverse Transcriptase
IFNγ	Interferon Gamma
IKK	Inhibitor Kappa Kinase
IL6	Interleukin-6
LPP	Lipid Phosphate Phosphatases
LPS	Lipopolysaccharide
MACS Buffer	Magnetic Activated Cell Sorting
MET	Methionine
MLE-12	Mouse Lung Epithelial Cells
MRM	Multiple Reaction Monitoring
NES	Nuclear Export Sequences
NFκB	Nuclear Factor Kappa B-Cells
NOX	NADPH Oxidase

$O_2^{\cdot -}$	Superoxide
PA	*Pseudomonas aeruginosa*
PKC	Protein Kinase C
PRR	Pattern Recognition Receptors
RIPA Buffer	Radioimmunoprecipitation Assay Buffer
ROS	Reactive Oxygen Species
S1P	Sphingosine 1 Phosphate
SAHA	Suberoylanilide hydroxamic Acid
SDS-PAGE	Sodium Dodecyl Sulfate Polyacrylamide Gel Electrophoresis
SphK1	Sphingosine kinase 1
SphK2	Sphingosine kinase 2
SPNS2	Spinster Homolog 2
SPP	S1P Phosphatases
SPT	Serine Palmitoyl Transferase
STAT	Signal Transducer and Activator of Transcription
TLR	Toll-like Receptors
TNFα	Tumor Necrosis Factor-alpha
TRAF	TNF Receptor-Associated Factor 2
TSA	Trichostatin A

SUMMARY

Sphingosine-1-phosphate (S1P), a simple bioactive sphingolipid, is recognized as a complex regulator of physiological and pathophysiological processes, with extensive ramifications for therapeutic development. Pulmonary infections and other lung disorders impair the ability of the lungs to exchange gases leading to acute or chronic disease state. S1P is a pleotropic signaling molecule, and has been implicated in a wide range of lung disorders. While sphingosine kinase 1 (SphK1)/S1P signaling axis has been implicated in various lung pathologies and is associated with disease severity and survival, SphK2 and the role of S1P generated in the nucleus has not been investigated in lung diseases. Infection of the lung by *Pseudomonas aeruginosa* (*PA*), a Gram-negative pathogen, can range from acute pneumonia in immunocompromised individuals to chronic lung function deterioration in cystic fibrotic patients. During acute infections, *PA* encroach the respiratory epithelium, and cause substantial tissue damage leading to lung inflammation and dysfunction of the epithelial barrier.

Inflammation of the lung, being the primary deterrent of the innate immune system against lung infection, is scrupulously regulated by various epigenetic mechanisms including histone modifications and HDAC activation/inhibition. While aberrant regulation of pro-inflammatory cytokines by epigenetic mechanisms has been reported to contribute to lung pathogenesis, the mechanisms still remain obscure and a subject of considerable interest. S1P, generated in the nucleus by the action of SphK2, has previously been reported to modify nuclear HDACs in breast cancer cells but the involvement of nuclear S1P signaling in modifying the epigenetic landscape has not been reported in any lung pathologies. The focus of this study is to interrogate the novel role of SphK2 in nuclear S1P generation and unravel the role of nuclear SphK2/S1P signaling axis in epigenetic regulation of *PA*-induced lung inflammation.

In the first specific aim of my thesis work, I hypothesized that nuclear S1P could be a key player in modulating host defense response against bacterial infection. S1P is generated in the cell by two kinases: SphK1, which is localized in the cytoplasm and SphK2 in the nucleus. S1P generated in the different compartments of the cell are spatio-temporally regulated and have distinct roles to play in regulating signaling pathways. Here I show, *in vivo* in mouse lungs, that in response to *PA* infection, SphK2 in the nucleus gets activated and subsequently generates nuclear S1P. I used novel murine model of *PA* infection involving *Sphk1*$^{-/-}$, *Sphk2*$^{-/-}$ mice along with C57BL/6 wild type (WT) mice, mimicking acute bacterial lung inflammation, to delineate the role of SphK2 and S1P signaling in the nucleus. *PA* infection activated SphK2 and it translated to increased S1P in the mouse lung and bronchoalveolar lavage fluids (BALFs) as evident from the LC-MS/MS mass spectrometry analysis. Elevated S1P also contributed to increased inflammation of the lung as we observed enhanced neutrophil migration into the alveolar space. Moreover, increased pulmonary leak accompanied inflated levels of pro-inflammatory cytokines IL-6 and TNF-α after *PA* infection. I also exploited the use of small molecule inhibitor ABC294640, a specific inhibitor of SphK2 to study its therapeutic potential in ameliorating *PA*-induced lung inflammation. Blocking SphK2 activity by ABC 294640, both pre- and post-infection, reduced S1P generation and blocked *PA*-induced lung inflammation.

The second specific aim of my thesis work is based on the hypothesis that nuclear S1P generated in response to *PA* infection could target the chromatin modifiers, particularly class I nuclear HDACs that regulate inflammatory cytokines and modulate their activity to contribute to lung pathogenesis. SphK2 mediated nuclear S1P generated in response to *PA* infection exist in close proximity to class I HDACs that reside in the nucleus. Class I HDACs, particularly HDAC 1, 2 & 3, are active participants of Toll-like receptor (TLR) signaling and predominantly regulate innate immunity

by controlling the expression of inflammatory cytokines in a negative fashion by deacetylating the chromatin. Both S1P and HDAC, exerting pleiotropic effects within the immune system, independently can modulate the epigenetic landscape of pro-inflammatory cytokines when interacting together. Equipped with the knowledge of existing literature that previously showed S1P blocking nuclear HDAC activity in breast cancer cells, I explored the mechanism in detail using *in vitro* as well as *in vivo* models to study epigenetic regulation of *PA*-induced lung inflammation. In mouse lung epithelial cells, *PA*-induced histone acetylation of H3K9 and H4K8, and blocking SphK2 by using siSphK2 and ABC294640 diminished histone acetylation patterns. Increased acetylation of histones H3 and H4 also correlated with increased IL-6 and TNF-α mRNA and protein levels. More importantly, blocking SphK2 and not SphK1 blocked the enrichment of histone H3K9 acetylation at IL-6 promoter regions as demonstrated by the Chromatin immunoprecipitation Assay (ChIP). I also identified a novel role of PKC isoform δ in phosphorylating SphK2 after *PA* infection; dominant negative PKC isoform δ abolished all the downstream signaling events, including phosphorylation of SphK2, S1P generation, IL-6 secretion and more importantly the enrichment of H3K9 acetylation at IL-6 promoter region. Further by elucidating the mechanism(s) by which SphK2 generated S1P blocks nuclear HDACs, I identified S1P mediated-NADPH oxidase 4 (NOX4) and its generation of reactive oxygen species (ROS) in the nucleus playing a momentous role in impairing the function of nuclear HDACs by oxidative modification. Consistent with these findings, I was able to establish the mechanistic link where SphK2 mediated S1P generation in the nucleus acts through NOX4 generated ROS to alter the epigenetic landscape of inflammatory cytokines.

This thesis work provides the first demonstration that SphK2 regulation is critical in the development of bacterial-induced lung inflammation. So far, evidences have pointed out only the role of SphK1 in

lung pathologies where the levels of SphK1 and S1P are elevated correlating with disease severity. Targeting SphK1 has also been advocated in the treatment of pulmonary diseases. The role of SphK2 in lung disorders needed a new line of investigation and my thesis research study have made an initial contribution by identifying SphK2 activation is decisive in bacterial induced lung inflammation and SphK2/S1P signaling is crucial for epigenetic regulation of inflammatory cytokine production.

In trying to understand the nuclear S1P signaling in *PA*-induced lung inflammation, I extended the study further to include S1P lyase, the enzyme that irreversibly degrades S1P into hexadecenal and ethanolamine phosphate. S1P lyase by itself and through degradation of S1P and generation of long chain fatty aldehyde could play an additional role in epigenetic regulation of *PA*-induced lung inflammation. In performing the preliminary studies, I have made some interesting observations including increased $\Delta 2$-hexadecenal levels in the nucleus after *PA* infection and a possible localization of S1P lyase in the nucleus. Blocking S1P lyase activity by 4-deoxypyridoxine (4-DP) also reduced histone H3K9 acetylation at the IL-6 promoter. Understanding the role of S1P lyase in *PA*-induced lung inflammation will add another dimension to the already completed thesis work of mine and will add to an array of potential therapeutic targets I have identified including SphK2, PKC δ and NOX4 in ameliorating lung injury.

1. REVIEW OF LITERATURE

1.1 Sphingolipids

Sphingolipids are a large and complex group of biomolecules that contain a sphingoid backbone, such as sphingosine, dihydrosphingosine, or phytosphingosine, linked to long-chain fatty acids (ceramides). Sphingolipids are classified based on the nature and location of the hydrophilic head groups, i.e., glycosphingolipids, and glycophospho sphingolipids, which participate in various signal transduction pathways (Weete 1974).

1.2.1 Sphingolipid Metabolism

De novo biosynthesis of sphingolipids begins in the endoplasmic reticulum (ER) with the condensation of L-serine and palmitoyl CoA, catalyzed by the rate-limiting enzyme serine palmitoyl transferase (SPT) (Alfred H Merrill 2002). The resulting ketosphinganine is rapidly reduced to dihydrosphingosine (DHS) by ketosphinganine reductase (Stoffel 1970), which is then N-acylated to dihydroceramide, mediated by ceramide synthases (Stiban, Tidhar, and Futerman 2010). Ceramides are generated by introduction of double bond in the DHS base, and then transported to the golgi apparatus, where ceramides are converted to complex sphingolipids like sphingomyelin and glycosphingolipids, or phosphorylated to generate ceramide-1-phosphate (Mitsutake, Kim, and Igarashi 2006). Ceramides are also generated through recycling/degradation of higher-order sphingolipids in the plasma membrane or lysosomes. Alternatively, in mammalian cells, in response to extracellular stimuli, ceramides are formed from sphingomyelin that can be further deacylated to sphingosine by ceramidases (Chalfant and Spiegel 2005). SphK 1 & 2 catalyze the conversion of sphingosine to S1P, which is irreversibly degraded by S1P lyase or dephosphorylated by S1P phosphatases (SPPs) (Saba and Hla 2004) (**Fig. 1**).

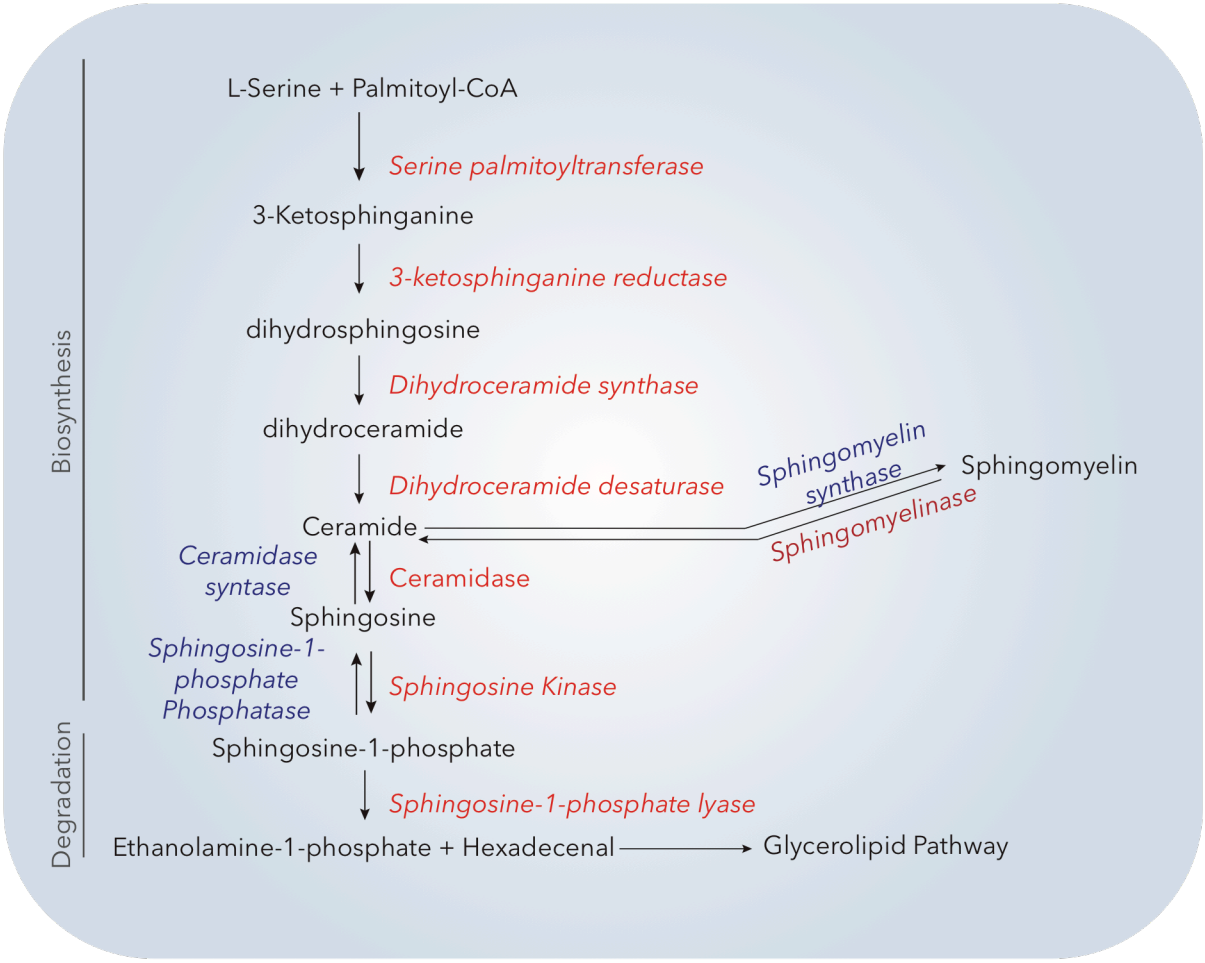

Fig. 1. ***De novo*** **Sphingolipid Metabolic Pathway**. This figure depicts the enzymatic steps in biosynthesis and degradation of sphingolipids.

1.2.2 Sphingosine-1-Phosphate Signaling

Intracellular level of S1P is tightly regulated by the enzymes that catalyze its synthesis and degradation. Activation of SphK 1 & 2 results in synthesis of S1P from sphingosine, whereas its degradation is catalyzed by reversible dephosphorylation to sphingosine by SPPs, lipid phosphate phosphatases (LPPs), or irreversible degradation by S1P lyase, a pyridoxal phosphate-dependent ER resident enzyme, to $\Delta 2$-hexadecenal and ethanolamine phosphate. ATP-binding cassette (ABC) transporters (Sato et al. 2007; Mitra et al. 2006; R. H. Kim et al. 2009; Kobayashi et al. 2009) and Spinster homolog 2 (Spns2) (Kawahara et al. 2009) are known to mediate export of intracellular generated S1P outside of the cells where S1P ligates to specific G-protein-coupled receptors, $S1P_{1\text{-}5}$, (Hla 2001) and generate downstream signals that play crucial roles in developmental and disease pathologies. S1P, a simple bioactive lipid, in recent years, has emerged as a critical mediator of diverse cellular processes that include, but not limited to, cell survival (Olivera et al. 1999), cytoskeletal reorganization (Garcia et al. 2001), endothelial barrier function(Wang and Dudek 2009), vascular maturation (Levkau 2008), adherens junction assembly (Mehta et al. 2005), immune regulation (Chi 2011; Spiegel and Milstien 2011), chemotaxis (J.-F. Lee et al. 2006), and morphogenesis (M. J. Lee et al. 1999),(M.-J. Lee et al. 2001) (**Fig. 2**).

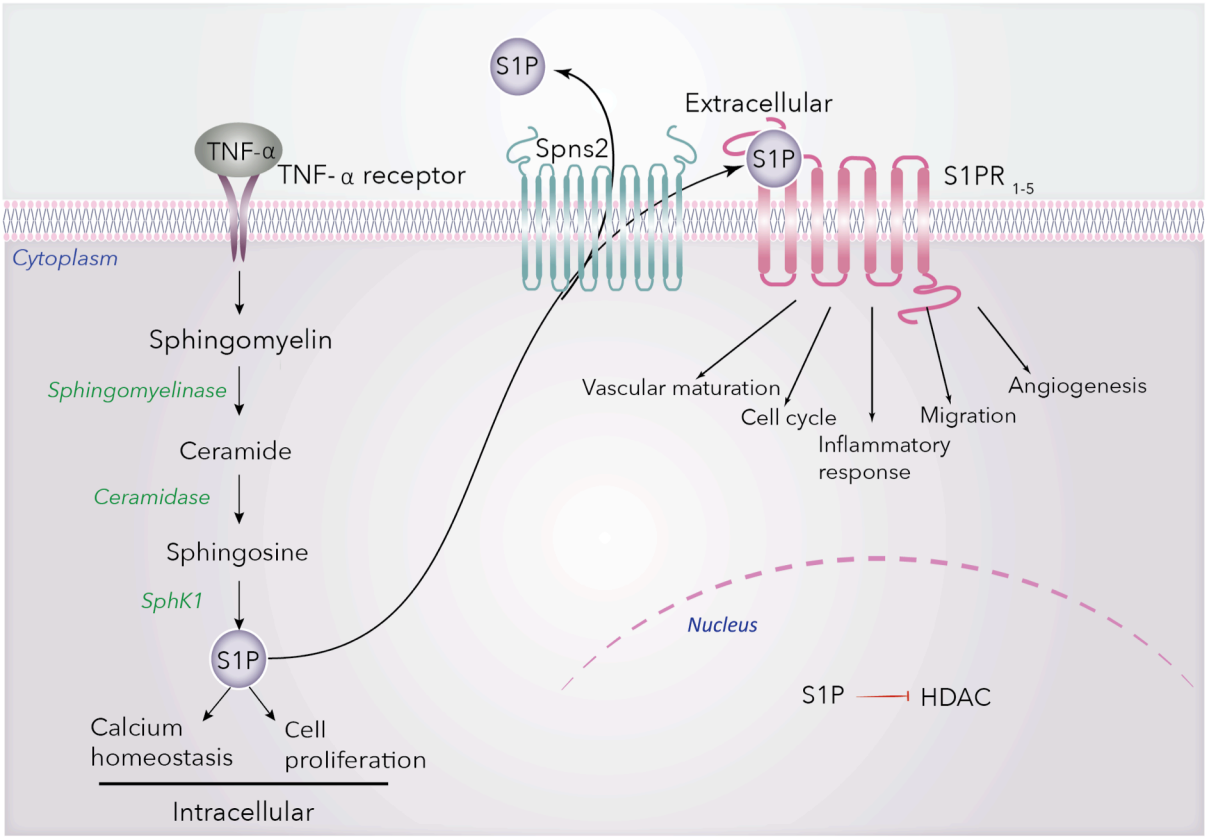

Fig 2. Sphingosine-1-phosphate signaling. S1P, generated by SphK1 or SphK2, can act intracellularly, regulating calcium homeostasis and cell proliferation. S1P, transported out of the cell by Spns2, ligates to S1P receptors 1-5 to generate downstream signaling pathways.

The subcellular localization and expression of the SphK 1 & 2 dictate the spatio-temporal S1P production and its function. While two nuclear export sequences (NES) direct SphK1 to the Cytoplasm, SphK2 has both nuclear export and import signals (N. Igarashi et al. 2003) (**Fig. 3**).

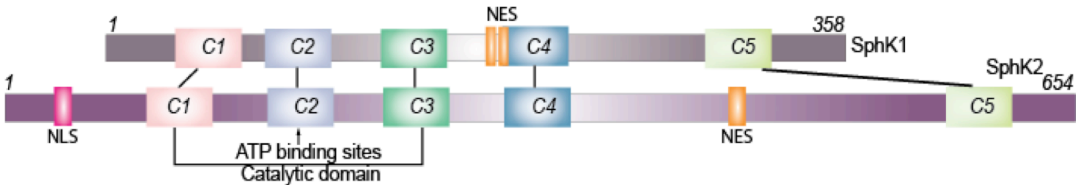

Fig 3: **Sphingosine kinase isoforms**: SphK1 & SphK2, have five conserved domains (C1-C5). The catalytic domain is located within the C1-C3 region and the ATP binding sites in the C2 domain. SphK1 also has two nuclear export signals (NES), while SphK2 has a nuclear localization signal (NLS) in addition to its NES.

Both SphK isoforms are activated in response to external stimuli, such as growth and survival factors. They undergo post translational modifications, translocation, protein-lipid, and protein-protein interactions that eventually result in increased S1P levels in the cells that play significant role in regulating various biological pathways (Alemany et al. 2007; Ebenezer, Fu, and Natarajan 2016). SphK1 is highly expressed in the lungs and heart, and SphK2 in the liver and spleen (Melendez et al. 2000). *In vivo* studies have shown that the SphK isoforms compensate for each other in SphK1 or SphK2 knock out mouse models, as they do not show any apparent phenotype; however, double knockouts result in embryonic lethality (Mizugishi et al. 2005). Moreover, both SphK isozymes also differ in regulating the sphingolipid metabolic pathway by having opposing roles in ceramide biosynthesis, thereby differentially regulating cell survival. In contrast to pro-survival SphK1, SphK2 catalytic activity induces apoptosis (Liu et al. 2003). Intracellularly, S1P is a known second messenger in calcium homeostasis that enhances endothelial cell barrier function in a Rac-dependent manner (Usatyuk et al. 2011). Recently, SphK2 generated S1P in the nucleus is shown to target nuclear HDACs, and is an integral component of the multiprotein HDAC repressor complex; however, the mechanism and its relevance in a clinical model is yet to be understood (Hait et al. 2009). SphK1 generated S1P has also been shown to be the missing cofactor for the E3 ubiquitin ligase TRAF2, leading to the activation of canonical nuclear factor kappa B (NFkB) pathway that regulates inflammatory and immune responses (Alvarez et al. 2010). S1P is also shown to allosterically mimic protein phosphorylation by binding to human telomerase reverse transcriptase, hTERT, and stabilizing it at nuclear periphery (Panneer Selvam et al. 2015). S1P generated by SphK1 has been well studied in respiratory disorders, but the mechanism of action of S1P generated in the nucleus by Sphk2 needs extensive study and its relevance to lung disorders need to be established (**Table I**).

Table I. Sphingosine Kinase Isoforms in Lung Diseases

Lung Disease	SphK Isoform	S1P Expression Levels
Sepsis	· Decreased SphK1 · Increased S1P Lyase	Low
Bronchopulmonary Dysplasia (BPD)	· Increased SphK1	Elevated
Idiopathic Pulmonary Fibrosis (IPF)	· Increased SphK1	Elevated
Pulmonary Hypertension (PH)	· Increased SphK1	Elevated
Ventilator-Induced Lung Injury (VILI)	· Decreased SphK1 · Increased S1P Lyase	Low
Lung Cancer	· Increased SphK1/SphK2	Elevated
Radiation-Induced Lung Injury (RILI)	· Increased SphK1/SphK2	Elevated
Pseudomonas aeruginosa (PA) induced Lung Inflammation	· Increased SphK2	Elevated (nuclear)

1.3 Respiratory Epithelium

Lungs, being the primary organ of the respiratory system, pack a large epithelial surface area into a dense volume. The conducting airway of the lungs, that is comprised of the trachea, bronchi and bronchioles, is lined by pseudostratified epithelium, which consists primarily of columnar ciliated cells (Whitsett and Alenghat 2015). Although ciliated cells dominate airway epithelial surface, other cell types, including secretory, neuroendocrine, and goblet cells are also found in lower numbers. In marked contrast to the diversity of the cell types in the airway, only two types line the alveoli. The squamous, alveolar type I cells (AT-I) cover 90% of the alveolar space in the adult lung and communicate with the endothelial cells of pulmonary capillaries. The self-renewing cuboidal alveolar Type II cells (AT-II) function as the precursors of Alveolar type I cells, in addition to secreting surfactant lipids and proteins that prevent lung collapse during ventilator cycle (Barkauskas et al. 2013).

1.3.1 Barrier Function of Lung Epithelial Cells

The Lung epithelial surface is in direct contact with the environment and functions as barrier to foreign particles, especially pathogens, thereby preventing infection and tissue injury. The mucociliary clearance of invading pathogens is also complemented by the innate and acquired immune responses that minimize inflammation and maintain tissue homeostasis (McKenzie et al. 2013). Conducting airway cells and AT-II cells express Pattern Recognition Receptors (PRRs) that include multiple Toll-Like Receptors (TLRs), of which TLR4 is activated in response to bacterial lipopolysaccharide (Armstrong et al. 2004),(Monick et al. 2003). Respiratory epithelial cells are responsible for the initial recognition of the pathogen through the activation of TLRs, signaling via the NF-kB and other inflammatory pathways, and subsequent production of inflammatory cytokines such as IL-6, IL-8, IL-

1β and TNF-α (McKenzie et al. 2013; Martin and Prince 2008). Epithelial cell-derived cytokines influence the recruitment of other cells from the immune system to modulate the inflammatory process in the lung. The invading pathogen influences the outcome of the inflammatory response, which could be either protective or pathological in nature (Parker and Prince 2011). Collectively, the respiratory epithelium plays a leading role in recognizing pathogens in the airway, initiating inflammatory signaling pathways and ensuing clearance of pathogens.

1.4 *Pseudomonas aeruginosa*

Pseudomonas aeruginosa is a motile, gram-negative, aerobic, opportunistic pathogen that is the leading cause of nosocomial infection, particularly in immunocompromised, ventilated and cystic fibrosis patients (Driscoll, Brody, and Kollef 2007). *P. aeruginosa* has a penchant for invading surface-exposed epithelial cells, such as the airways, and causes a spectrum of lung disorders ranging from acute pneumonia in immunocompromised patients to severe chronic deterioration of lung function in patients with cystic fibrosis (Oliver and Mena 2010). During acute infection, *PA* invades the respiratory epithelium, disseminates and cause epithelial barrier dysfunction. *PA* pathogenesis is mediated by a wide array of secreted toxins of type III and VI secretion systems, lipopolysaccharide (LPS), flagellin, pili, matrix pigments, proteases, and adhesions that facilitate bacterial adhesion and eventual modulation of host cell signaling pathways (Williams, Dehnbostel, and Blackwell 2010).

1.4.1 Recognition of *Pseudomonas aeruginosa* by Toll-Like Receptors

P. aeruginosa and its derived products are specifically recognized by toll receptors, TLR2 (Travassos et al. 2004; Epelman et al. 2004)., TLR4 (Hajjar et al. 2002; Pier 2007) and TLR5. TLR4 shares several *P. aeruginosa* ligands with TLR2, including LPS and certain outer-membrane proteins. *P. aeruginosa* derived LPS ligation to TLR4 induces a potent immune response that result in severe inflammation of

the lung. Flagellin, the primary component of *PA* flagellum, acts as a ligand for TLR5 (Hayashi et al. 2001). Bacterial mutants with over expressed flagellin cause intense inflammation, whereas those that lacked flagellin dodge the immune system and cleared from lungs leisurely (Amiel et al. 2010). *PA* derived products binding to TLR triggers a set of complex molecular signaling events, the prominent consequence being the generation of soluble mediators of immune response that are required for host defense against the pathogen.

1.4.2 Cytokine and Inflammatory Mediators in *Pseudomonas aeruginosa* Infection

Inflammation of the airways is associated with elevated production of pro-inflammatory cytokines in the lung by airway epithelial cells, macrophages, and neutrophils (**Table II**). Elevated concentrations of IL-1β, IL-6, IL-8 and TNF α has been reported in sputum and BALFs of Cystic Fibrosis (CF) patients (Richman-Eisenstat 1996). The transcription factor, nuclear factor-Kappa B, (NFκB) plays an important role in regulating the production of the pro-inflammatory cytokines (Barnes and Karin 1997). IL-6 is responsible for mediating the acute-phase reaction and TNF-α facilitates the chemotaxis of neutrophils to the site of inflammation. Excess release of oxidants and proteases by the migrating neutrophils and tilting of balance towards the pro-inflammatory cytokines like IL-6 and IL-8 exacerbate the lung tissue damage in CF lung (Berger 1991). C-reactive protein, a surrogate marker of IL-6 and TNF-α, has been found to be elevated during lung deterioration and decreased levels have been noted following antibiotic therapy (Elborn et al. 1993). Altered cytokine profiles play a crucial role in the development of clinical features of lung diseases and therapy targeted at regulating the cytokine levels carry enormous potential in ameliorating *PA* mediated lung inflammation.

1.5 Epigenetic Regulation of Lung Inflammation and Repair

Epigenetics is defined as the heritable changes in the expression of genes without involving changes to the DNA sequence. The molecular basis of epigenetic regulation is complex and involves histone modifications, DNA methylation and gene regulation by non-coding RNAs. Epigenetic modifications are reversible and the epigenome is as crucial as the genome and environmental factors such as nutrients, toxins, infections and hypoxia have shown to determine the epigenetic signature and susceptibility to disease (Barros and Offenbacher 2009; Campos and Reinberg 2009). Inflammatory response is a gene-specific signal that involves sophisticated epigenetic mechanisms, including DNA methylation and covalent histone modifications are shown to be critical in the regulation of inflammatory cytokines, in addition to regulation of transcription factors NFκB, FOXP3 and STAT family members (Bayarsaihan 2010; Medzhitov and Horng 2009).

Table II. Inflammatory mediators of lung inflammation

Cytokine	Action	Pro/Anti Inflammation
IL-1β	· Amplify neutrophil adherence to the endothelium · Mobilize neutrophils	Pro-inflammatory
IL-6	· Induce B-lymphocyte maturation · Induce T-lymphocyte activation · Regulates acute-phase reaction	Pro-inflammatory
IL-8	· Induce Neutrophil activation · Induce the expression of adhesion molecules · Accelerate the chemotaxis of neutrophils	Pro-inflammatory
IL-10	· Arrest the secretion of TNF-α and other cytokines · Arrest antigen presentation	Anti-inflammatory
TNF-α	· Aid in the chemotaxis of neutrophils · Amplify neutrophil adherence to the endothelium · Activate the production of chemoattractants for neutrophils · Boost intermediary metabolism	Pro-inflammatory

1.5.1 Histone Modifications

Nucleosome, which form the basic unit of chromatin, is composed of segments of DNA wrapped around core histones that are made up of two copies H2A, H2B, H3 and H4 (Campos and Reinberg 2009). The covalent post-translational modification of N-terminal histone tails which includes acetylation, phosphorylation, methylation, Ubiquitination, SUMOylation and ADP-ribosylation impact gene expression by altering chromatin structure and recruiting histone modifiers (Fuchs et al. 2006). Acetylation and methylation occur in lysine and arginine residues and control the accessibility of the chromatin. Acetylation of the lysine residues at the N-terminus of histone proteins remove the positive change, thereby reducing the affinity between DNA and histones, creating a transcription permissive environment (Campos and Reinberg 2009; Cheng and Blumenthal 2010). Acetylated H3K9 (H3K9ac) and H4K8ac are associated with transcriptional activation and these modifications are carried out by Histone Acetyl Transferases (HATs) (Marks et al. 2001). On the other hand, Histone methylation can keep chromatin in an either "open" or "closed" state. Trimethylation of Histone H3 on Lysine 4 and 36 (H3K4me3, H3K36me3) is an indicator of open chromatin for active transcription in contrast to histone methylations on Lysine 9 and 27 (H3K9me3, H3K27me3) that are associated with closed chromatin (Dong and Weng 2013). Methylation and demethylation of histones are carried out by Histone Methyl Transferases (HMT) and Histone Demethylases (HDM), respectively.

1.5.2 Histone Modifications in Inflammation

Acetylation of histones by HATs, such as CREB-binding protein (CBP) and its close homolog P300 activates inflammatory genes, whereas elevated HDAC activity results in decreased inflammatory gene repression. In chronic obstructive pulmonary disease (COPD), decreased HDAC activity and increased histone acetylation at promoters of IL-1, IL-2, IL-8, IL-12 is mediated by NF-kB leading to

transcriptional activation and elevated cytokine secretion (Villagra, Sotomayor, and Seto 2010). Also, there was increased recruitment of NF-κB at the promoters of cytokines and chemokines whose promoters are histone H3 acetylated IKK-α mediated phosphorylation at Histone H3, Ser 10 and CBP-assisted histone acetylation at H3K9 is shown to be critical for subsequent CBP-mediated acetylation of Histone H3 Lys 14 in NFkB dependent promoters (Barnes 2008). .

HDACs opposes HAT activity by removing the acetylation marks and hence involved in silencing TLR-4 target genes by modifying the chromatin (Foster, Hargreaves, and Medzhitov 2007). Class I HDACs, which are localized in the nucleus, are responsible for negatively regulating TLR response signaling of NF-kB by reversible deacetylation. HDAC 1 acts as feedback regulator of TLR responses by inhibiting inflammatory gene promoters including Cox-2 (Deng, Zhu, and Wu 2004); IL-12 (Lu et al. 2005); p40 (Deng, Zhu, and Wu 2004) and IFN-B (Nusinzon and Horvath 2006); this probably could be HDAC 1 exerting its effect on NF-κB regulatory subunits binding to the promoters (Ashburner, Westerheide, and Baldwin 2001; Choi and Jeong 2005; Elsharkawy et al. 2010). HDAC1 deacetylation of histone H4 is through its interaction with activating transcription factor (ATF), which is an inducible negative regulator of TLR-signaling (Gilchrist et al. 2006).

The repressive effect on TLR-signaling is not just limited to HDAC1; other nuclear HDACs such as HDAC 2, 3 & 8 have similar function as negative regulators of TLR-mediated responses. HDAC 3 switches off NF-kB mediated inflammatory responses by deacetylating p65 subunit and subsequent nuclear export of NF-kB (Kiernan et al. 2003). In LPS mediated responses, HDAC 2 is inactivated by S-nitrosylation in order to activate the inflammatory gene expression. Selective loss of HDAC2 function in alveolar macrophages has been shown to correlate with disease severity in COPD. Nitration of

HDAC2 at Y253 during oxidative stress promotes its proteosomal degradation leading to enhanced inflammatory response in macrophages (Osoata et al. 2009).

1.6 HDAC Family

In humans, 18 HDAC enzymes are grouped into four different classes (**Table III**). Class I, II and IV HDACs are Zn2+ dependent for their enzymatic activity. Class 1 HDACs (HDACs 1, 2, 3, and 8) reside in the nucleus because of their nuclear localization sequence and are the most widely studied for their role in modifying histones and repressing transcription. Class II HDACs are further classified into Class II a (HDACs 4, 5, 7 and 9) and II b (HDACs 6 & 10) based on their domain organization. Class IIA HDACs have N-terminal transcription factor binding domains through which they control gene expression by recruiting transcriptional co-repressors and co-activators, and a C -terminal nuclear export signal that prevents them from acting as transcriptional repressors. Class IIb HDACs have tandem deacetylase domains and while HDAC 6 is predominantly localized in the cytoplasm, HDAC 10 shuttles between nucleus and cytoplasm. HDAC 11 is the sole member of HDAC IV. Seven Sirtuins (SIRT 1-7), require NAD^+ for their activity, comprises the class III HDACs (Delcuve, Khan, and Davie 2012).

1.6.1 Class I HDAC Complexes

Class I HDACs are ubiquitously expressed nuclear enzymes that are components of multiprotein co-repressor complexes (de Ruijter et al. 2003). HDAC 1 & 2 share almost 85% homology and form either homo or hetero dimers, which presumably allows them to act independently or together and is imperative for HDAC activity (Gregoretti, Lee, and Goodson 2004). HDAC 1 and 2 are integral components of multiprotein co-repressor complexes Sin3, Nucleosome-remodeling NuRD, and

CoREST, that are recruited by the transcriptions factors such as NF-kB, Sp1, Sp3, p53 and YY1 to the regulatory regions of the chromatin (de Ruijter et al. 2003)·(Yang and Seto 2008).

Table III. Classes of HDAC

HDAC Class	HDAC Family Member	Localization	Cofactor	Function from Knockout Experiments
I	HDAC1	Nucleus	Zn-dependent	Participates in overall HDAC Activity
	HDAC2	Nucleus	Zn-dependent	Mediates cardiac muscle production
	HDAC3	Nucleus	Zn-dependent	Participates as cell cycle checkpoints as well as pro-apoptosis activities
	HDAC8	Nucleus	Zn-dependent	Unknown
II A	HDAC4	Nucleus and Cytoplasm	Zn-dependent	Regulates ossification and chondrocyte activity
	HDAC5	Nucleus and Cytoplasm	Zn-dependent	Participates in cardiac stress response
	HDAC7	Nucleus and Cytoplasm	Zn-dependent	Participates in endothelial cell-cell adhesion
	HDAC9	Nucleus and Cytoplasm	Zn-dependent	Regulates myocardial cell division
II B	HDAC6	Cytoplasm	Zn-dependent	Participates in cell recovery in oxidative stress
	HDAC10	Cytoplasm	Zn-dependent	Unknown
III	SIRT 1-7	Nucleus and Cytoplasm	NAD-dependent	Might regulate metabolism, stress response, DNA repair, apoptosis, as well as cell senescence
IV	HDAC11	Nucleus	Zn-dependent	Unknown

1.6.2 Sin3 Complex

The catalytic core of Sin3 complex that is composed of HDAC1/2 along with histone binding proteins RbAp46, RbAp48 and core proteins, Sin3A and Sin3B forms a platform for the addition of other modules with enzymatic activity for nucleosome remodeling, histone methylation and DNA methylation (Delcuve, Khan, and Davie 2012).

1.6.3 NuRD Complex

The NuRD complex links two chromatin-modifying activities, both HDAC- and ATP-dependent, carried out by HDAC 1 and/or HDAC2 and Mi-2α and/or Mi-2β. The other components include the regulatory proteins, RbAP46/RbAp48 and Methyl-CpG-binding domain containing proteins, MBD2/MBD3 (Delcuve, Khan, and Davie 2012).

1.6.4 CoREST

HDAC 1 & HDAC 2, along with KDM1 forms the core of CoREST complex, which then interact with other chromatin remodeling complexes like SWI/SNF to form larger repressor complexes to regulate neuronal and cell-cycle genes (M. G. Lee et al. 2005).

This illustrates the various combinations of interactions that HDAC1 and HDAC2 homo- or heterodimer can form with different proteins, which determine the activity, substrate specificity, and the genomic location of the repressor complex.

1.7 Reactive Oxygen Species

Reactive oxygen species (ROS) are oxygen derivatives that are more reactive than molecular oxygen. Superoxide ($O_2^{\cdot-}$) is the primary ROS, which is formed by one-electron reduction of molecular oxygen, and its reduction by dismutase yields hydrogen peroxide (H_2O_2). Electron exchange between $0_2^{\cdot-}$ and H_2O_2 or reduction of H_2O_2 gives rise to hydroxy radical(OH^-). ROS can act as signaling molecules

under compartmentalized, strictly regulated conditions but abundant production of ROS damages lipids, proteins and DNA. Oxidation of amino acids, especially cysteine (Cys) and methionine (Met) by ROS is known to affect the functional properties of the proteins (Morrell 2008). NADPH Oxidase (NOX) family of proteins is one of the multiple sources contributing to the production of ROS.

1.8 Protein Kinase C

Protein Kinase C (PKC) is a family of serine/ threonine kinases that are activated by the signals that trigger cell surface receptors that result in diacylglycerol (DAG) production. PKC isozymes, in addition to DAG, can also be activated by phorbol esters and require phosphatidyl- serine and/or Ca^{2+} for optimal enzymatic activity (Mochly-Rosen, Das, and Grimes 2012). PKC isoforms are differentially distributed throughout the cell and the subcellular localization is key to its regulation of the activity (Mochly-Rosen and Gordon 1998). PKC isoforms become catalytically active by phosphorylation that localize the protein to specific cell compartments enabling it to act on plethora of substrates, thus modifying diverse cellular functions. PKC family members share a single polypeptide, comprised of N-terminal regulatory and C-terminal catalytic regions (**Fig. 4**). Based on their structure and cofactor regulation, PKC isoforms are classified into three major groups: Conventional, Novel and Atypical (Wu-Zhang and Newton 2013) (**Table IV**). PKCs, in addition to phosphorylating Serine/threonine residues, can also function as an ATPase and a phosphatase (Wu-Zhang and Newton 2013). Increased activation of PKC is noted in various cardiovascular (Ferreira, Brum, and Mochly-Rosen 2011) and lung disorders (Dempsey, Cool, and Littler 2007), with PKC being a central mediator in regulating various signaling cascades. PKC isoforms are master regulators of inflammation signaling pathways in the lungs, regulating alveolar epithelial barrier function, neutrophil trafficking and pro-inflammatory signaling (Koyanagi et al. 2007).

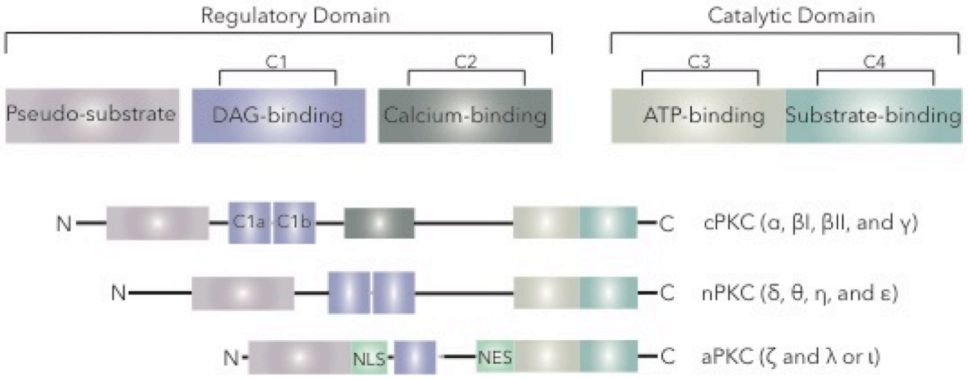

Fig. 4. Domain Structure of PKC Isoenzymes. This figure indicates the domain structure of PKC isoenzymes.

Table IV. Classes of PKC

PKC Class	PKC Isozyme	Cofactor
Conventional	· PKC-α · PKC-β1 · PKC-β1 · PKC-γ	· DAG · Ca^{2+} · Phospholipid
Novel	· PKC-δ · PKC-ε · PKC-η · PKC-θ	· DAG
Atypical	· PKC-ι · PKC-ζ	· Phosphatidyl Serine

1.9 NADPH-Oxidases

NADPH-oxidase (NOX) families of proteins are enzymes dedicated to generate $O_2^{\cdot-}$ and/or H_2O_2. Seven members of NOX family proteins (NOX 1-5, Duox1 and Duox2) have been identified so far (**Table V**). NOX1, NOX2, NOX3, NOX4 are identical in size and domain structure which consists of C-terminal flavoprotein domain containing an NADPH-binding region and a FAD binding region (Aitken et al. 1997); the N-terminal hydrophobic domain containing two heme-binding sites (Maturana, Krause, and Demaurex 2002). NOX isoforms are expressed in specific lung cells and they mediate diverse signaling pathways. NOX2 regulates cell cycle (Chaube et al. 2005) in alveolar epithelial cells and NOX4-derived ROS induced in response to lung injury in AT II cells is shown to promote apoptosis in response to lung injury (Bedard and Krause 2007). DUOX 1/2 are expressed in AT II cells and play a critical role in regulating acid release during lung development (Fischer 2009). NOX 2 and NOX 4 have been shown to localized to the nucleus/perinuclear region (Pendyala et al. 2009) and NOX-4 and not NOX-2 mediates *PA* induced endothelial barrier dysfunction(Fu et al. 2013).

Table V. NOX Family Proteins

NADPH Oxidase Family	Localization	Activation	Function
NOX 1	· Transmembrane · Smooth Muscle Cells	· Rac Dependent · Activated by proteins such as NOXa1 and NOXo1	· Generates ROS · Induces thromboxane A synthase
NOX 2	· Transmembrane · Endothelial · Mesenchymal · Epithelial	· Rac Dependent · Activated by $p47^{phox}$ and $p67^{phox}$	· ROS production via PIP3 signaling · Promotes cell-cycle progression from G0/G1 to S and G2 to M phases
NOX 3	· Transmembrane	· Suppressed by TLR4	· Generates ROS
NOX 4	· Transmembrane · Endothelial · Mesenchymal · Epithelial · Smooth Muscle Cells	· Rac Independent	· Generates H2O2 · Responds to hyperopia
NOX 5	· Transmembrane	· Always Active	· Generates ROS
DUOX 1	· Thyroid Tissue · Airway epithelia · Prostate	· Rac independent · Ca^{2+}	· Generates ROS · Lung Defense System
DUOX 2	· Thyroid Tissue · Airway epithelia · Prostate · Salivary glands · Gastrointestinal tract · Rectal mucosa	· Rac independent · Ca^{2+}	· Generates ROS · Biosynthesis of thyroid hormone · Lung Defense System

2. OBJECTIVES

2.1. To determine the role of Sphingolipid metabolism in *Pseudomonas aeruginosa* induced lung inflammation.

2.2. To elucidate the role of Sphingosine Kinase-2 mediated nuclear Sphingosine-1-phosphate signaling in epigenetic regulation of pro-inflammatory cytokine secretion.

3. METHODS AND MATERIALS

3.1 Reagents

10X TBS (170-6435, BioRad Hercules, CA), 10X TAE Buffer (161-0743, BioRad, Hercules, CA), 10X Tris/Glycine/SDS Buffer (161-0772, BioRad, Hercules, CA), 10X Tris/Glycine Buffer (161-0771, BioRad, Hercules, CA), RIPA Buffer (R0278, Sigma-Aldrich, St. Louis, MO), 1X TE Buffer (51235, Lonza, Basel, Switzerland), PBS (21-040-CV, Corning, Corning, NY), Dimethyl Sulphoxide (DMSO), Hybri-Max (D2650, Sigma-Aldrich, St. Louis, MO), Formalin Solution, neutral buffered, 10% (HT501128, Sigma-Aldrich, St. Louis, MO), ChIP Lysis Buffer (sc-45000, Santa Cruz Biotechnology, Dallas, TX), Restore PLUS Western Blot Stripping Buffer (46430, Thermo Fisher Scientific, Waltham, MA), ACK Lysis Buffer (10-548E, Lonza, Basel, Switzerland), Formaldehyde (BP531-500, Thermo Fisher Scientific, Waltham, MA), Sodium Bicarbonate (7.5%) (25080-094, Thermo Fisher Scientific, Waltham, MA), 0.5 M EDTA (15575-038, Invitrogen, Carlsbad, CA), DEPC-Treated Water (G-3223-125, GeneMate BioExpress, Kaysville, UT), SDS 10% Solution (AM9822, Invitrogen, Carlsbad, CA), Sodium Chloride Solution (S6316, Sigma-Aldrich, St. Louis, MO), Molecular Biology Grade Water (46-000-CM, Corning, Corning, NY), HEPES (15630-080, Gibco, Gaithersburg, MD), Absolute Ethanol (BP2818-500, Fisher Scientific, Waltham, MA), Methanol (A452-4, Fisher Chemical, Waltham, MA), Isopropanol (67-63-0, Sigma-Aldrich, St. Louis, MO), Chloroform (C606SK-1, Fisher Scientific, Waltham, MA), TRIzol Reagent (15596018, Life Technologies, Carlsbad, CA), GeneSilencer siRNA Transfection Reagent (T500750, Genlantis, San Diego, CA), Triton X (CAS 9002-93-1, Sigma-Aldrich, St. Louis, MO), FastStart Universal SYBR Green Master (Rox) (19317900, Sigma-Aldrich, St. Louis, MO), DAPI (4', 6-diamidino-2-phenylindole) (D1306, Thermo Fisher Scientific, Waltham, MA), ProLong Gold Antifade Reagent with DAPI (P36935, Thermo Fisher Scientific, Waltham, MA), LE Agarose (E-3120-500, GeneMate

BioExpress, Kaysville, UT), Luria Broth (L24040-500, Grainger, Lake Forest, IL), Novex Wedgewell 4-20% 10 well Tris-Glycine Gel (XP04200BOX, Thermo Fisher Scientific, Waltham, MA), Novex Wedgewell 10% 10 well Tris-Glycine Gel (XP00100BOX, Thermo Fisher Scientific, Waltham, MA), Novex Wedgewell 4-20% 15 well Tris-Glycine Gel (XP04205, Thermo Fisher Scientific, Waltham, MA), Novex Wedgewell 10% 15 well Tris-Glycine Gel (XP00105BOX, Thermo Fisher Scientific, Waltham, MA), 2-Mercaptoethanol (M3148, Sigma-Aldrich, St. Louis, MO), Lamelli 6X, Nonreducing Sample Buffer (BP-111NR, Boston BioProducts, Ashland, MA), Pierce BCA Protein Assay Kit (23225, Thermo Fisher Scientific, Waltham, MA), Pierce ECL Western Blotting Substrate (32106, Thermo Fisher Scientific, Waltham, MA), Tween 20 (BP337-100, Fisher Scientific, Waltham, MA), Bovine Serum Albumin (A7906-100G, Sigma-Aldrich, St. Louis, MO), ECL Prime Western Blotting Detection Reagent (RPN2232, GE Healthcare Life Sciences, Pittsburgh, PA), Precision Plus Protein Dual Color (161-0374, BioRad, Hercules, CA), Protein A/G Plus-Agarose (sc-2003, Santa Cruz Biotechnology, Dallas, TX), Dynabeads Protein G for Immunoprecipitation (10004D, Invitrogen, Carlsbad, CA), Control siRNA (sc-37007, Santa Cruz Biotechnology, Dallas, TX), PKC δ siRNA (sc-36246, Santa Cruz Biotechnology, Dallas, TX), SphK2 siRNA (sc-39226, Santa Cruz Biotechnology, Dallas, TX), NOX4 siRNA (sc-41587, Santa Cruz Biotechnology, Dallas, TX)

3.2 Inhibitors

Phosphatase Inhibitor (524625-1SET, EMD Millipore, Billerica, MA), Protease Inhibitor (539134- 1SET EMD Millipore, Billerica, MA), ROCK Inhibitor (Y-27632, Sigma-Aldrich, St. Louis, MO).

3.3 Antibodies

HDAC2 (IP Preferred) (2545S, Cell Signaling Technology, Danvers, MA), Acetyl-Histone H4 (8647P, Cell Signaling Technology, Danvers, MA), Acetyl-Histone H3 (9649P, Cell Signaling Technology, Danvers, MA), Histone H3 (9715, Cell Signaling Technology, Danvers, MA), Histone H4 (2592S, Cell Signaling Technology, Danvers, MA), SphK2 (Thr614) (A8423, Assay BioTech, Fremont, CA), SphK1 (ab37980, Abcam, Cambridge, UK), Anti-PKC delta (phospho S299) (ab133456, Abcam, Cambridge, UK), NOX4 (H300) (sc-30141, Santa Cruz Biotechnology, Dallas, TX), Lamin B1 (ab16048, Abcam, Cambridge, UK), Actin (A15441, Abcam, Cambridge, UK), GAPDH (sc-25778, Santa Cruz Biotechnology, Dallas, TX), EpCAM Monoclonal Antibody (13-5791-82, eBioscience, San Diego, CA), Goat Anti-Mouse IgG (170-6516, BioRad, Hercules, CA), Goat Anti-Rabbit IgG (170-6515, BioRad, Hercules, CA), Donkey-anti Rabbit IgG 568 (A10042, Thermo Fisher Scientific, Waltham, MA), Goat-Anti Mouse IgG 568 (A11031, Thermo Fisher Scientific, Waltham, MA), Alexa Fluor 488 (A21206, Thermo Fisher Scientific, Waltham, MA), Alexafluor 647 (A21244, Thermo Fisher Scientific, Waltham, MA), Fetal Bovine Serum Heat Inactivated (12306C, Sigma-Aldrich, St. Louis, MO), DMEM (11995-065, Gibco, Gaithersburg, MD), L-Glutamine (25030-081, Gibco, Gaithersburg, MD), Penicillin/Streptomycin (15140122, Gibco, Gaithersburg, MD), 0.05% Trypsin (25300-054, Gibco, Gaithersburg, MD), Ethidium Bromide (161-0433, BioRad, Hercules, CA), 6X DNA Loading Dye (R0611, Thermo Fisher Scientific, Waltham, MA), Quick-Load Purple 2-Log DNA Ladder (N0550G, New England BioLabs, Ipswich, MA).

3.4 Assay Kit

Amplex Red Hydrogen Peroxide/Peroxidase Assay Kit (A22188, Thermo Fisher Scientific, Waltham, MA), Mouse IL-6 ELISA (M6000B, R&D Systems, Minneapolis, MN), Mouse TNF-α Immunoassay

(MTA00B M6000B, R&D Systems, Minneapolis, MN), HDAC Fluorometric Activity Assay Kit (10011563, Cayman Chemical, Ann Arbor, MI), QIAquick PCR Purification Kit (28104, Qiagen, Hilden, Germany).

3.5 Enzymes

RNAse A (EN0531, Thermo Fisher Scientific, Waltham, MA), Proteinase K (P8107S, New England BioLabs, Ipswich, MA), Micrococcal nuclease (MO247S, New England BioLabs, Ipswich, MA), Dispase (04942078001, Roche Diagnostics, IN), DNase I (M0303S, New England Biolabs, USA).

3.6 Quantitative Real-Time PCR:

All Primers used for Real time PCR analysis were obtained from IDT, Coralville, IA.

IL-6 Forward, 5′-CCAAGAGGTGAGTGCTTCCC-3′,

IL-6 Reverse Primer, 5′-CTGTTGTTCAGACTC TCTCCCT-3′,

TNF-α Forward Primer, 5′-CCCTCACACTCAGATCATCTTCT-3′,

TNF-α Reverse Primer, 5′-GCTACGACGTGGGCTACAG-3′,

GAPDH Forward Primer, 5′-AGGTCGGTGTGAACGGATTTG-3′,

GAPDH Reverse Primer, 5′-TGTAGACCATGTAGTTGAGGTCA-3′,

ChIP DNA primers targeting the NFkB binding site in the proximal promoter region of mouse IL-6 gene:

Forward Primer, 5′-CCCACCCTCCAACAAAGATT-3′,

Reverse Primer, 5′-GAATTGACTATCGTTCTTGGTG-3′

3.7 Sphingosine Kinase Activity Assay using [γ-^{32}P] ATP

Mouse lung alveolar epithelial (MLE-12) cells in 100-mm dishes were treated with vehicle or heat-inactivated *Pseudomonas aeruginosa* (1.5×10^8 pfu/ml) for 2 h followed by isolation of nuclear fraction.

The nuclear fractions (40 μg protein) were subjected to SphK activity assay in Hepes buffer (pH 7.4) containing 10 mM $MgCl_2$, and 1 mM DTT in the absence or presence of 1μM sphingosine (Sph), dihydro Sph or FTY720 in the presence of 0.1% fatty acid BSA and 10 μM [γ-^{32}P] ATP (Specific activity 10,000 dpm/pmol) in a final volume of 100 μl for 30 min at 37^{0}C. The reaction was terminated by the addition of 0.8 ml of 1N HCl followed by 1 ml of methanol and 1 ml chloroform to extract the lipids. The lower chloroform layer was subjected to thin-layer chromatography, and autoradiography and radioactivity associated in S1P, DH S1P or FTY720-P was quantified by scintillation counting as described under Materials and Methods. Values are means $\pm$SEM of three independent experiments and expressed as p-moles of product formed/mg protein/min.

3.8 Analysis of Sphingoid Base-1-Phosphates, Ceramides and Sphingoid Bases by Mass Spectrometry

Analysis of sphingoid base-1-phosphates, ceramides, and sphingoid bases were performed by electrospray ionization tandem mass spectrometry (ESI-LC/MS/MS). The instrumentation employed was Sciex 6500 QTRAP hybrid triple quadrupole linear ion-trap mass spectrometer (AB Sciex, Redwood City, CA) equipped with an Ion Drive Turbo V ion spray ionization source interfaced with a Shimadzu Nexera X2 UHPLC system. All lipid molecules and their derivatives were separated using Ascentis Express RP-Amide 2.7 μm 2.1 x 50 mm column and gradient elution from methanol: water: formic acid (65:35:0.5, 5 mM ammonium formate) to methanol: chloroform: water: formic acid (90:10:0.5:0.5, 5 mM ammonium formate). S1P and DHS1P were analyzed as *bis*-acetylated derivatives with D7-S1P as the internal standard employing negative ion ESI and MRM analysis basically as described in (4). Ceramides and sphingoid bases were analyzed with D7-16:0-ceramide and D7-Sph as internal standards using positive ion ESI and MRM analysis. To facilitate ceramide analysis, total lipids

were hydrolyzed using a methylamine reagent for 2 h at 55°C. Reagents were evaporated with nitrogen stream; the residual non-saponified lipids were dissolved in 0.2 ml of methanol and subjected to the LC-MS/MS analysis of ceramides. Standard curves were created for all measured analytes by mixing a fixed amount of the internal standard with variable amounts of corresponding analytes (Sph, DHSph, S1P, DHS1P, and variable ceramide species N-acylated with 16:0-24:1 fatty acids, all from Avanti Polar Lipids). The linearity and the correlation coefficients of the standard curves were obtained via linear regression analysis. Quantification of ceramide molecules for which there are no standards available was performed with the best closest approximation to the available standards.

3.9 ChIP Assay

MLE-12 cells grown to ~90% confluence on 100-mm dishes were treated with heat killed *PA*103 for 3 h. Formaldehyde was added directly to the cell culture medium to a final concentration of 1% and incubated for 9 min. Glycine was then added to a final concentration of 125 mM and dishes were incubated in room temperature for 5 min, washed with PBS, cells were collected in a 15 mL tube, centrifuged at 800 x g for 5 min, and pellet was collected. The pellet was resuspended in ChIP lysis buffer (Santa Cruz) with protease and phosphatase inhibitors, and incubated at 4°C with rotation for 10 min. Samples were centrifuged at 2000 x g for 5 min and 1 mL Micrococcus nuclease (MNase) digestion buffer containing $CaCl_2$ was added to re-suspend the pellet, and samples were incubated at 37°C for 10 min. EDTA was added to a final concentration of 5 mM and samples were sonicated 3 times, 12 sec each, at a power of 6. Lysates were centrifuged at 10,000 x g for 10 min. 50µl of chromatin was removed for analysis and the remaining supernatant was stored in -80°C. For chromatin analysis, 100µl of nuclease-free water, 6µl of 5M NaCl, and 2µl RNAse A was added to the 50µl sample and incubated at 37°C for 30 min. Following incubation, 2µl Proteinase K was added and samples were incubated at

65°C for 2 h. DNA was purified using Qiagen QiA Quick PCR purification kit; protein concentration was measured with a nano-drop and amount of digested DNA was viewed by loading 10µl of sample on a 1.2% agarose gel with 100bp DNA marker. 10µg of digested chromatin was used for each immunoprecipation (IP). 50µl Protein A/G agarose beads were added to the digested DNA and samples were incubated for 1 h at 4°C with rotation. Samples were centrifuged at 4,000 x g for 5 min and the supernatant was transferred to a new tube. 10µl of supernatant was kept aside for input fraction. Chromatin DNA was immunoprecipitated using 5µg Acetylated Histone H3K9 antibody, 2µg of negative control (IgG), and 2µg of positive control ($H_3K_4Me_3$) for 4 h at 4°C with rotation. 50µl of Protein A or G magnetic beads were added and samples were incubated for 2 h at 4°C with rotation. Magnetic beads were pelleted using Dyna mag^{-2} Magnet stand (Invitrogen) and supernatant discarded. Magnetic pellets were washed with low salt wash buffer, high salt wash buffer, LiCl wash buffer, and 1 X TE buffer, twice. 250µl of Elution buffer was added to input fractions and allowed to incubate at room temperature for 30 min with rotation. Samples were then incubated overnight at 65°C. Samples were treated with 2µl RNAse for 30 min at 37°C. After incubation, 2µl Proteinase K was added and incubated for 1 h at 55°C. Magnetic beads were pelleted and supernatant was collected; DNA was isolated using Qiagen QiA Quick PCR purification kit. Real time PCR was performed using specific primers designed to amplify NF-kB binding site in IL-6 proximal promoter region.

3.10 Exposure of Epithelial Cells to Heat-Inactivated *Pseudomonas aeruginosa*

Primary human bronchial epithelial cells (HBEpCs) (Lonza) were cultured in Basal Epithelial Cell Basal Medium (BEBM) supplemented with growth factors (Lonza) and 100 U/mL penicillin/streptomycin. HBEpCs between 2-8 passages were used. Mouse lung epithelial cell line (MLE-12) was cultured in DMEM complete medium (5% FBS, 100 U/mL penicillin and streptomycin) at 37^0C and 5 % CO2 and

cells were allowed to grow approximately 90 % confluence before exposure to bacterial. Cells were exposed to heat-inactivated *PA* at a multiplicity of infection (MOI) of 50 in serum free BEBM or DMEM medium containing 1% serum for varying time periods. Cells were rinsed in ice-cold PBS and harvested, cell lysates prepared and immunoblotted.

3.11 HDAC Activity Assay

HDAC activity was measured in cell nuclei isolated from MLE-12 cells or HBEpCs as outlined above using a commercially available kit according to the manufacturer's instruction (Cayman).

3.12 Human Cystic Fibrosis Lung Specimens

Six cases of advanced cystic fibrosis subjected to lung explanatation were selected from the archives from the Department of Pathology of the Colorado Children's Hospital. The CF lung donors were 4 males and 3 females, ages 16-24 years old. These lungs had characteristic gross and microscopic features of cystic fibrosis. These consist of bronchiectasis and bronchiolectasis, with extensive peri-airway fibrosis. Microscopically, the airways had characteristic mucus accumulation admixed with large numbers of neutrophils. The inflammatory process extended to adjacent alveolar structures. Six normal lungs, not used for transplantation, were obtained from anonymous lung donors. They were histologically normal. The study was approved by the University of Colorado Institutional Review Board.

3.13 IL-6 Gene Expression

Total RNA was isolated from cells that were treated with vehicle and *PA*103 for 3 h using TriZOL reagent (Life Technologies), according to the manufacturer's protocol. cDNA was generated using random primers and Real time PCR was done using Mouse IL-6 primers on the iCycler (BioRad).

3.14 Immunoblotting

HBEpCs, MLE-12 cells or primary ATII cells (~90 % confluence) were stimulated with vehicle or 50 MOI (1 x 10^8 CFU/ml) of heat-killed *PA*103 for 2 h, washed with PBS, and lysed with 100µl of RIPA buffer, with protease and phosphatase inhibitors. Lysates were then sonicated for 10 seconds at a setting of 3 in a probe sonicator and centrifuged at 10,000 x g for 10 min at 4°C. Supernatants were collected and protein concentration was measured using BCA protein assay kit. Samples for Western blotting were prepared with 10-20µg protein and 6x Laemmli buffer, placed on a heat block at 100°C for 5 minutes. The cell lysates were separated by Sodium dodecyl sulfate polyacrylamide gel electrophoresis (SDS-PAGE) on 10% or 4-20% precast gel (Invitrogen) at 225 V for 40 min. Blots were transferred onto 0.22nm nitrocellulose membranes for 1.5 h at 70 volts. Membranes were rinsed in wash buffer (Tris buffer saline + Tween 20) for 5 minutes following transfer, then blocked in blocking buffer (Tris buffer saline + Tween 20 + 1% BSA) for 2 h, and were probed with the primary antibody of interest overnight at 4°C. The next day, membranes were washed with washing buffer 3 times, 10 min each, incubated with respective HRP-conjugated secondary antibody for 1 h, and washed with washing buffer 3 times,10 min each. Protein bands were detected using super signal luminol enhancer. Band intensities were quantified by densitometry using ImageJ software.

3.15 Immunofluorescence Microscopy

MLE-12 or primary ATII cells grown on chamber slides were grown to ~90% confluence and starved in 2% FBS overnight. Cells were then treated with *PA*103 for 3 h, fixed with 3.7% formaldehyde, permeabilized with 0.25% Triton X, and incubated with blocking buffer for 1 h (PBS + Tween 20 + 2% BSA). Cells were then incubated with appropriate primary and secondary antibodies (1:200 dilution) in PBS-T containing 2% BSA. Glass cover slips were mounted on the chamber slides with mounting fluid

containing DAPI. Cells were examined using an Olympus fluoview 1000 and Nikon Eclipse TE2000-S immunofluorescence microscope and Hamamatsu digital camera with 60X oil immersion object and MetaVue software. Analysis was done using FIJI software.

3.16 Immunoprecipitation

After appropriate treatments, cells were pelleted in ice-cold PBS, lysed in standard lysis buffer (Cell Signaling), and sonicated. Lysates were then centrifuged at 1,000 x g for 10 min at 4°C. Supernatants were collected and protein assayed using BCA protein assay kit. For immunoprecipitation (IP), equivalent amounts of protein (1 mg) from each sample were pre-cleared with control IgG conjugated to A/G agarose beads at 4°C for 1 h, centrifuged at 1,000 x g for 10 min at 4°C in a microfuge centrifuge. Supernatants were collected and incubated overnight with primary antibody conjugated to A/G agarose beads at 4°C, with rotation. After 18-24 h, the samples were centrifuged at 1,000 x g for 5 min at 4°C in a refrigerated microfuge centrifuge and the pellet containing the agarose beads were washed three times with lysis buffer. After brief centrifugation at 1,000 x g for 5 min, the beads were collected by removing supernatant buffer, and 40-100 μl of SDS sample buffer [100 mM Tris-HCl (pH 6.8), 4% SDS, 0.1% bromophenol blue, 20% glycerol, 200 mM DTT] was added to the beads and boiled. Lysates were then subjected to 10% SDS-PAGE followed by Western blotting. Proteins were detected by immunoblotting using appropriate primary antibodies, and HRP-conjugated anti-rabbit or anti-mouse secondary antibodies.

3.17 Isolation of Alveolar Type II Epithelial Cells from Mouse Lung

Alveolar type II (ATII) epithelial cells from 8-week-old WT mice were isolated as described. Briefly, mice were anesthetized with intraperitoneal injection of ketamine, and euthanized. The trachea was exposed by dissection and a cannula was inserted and lungs were perfused with 1.5 ml of dispase II

and tied immediately with a suture thread. Lungs were collected, incubated in 1 ml of dispase II for 45 min at 37°C, transferred to 100-mm petri-dishes containing 10 ml of DMEM medium plus 25 mM HEPES, 1% Pen/Strep, and 20 U/ml of DNase I and gently teased with forceps, until only connective tissue were visible. The cell suspension was then passed through a 70 micron mesh; cells were resuspended in DMEM media containing 25 mM HEPES, 10% FBS, and 1% Pen/Strep and incubated at 37°C for 2 h on IgG coated plates. Following incubation, non-adherent cells were centrifuged at 1500 rpm for 5 min and the supernatant discarded. 1 ml ACK lysis buffer was added to the pellet and incubated for 1 min, and DMEM media was added to neutralize the buffer. Cells were collected and centrifuged for 5 min at 1500 rpm, supernatant was discarded, and 1 ml of ACK lysis buffer was added again until no RBC's were present. When RBC's were no longer present, 4 μl of anti-EpCAM biotin conjugated antibody was added and incubated at 37°C for 20 min in the dark. Following incubation, cells were washed in 1 ml of FACS buffer, then resuspended in 500 μl of FACS buffer (1X PBS + 2% FBS) with 20 μl streptavidin coated conjugated magnetic beads and incubated for 30 min. Cells were then washed in 1 ml of MACS buffer, twice, then resuspended in 200 μl MACS buffer and in an IMAC apparatus, allowing cells to bind for 8 min. Bound fractions were resuspended in 1 mL of fresh MACS buffer and unbound fractions were removed. Cells were then resuspended in DMEM media containing 25 mM HEPES, 10% FBS, 1% Pen/Strep, and 10 μM/ml ROCK inhibitor and incubated in collagen (rat-tail), and incubated at 37°C. The medium was changed every 2 days, and the primary ATII cells were used within 7 days of isolation. The purity of the ATII epithelial cells was verified using flow cytometry for co-staining with Ep-CAM and cytokeratin and co-staining with Ep-CAM and SP-A.

3.18 Isolation of Epithelial Cell Nuclear Fraction

Nuclei from MLE-12 cell or HBEpCs (~90% confluence) were prepared by sucrose density gradient differential centrifugation. Briefly, nuclei were prepared from MLE-12 or HBEPC cells, grown in 100-mm dishes. After *PA* infection for 2 h, cells were washed three times with PBS, trypsinized, and then centrifuged at 300 x g for 10 min. The cell pellets were washed again with PBS and resuspended in 5 ml buffer A (10 mM HEPES-KOH [pH 7.9], 1.5 mM $MgCl_2$, 10 mM KCl, 0.5 mM DTT), and homogenized ten times using a Dounce homogenizer with a tight pestle. Cell homogenates were centrifuged at 200 x g for 5 min at 4°C and supernatant was collected and stored as cytoplasmic fraction. The pellet was resuspended in 3 ml of 0.25 M sucrose, 10 mM MgCl2, and layered over 3 ml 0.35 M sucrose, 0.5 mM $MgCl_2$, and centrifuged at 1,400 x g for 5 min at 4 °C. The nuclear pellet was collected, resuspended in RIPA buffer, sonicated for 10 sec at setting 5, and centrifuged for 10,000 x g for 10 min at 4 °C and the supernatant collected as nuclear fraction.

3.19 Lipid Extraction

Lipids from cells or subcellular fractions were extracted by a modified Bligh and Dyer procedure (BLIGH and DYER 1959) with the use of 2% formic acid for phase separation mostly as described. D7-S1P (30 pmol), D7-16:0-ceramide (*N*-16:0-D7-sphingosine, 60 pmol) and D7-sphingosine (30 pmol) were employed as internal standards, and were added during the initial step of lipid extraction. The extracted lipids were dissolved in methanol/chloroform (4:1, v/v), and aliquots were taken to determine total phospholipid content as described (Berdyshev et al. 2006). Samples were concentrated under a stream of nitrogen, re-dissolved in methanol, transferred to auto sampler vials, and subjected to sphingolipid LC-MS/MS analysis. All standards were from Avanti Polar Lipids (Alabaster, AL).

3.20 Measurement of H_2O_2

BAL fluid from mice were collected and centrifuged at 10,000 × g, for 20 min at 4°C, and H_2O_2 measurements were performed immediately using Amplex Red Hydrogen Peroxide/Peroxidase kit (Invitrogen), according to the manufacturer's instruction.

3.21 Measurement of IL-6 and TNF-α

Media from MLE-12 cells, HBEpCs or BAL fluids were centrifuged at 300 x g for 10 min, and IL-6 and TNF-α levels in the supernatants were measured using a commercially available ELISA kit, according to the manufacturer's instruction (R&D).

3.22 *Pseudomonas aeruginosa* Infection on Mouse Lungs

All animal experiments were approved by the Institutional Animal Care and Use committee at University of Illinois at Chicago. Adult male and female C57BL/6J wild type, SphK1 (*SphK1*$^{-/-}$), and SphK2 (*SphK2*$^{-/-}$) knockout mice (20-25 g) in the same background was used for *in vivo* lung infection studies. Mice were administrated with sterile PBS or *PA*103 strain in PBS intratracheally at dose of $1x10^6$ CFU/mouse under anesthesia. After 24 h of infection, BAL fluids were collected using 1 ml of sterile Hanks Balanced Salt solution to determine total and differential cell counts, protein concentration, H_2O_2 and cytokines levels as described. Left lung was removed and fixed for hematoxylin-eosin staining or immunohistochemistry, while right lung was snapped in liquid nitrogen and stored at – 80^0C for further analysis for Western blot. For survival studies, mice were administered 1×10^7 CFU/animal of *PA*103 and monitored at least 4 times daily for 4 days.

3.23 PKC Activity

MLE-12 cells grown to ~90% confluency was treated with heat killed *PA*103 for different time points and lysed with RIPA buffer. Cell lysates were then sonicated and centrifuged at 10,000 x g for 10

minutes and PKC activity was measured with a kit according to the manufacturer's instruction Kit (Enzo Biosciences).

3.24 Preparation of *Pseudomonas aeruginosa* culture.

The parent strain *PA* 103 was used for all the experiments. Preparation of the cultures and determination of colony-forming units (CFU) were carried out as described (Fu et al. 2013). The bacterial concentration was confirmed by plating out the diluted samples on sheep blood agar plates. For *in vitro* experiments, the bacterial preparations that were heat-inactivated at 60°C for 20 min were used.

3.25 RNA-Seq. Analysis

In the analysis of 3′ mRNA-seq data, the short reads of 12 samples of 4 groups (Ko.*PA*, KO.CTRL, WT.PA, WT.CTRL) were mapped to the UCSC mouse mm10 reference genome using BWA mem with soft-clipping. The raw counts of transcripts mapped to each gene were quantified using feature Counts base on the mapping results, given the transcriptome annotation of UCSC mm10. The genes with zero counts across all samples were filtered from further analysis. In each sample, the raw counts were normalized to count per million (CPM) for each gene by using R Bioconductor Package edgeR (PMID for edgeR: 19910308). The Differentially Expressed Genes (DEGs) were identified using edgeR as well. First, the General Linear Model (GLM) Likelihood Ratio Test (LRT) was performed as omnibus test for DEGs where the mean expression value of a gene in any group is significantly different than in other sample groups. The raw *p*-values were adjusted by Benjamini–Hochberg correction. Second, the pairwise comparisons were performed between KO.*PA* vs. KO.CTRL, WT.*PA* vs.

WT.CTRL, and WT.*PA* vs. KO.*PA*. The exact test was performed on each gene between each pair of sample groups to identify to the significant pairwise DEGs. The *p*-values from the exact test were also corrected by Benjamini–Hochberg correction.

3.26 Transfection of MLE-12 or HBEpCs with Small Interfering RNA

Depletion of endogenous SphK1 and SphK2 proteins in cells was carried out using gene-specific siRNA. Pre-designed siRNA of mouse and human SphK1, SphK2, or nonspecific/non-targeting siRNA, were used to transfect MLE-12 or HBEpCs. Each siRNA contained at least 3 different sequences targeting the mRNA of each gene. Prior to transfection, cells were starved in basal medium containing 2% FBS for 24 h. Next day, 50 nM scrambled or gene specific siRNA complexes were prepared in Gene Silencer transfection reagent according to the manufacturer's recommendation and cells were transfected in serum-free media for 4 h and the media was replaced with fresh complete medium supplemented with 10% FBS and growth factors. After 72 h post-transfection, cells were stimulated with vehicle or *PA* for 3 h, and knockdown of target protein was confirmed by Western blotting.

3.27 Data Analysis

All *In vitro* cell culture experiments were performed at least in triplicate. Means and standard errors were calculated based on the value of individual treatments and number of experiments. For *In-vivo* animal studies, 5-8 mice per group were used and means plus standard error were calculated based on the number of animals used in each group. Statistical analysis of the difference between the two means when comparing two groups was assessed by 2-tailed t-test when comparing 2 groups (assuming normal distribution of data), ANOVA (with Tukey post-hoc test) when comparing multiple groups, and Mantel-Cox (log rank) test for survival plots using Graphpad Prism 7 software.

4. RESULTS-I

4.1. Hypothesis: Sphingosine-1-phosphate generation in response to PA-induced Lung inflammation modulates host defense response.

4.1.1 *Pseudomonas aeruginosa* infections alter sphingolipid levels in mouse lungs and bronchoalveolar lavage fluids.

We investigated first whether *PA*-infection can induce change in the sphingolipid levels in the mouse lung. We treated C57BL WT mice with *PA* for 48 h, isolated the lungs and BALF and quantified sphingolipid levels by mass spectrometry. In the lung tissues, S1P increased significantly after 24 h **(Fig. 5A)**, and sphingosine levels almost doubled at 48 h **(Fig. 5B)**. We also observed increased ceramide levels as early as 6 h post-*PA* infection **(Fig. 5C)**. We also measured the sphingolipid levels in the BALF after *PA* stimulation and observed an increase in S1P and ceramide levels starting as early as 6 h **(Fig. 5D and Fig. 5F);** however, sphingosine levels were significantly lower in BALF at all the time points **(Fig. 5E)**. These results suggest that *PA* infection has an effect on the sphingolipid metabolism in the lungs and elevated S1P and/or ceramide in the lung tissue and BAL may play a role in the development of *PA* mediated lung inflammation and injury.

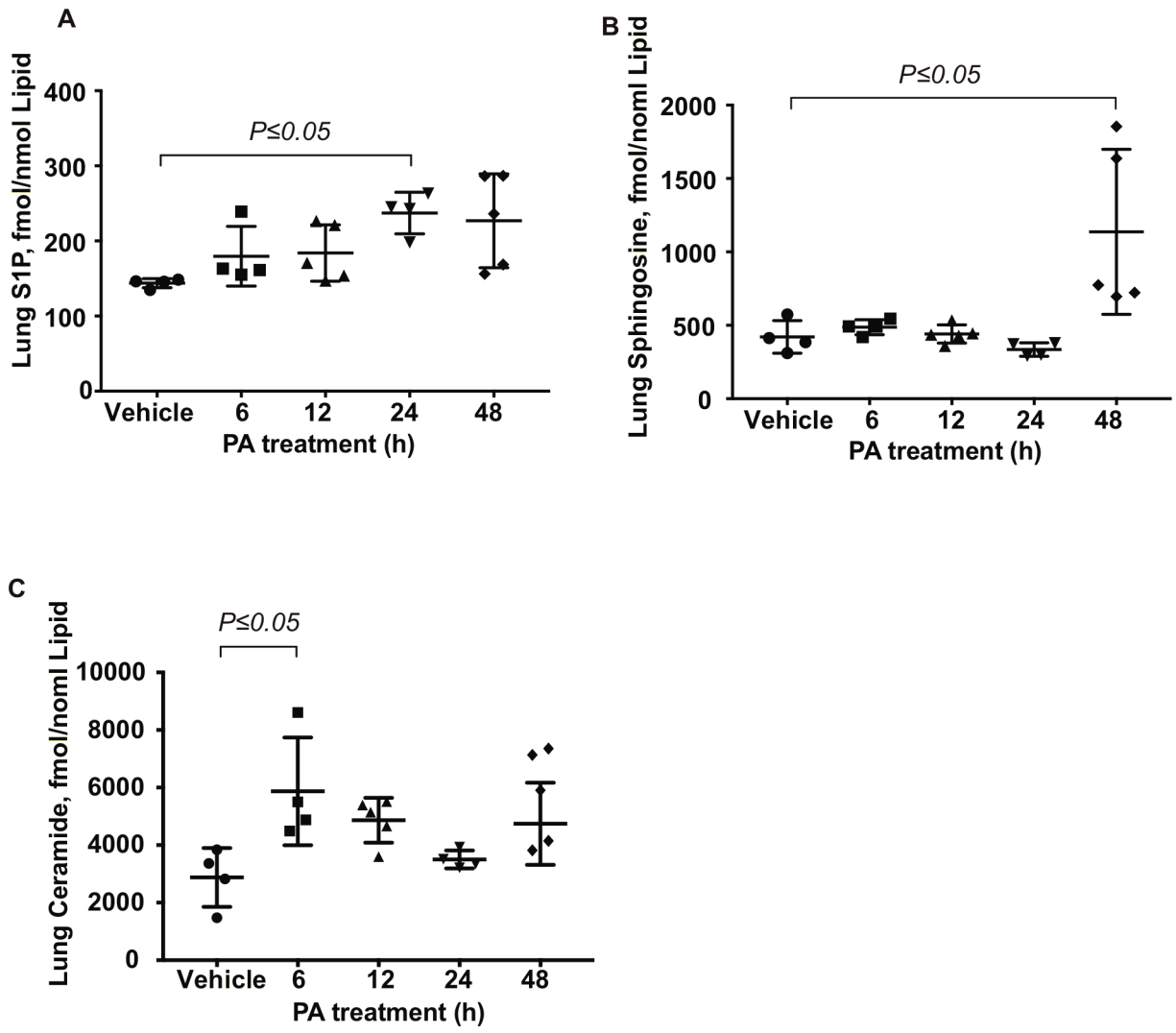

Figure 5: *Pseudomonas aeruginosa* (*PA*) infection alters sphingolipid levels in mouse lungs. Wild-type mice were challenged intratracheally either sterile PBS or *Pseudomonas aeruginosa (PA)* 103 (1 x 10^6 CFU/animal) in a total volume of 50 µl for 24 h. Animals were sacrificed, Lungs were removed and frozen in liquid N_2 immediately. Lipids were extracted from BAL fluid and lung tissues as described in METHODS. Quantification of S1P, sphingosine and ceramide levels in lung tissues from control and *PA*103 infected mice (1 x 10^6 CFU/mouse) 24 h post-infection by LC-MS/MS as described in METHODS. Sphingosine-1-phosphate (S1P), sphingosine and ceramide levels in lung tissues (**A-C**) were quantified by Mass Spectrometry. Data are from one experiment with five animals (n=5) used for each treatment, and data are expressed as means ± SEMs.

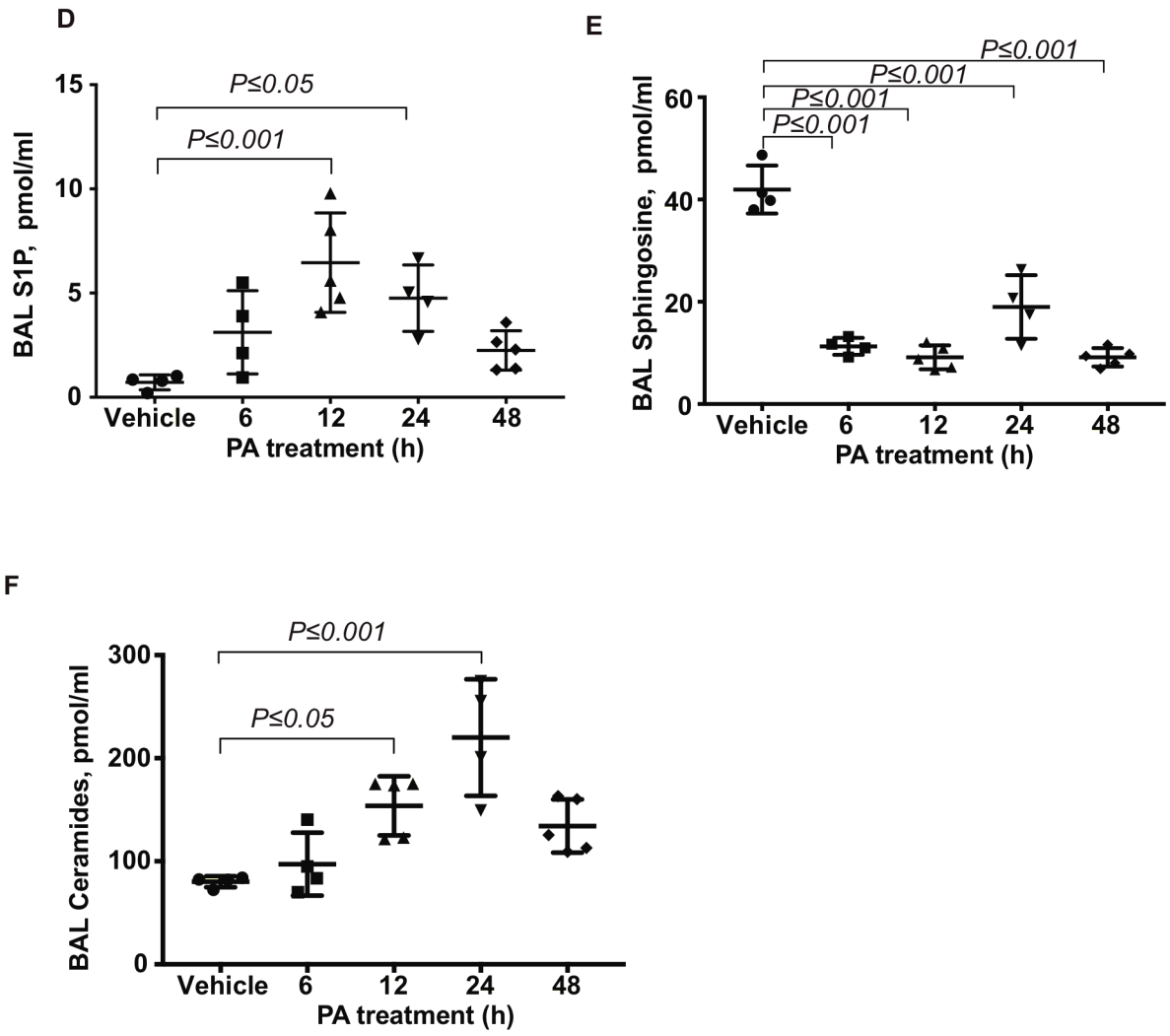

Figure 5: Pseudomonas aeruginosa (*PA*) infection alters sphingolipid levels in mouse bronchoalveolar lavage fluids. Wild-type mice were challenged intratracheally either sterile PBS or *Pseudomonas aeruginosa (PA*) 103 (1 x 10^6 CFU/animal) in a total volume of 50 µl for 24 h. Animals were sacrificed, bronchoalveolar (BAL) fluid was collected, centrifuged and analyzed. Lipids were extracted from BAL fluid as described in METHODS. Quantification of S1P, sphingosine and ceramide levels in BAL fluids from control and *PA*103 infected mice (1 x 10^6 CFU/mouse) 24 h post-infection by LC-MS/MS as described in METHODS. Sphingosine-1-phosphate (S1P), sphingosine and ceramide levels in BAL fluid (**D-F**) were quantified by Mass Spectrometry. Data are from one experiment with five animals (n=5) used for each treatment, and data are expressed as means $\pm$ SEMs.

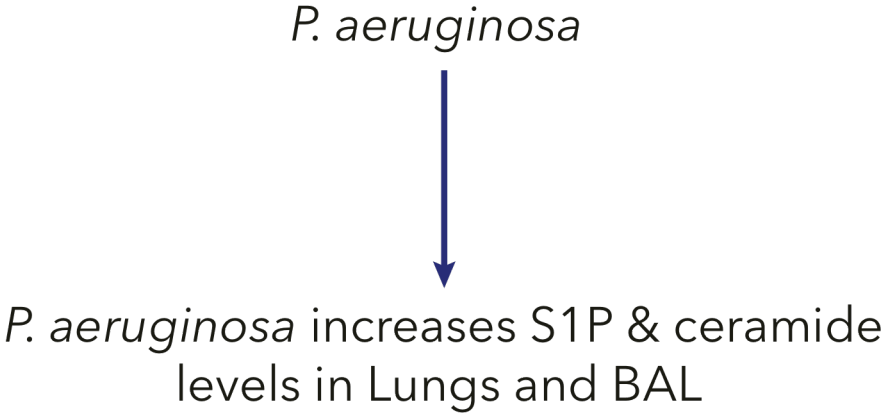

Fig. 6 Schematic diagram depicting *PA*-induced sphingoid base levels in lungs and BAL fluids

4.1.2 SphK2, but not SphK1, deficient mice are protected from *PA*-mediated lung inflammation

To determine which of the isoforms of sphingosine kinase is leading to the elevated levels of S1P in *PA*-mediated lung inflammation, we infected WT, *Sphk1*$^{-/-}$, and *Sphk2*$^{-/-}$ mice with *PA*. Compared to WT, *Sphk2*$^{-/-}$ mice showed decreased infiltration of inflammatory cells, especially the neutrophils into the alveolar space **(Fig. 7A)**. Elevated neutrophils counts were also validated by differential cell counts using Cytospin where SphK2 knock down mice showed decreased neutrophils counts after *PA* infection compared to WT and SphK1 knock down siblings **(Fig. 7B&C)**. Genetic deletion of SphK2 in mice also resulted in reduced pulmonary leak as evident from decreased cell counts **(Fig. 7D)** and protein concentration **(Fig. 7E)** in the BAL compared to their WT siblings. In contrast, SphK1 deletion had no notable effect on *PA*-induced lung inflammation. Loss of SphK2 in mice also resulted in decreased inflammation as observed in diminished levels of pro-inflammatory cytokines. While significant reduction of IL-6 **(Fig. 7F)** and TNF-α **(Fig. 7G)** levels was noted in SphK2 knock down mice compared to WT mice, no such change in the levels of IL-1β **(Fig. 7H)** and MIP-2 **(Fig. 7I)** were observed in *Sphk2*$^{-/-}$ compared to WT. Knock down of SphK2, but not SphK1, blocked *PA*-induced ROS production in the mouse lung, compared to WT **(Fig. 7J)**. Interestingly, knock down of SphK2 also increased the survival of mice infected with *PA* compared to SphK2 knock down and WT littermates **(Fig. 7K)**. To further validate the effect of SphK2 knock down in *PA* infection, we enumerated the bacterial colony count, which was similar in WT, *Sphk1*$^{-/-}$, and *Sphk2*$^{-/-}$ mice, at 6hrs and 24 h post-*PA* infection **(Fig. 7L)** suggesting bonafide SphK2 knock down effect rather than difference in the survival of bacteria in the lung. Taken together these data suggest that S1P generated in response to *PA*-induced lung inflammation is SphK2 and not SphK1 dependent.

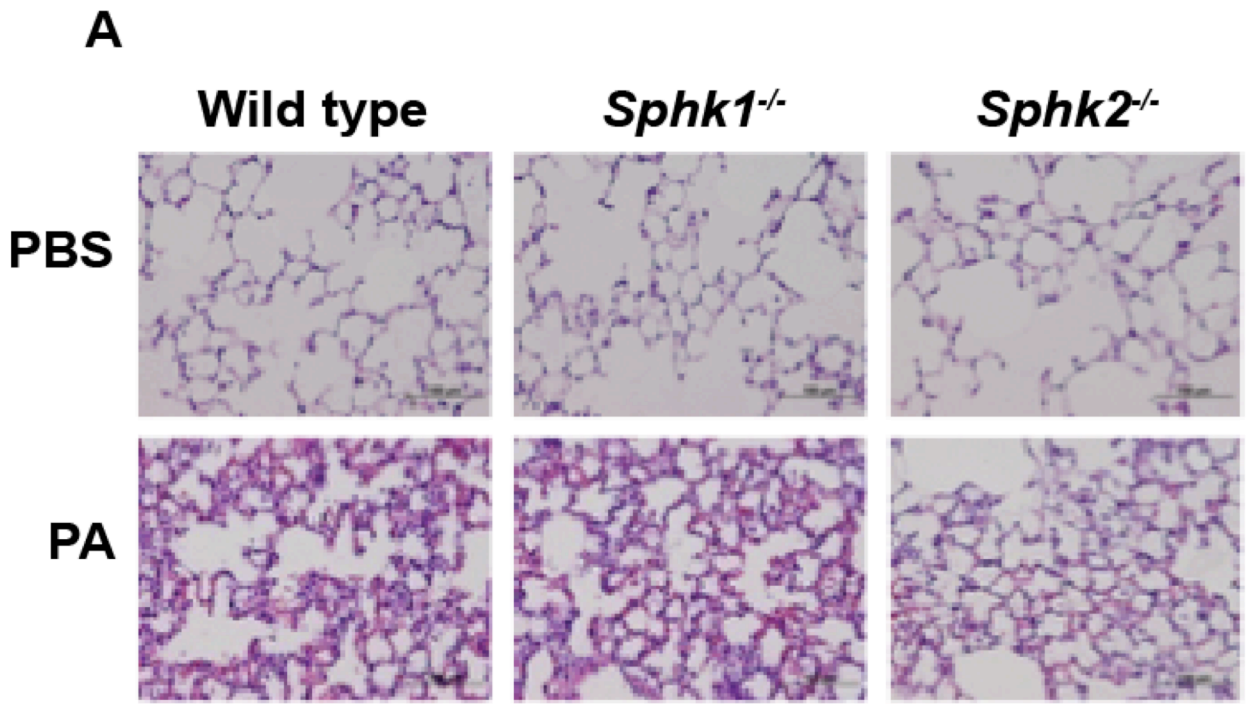

Figure 7: Deletion of SphK2 prevents *PA*-induced alveolar infiltration of neutrophils. C57BL/6J, *Sphk1*$^{-/-}$ and *Sphk2*$^{-/-}$ mice were challenged intratracheally with sterile PBS or *PA*103 as outlined in Figure 5. (**A**) Representative Hematoxylin-Eosin staining of lung sections from mice, scale bars, 100 μm showing infiltration of neutrophils in alveolar space. *Sphk2*$^{-/-}$ mice have less neutrophil migration compared to *PA* treated WT C57BL/6J mice. Data are expressed as means $\pm$ SEMs from one experiment (number of animals per group =5)

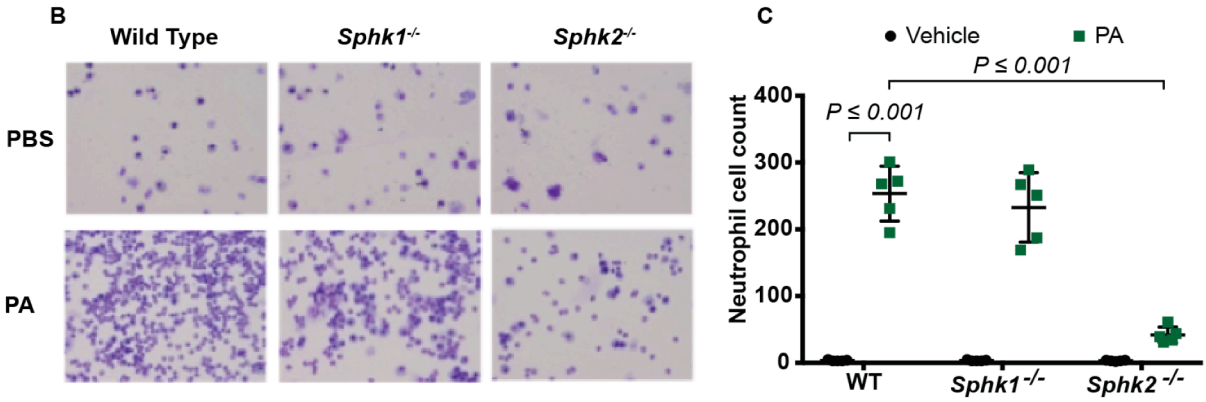

Fig 7. *PA*-induced neutrophil influx in alveolar space is attenuated by SphK2 deficiency. Wild-type mice were challenged intratracheally either sterile PBS or *Pseudomonas aeruginosa* (*PA*) 103 (1 x 10^6 CFU/animal) in a total volume of 50 µl for 24 h. Animals were sacrificed, bronchoalveolar (BAL) fluid was collected, and an aliquot was subjected to Cytospin and differential cell count. Shown is representative image of BAL fluid from five mice. Neutrophils were the predominant infiltrating immune cells into the alveolar space after *PA* challenge, which was attenuated in *Sphk2*$^{-/-}$ mice compared to WT and *Sphk1*$^{-/-}$ mice.

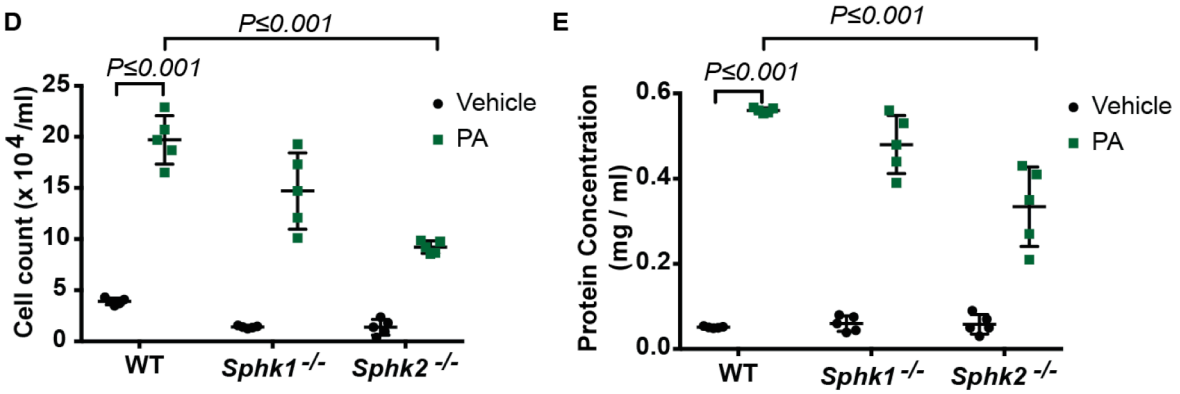

Fig 7. Deletion of SphK2 prevents *PA*-induced pulmonary leak. C57BL/6J, *Sphk1*$^{-/-}$ and *Sphk2*$^{-/-}$ mice were challenged intratracheally with sterile PBS or *PA*103. BAL fluids from control and *PA* challenged WT, SphK1, and SphK2 KO mice were analyzed for otal infiltrated cell number (**D**), and total protein levels **(E)**. *Sphk2*$^{-/-}$ mice had significantly reduced BAL cell count and protein concentration when compared to WT and *Sphk1*$^{-/-}$ mice. Data are expressed as means $\pm$ SEMs from one experiment (number of animals per group =5).

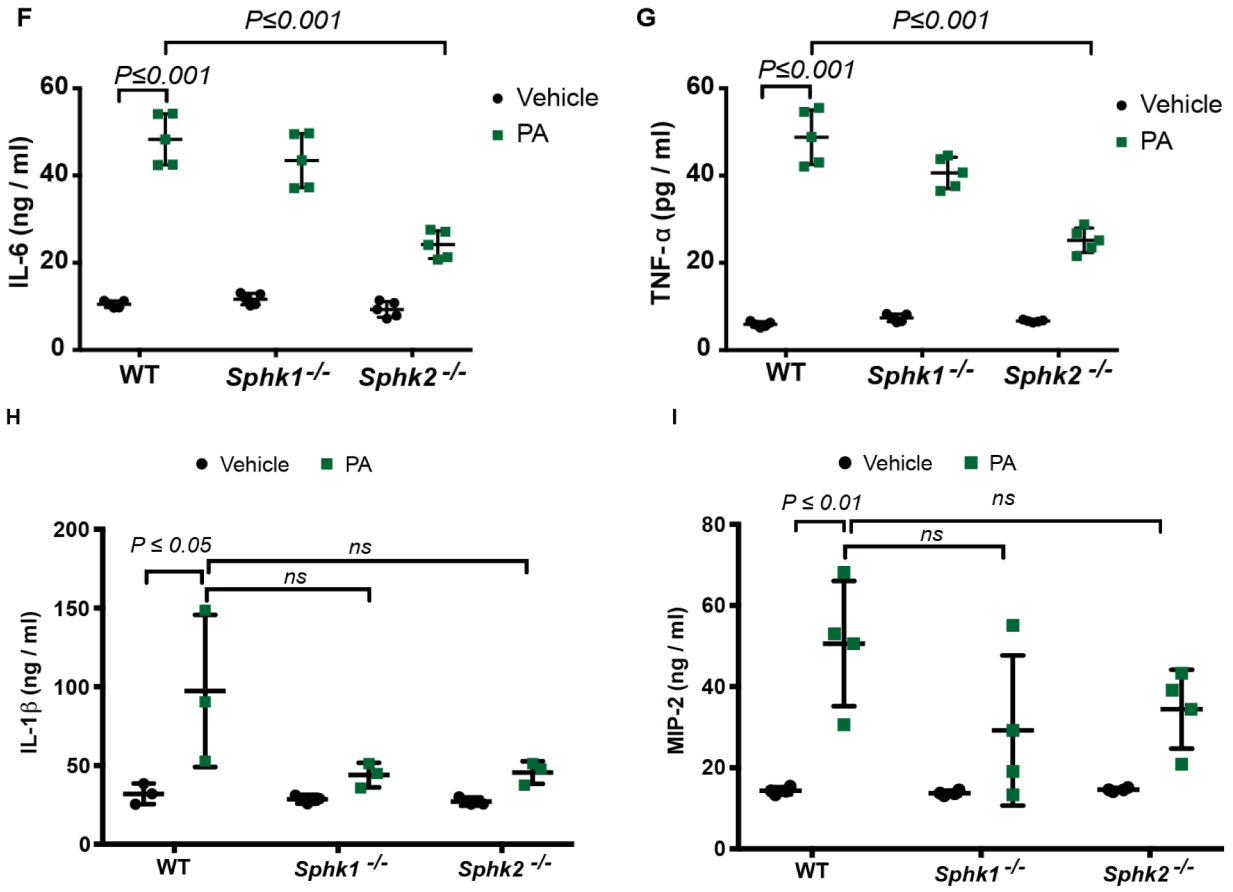

Fig 7. Deletion of SphK2 prevents *PA*-induced lung inflammatory cytokine secretion. C57BL/6J, *Sphk1*$^{-/-}$ and *Sphk2*$^{-/-}$ mice were challenged intratracheally with sterile PBS or *PA*103. BAL fluids from control and *PA* challenged WT, SphK1, and SphK2 KO mice were analyzed for concentration of IL-6 **(F)** and TNF-α **(G)**. **SphK2 deficiency had no effect on *PA*-induced IL-1β and MIP-2α secretion.** BAL fluids from (**A**) were analyzed for pro-inflammatory cytokine levels using commercial ELISA kits. Deletion of SphK2 had no effect on *PA*-induced secretion of IL-1β (**H**) and MIP-2(**I**) in BAL fluid. Values are means $\pm$ SD from one experiment (n=5 animals per group). Data are expressed as means $\pm$ SEMs from one experiment (number of animals per group =5).

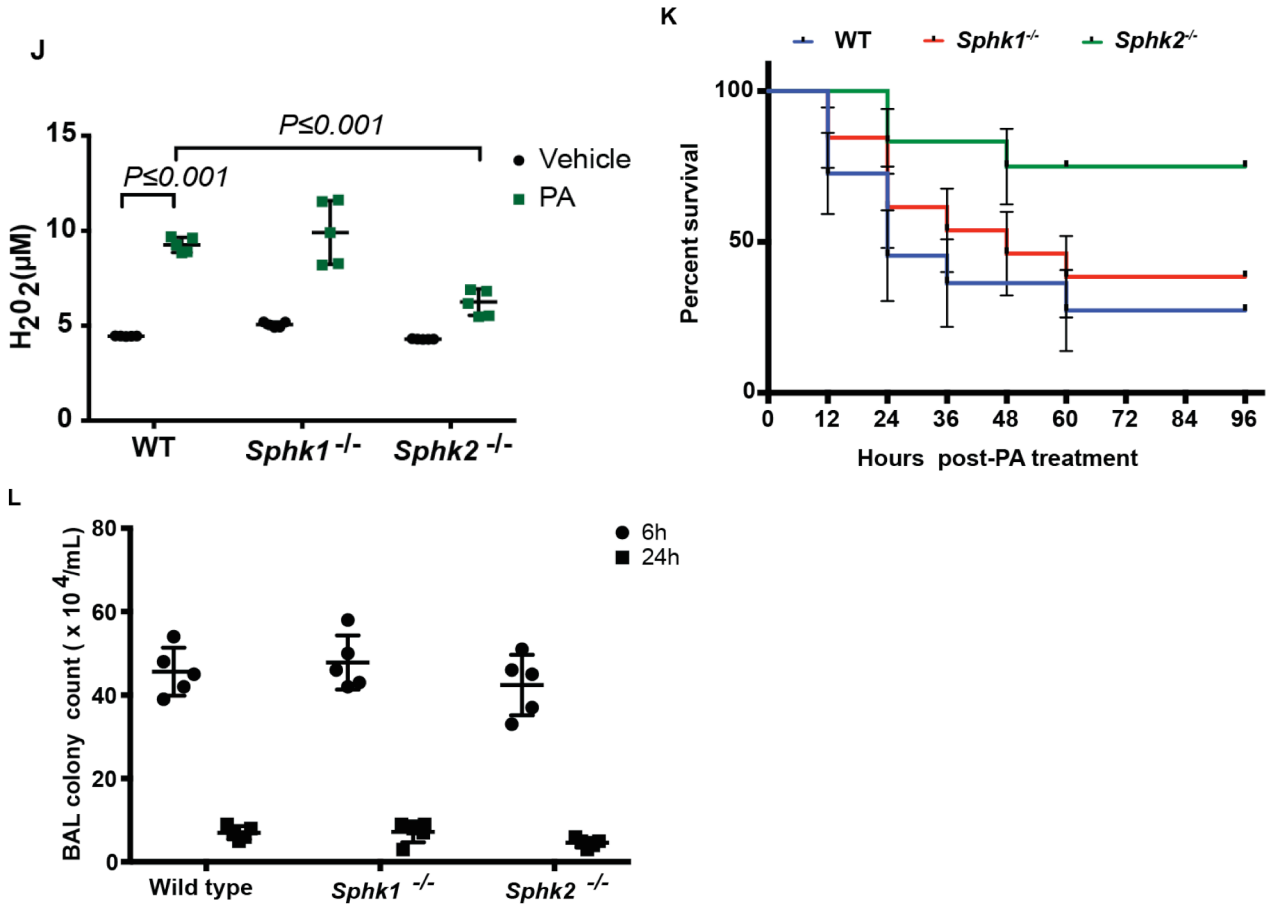

Fig 7. Deletion of *Sphk2* blocks ROS and increases survival of mice after *PA* challenge. C57BL/6J, *Sphk1*$^{-/-}$ and *Sphk2*$^{-/-}$ mice were challenged intratracheally with sterile PBS or *PA*103. BAL fluids from control and *PA* challenged WT, SphK1, and SphK2 KO mice were analyzed for H_2O_2 (**J**). *Sphk2*$^{-/-}$ mice had lower H_2O_2 levels compared to WT and *Sphk1*$^{-/-}$ mice. **Survival of WT, *Sphk1*$^{-/-}$ and *Sphk2* $^{-/-}$ mice exposed to high dose of *PA*.** Wild-type (WT), *Sphk1*$^{-/-}$ and *Sphk2*$^{-/-}$ mice were challenged intratracheally either sterile PBS or *PA* 103 (1 x 10^7 CFU/animal) in a total volume of 50 μl and animals were monitored for a period of 96 h (n=10 in each group). Mice deficient in SphK2 showed significantly lower mortality (~25%) compared to WT and SphK2 KO mice **(K)**. Significance was calculated using two-way ANOVA. **Colony formation in wild type, *Sphk1*$^{-/-}$ and *Sphk2*$^{-/-}$ mice after infection of mouse lung with *PA*.** Wild-type (WT), *Sphk1*$^{-/-}$ and *Sphk2*$^{-/-}$ mice were challenged intratracheally either sterile*PA* 103 (1 x 10^6 CFU/animal) in a total volume of 50 μl for a period of 6 and 24 h (n=5 in each group). BAL fluid was collected at 6 h and 24 h after *PA* treatment, diluted a thousand times with sterile PBS. Hundred micro litters of diluted BAL fluid was used to culture overnight at 37 ^oC on blood agar plate for bacterial colony counting. Colonies were enumerated when visible, and counted. No difference in the colony formation was noted in WT, *Sphk1*$^{-/-}$ and *Sphk2*$^{-/-}$ mice at 6 and 24 h after infection of the lung with *PA* **(L)**.

4.1.3 SphK2 genetic deletion affects *PA*-induced gene expression in mouse lung

To further understand the effect of SphK2 genetic deletion on *PA*-induced host gene expression and changes in mouse lung, we performed RNA Seq analysis. C57BL/6J and *Sphk2*$^{-/-}$ mice were challenged intratracheally with sterile PBS or *PA*103 and lung tissue was collected and RNA was isolated immediately. The RNA Seq experiment was conducted using Lexogen Quantseq 3'mRNA kit and mapped using bowtie local alignment and quantified using htSeq. Differentially expressed genes (FDR cut off 0.05) were used for unsupervised hierarchical clustering of samples. A heat map showing the expression pattern of 1108 differentially expressed genes (DEGs, adjust p-value<0.05 from pairwise comparison) in 12 samples of 4 groups, including: Knockout with *PA* infected (KO *PA*), Wildtype with *PA* infected (WT *PA*), Knockout without *PA* infection (KO Ctrl) and Wildtype without *PA* infection (KO Ctrl), and 3 samples for each group was generated. Analysis of the top 35 genes that were differentially regulated, we found that they fall into three related categories: Inflammation, Immune response, injury and cytokine activity in GO category (biological process & Molecular function). A number of cytokines including IL-6, TNFα, IL1β, IL-10, IL-12 were all differentially regulated in SphK2 knock out mice with *PA* treatment compared to control *PA* treated group.

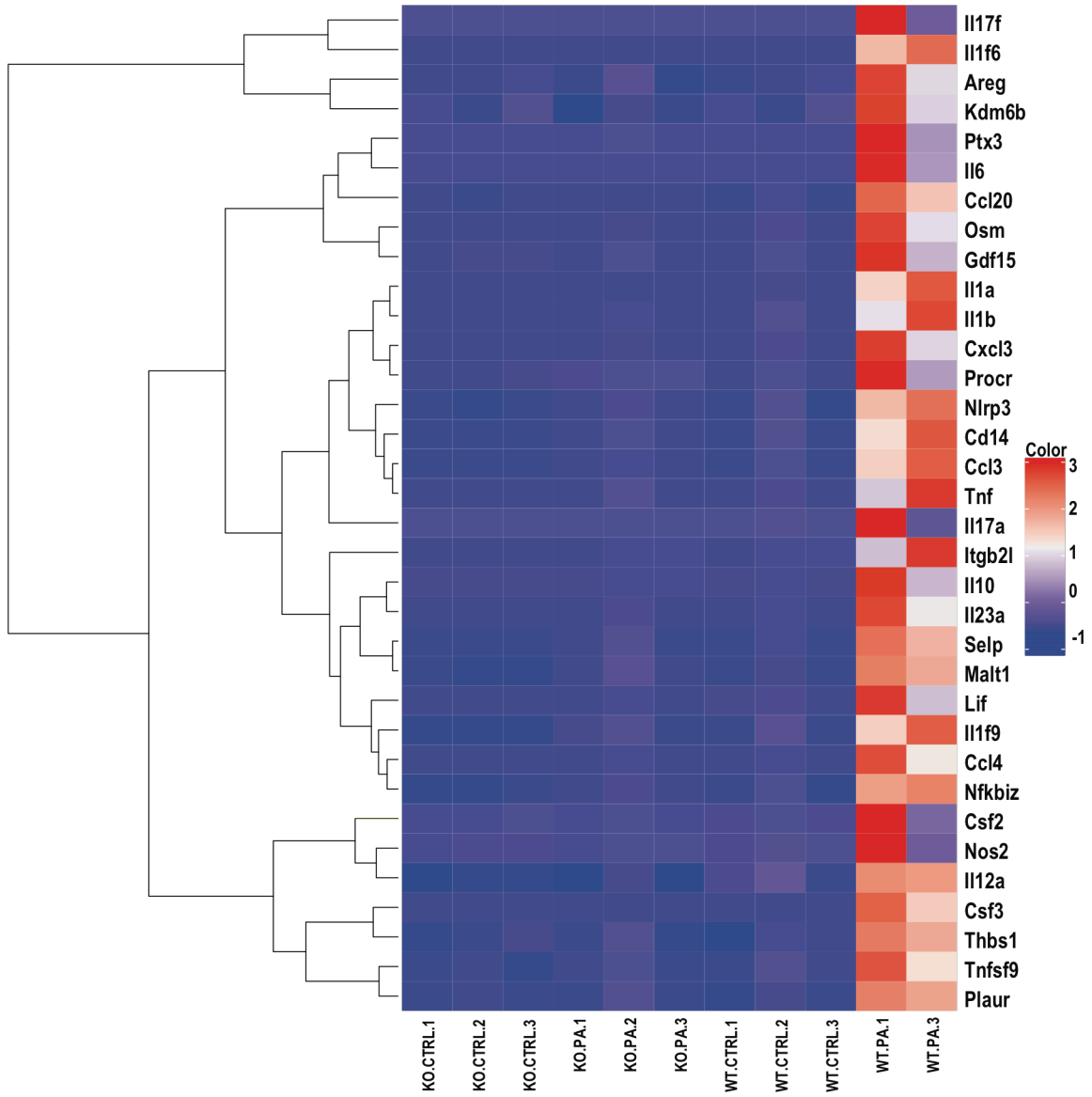

Fig. 8: Differential expression of 35 genes 24 h after *PA* challenge of Wild type and SphK2 KO mouse lung. A heat map shows the expression pattern of 35 differentially expressed genes determined after *PA* challenge of Wild type (WT), WT + *PA*, SphK2 KO, SphK2 KO + *PA* by unsupervised hierarchical clustering of samples from RNA-seq. Inflammatory cytokines including IL-6 form the bulk of the top 35 differentially expressed genes.

4.1.4 Inhibition of SphK2 ameliorates *PA*-induced lung inflammation in mice

To further investigate the role of SphK2 in *PA*-induced lung inflammation, we analyzed the effect of ABC294640, a specific inhibitor of SphK2 for its prophylactic and therapeutic potential. Wild type mice were intraperitoneally treated with ABC294640 (10 mg/kg body weight) 1 h before intratracheal *PA* challenge and observed for the prevention of development of lung inflammation. Compared to vehicle-challenged mice, treatment with ABC294640 reduced infiltration of inflammatory cells into the alveolar space **(Fig. 9A)**. Reduced pulmonary leak was also observed in ABC294640 treated mice as evident from low levels of proteins and cell counts **(Fig. 9B)** in the BALF **(Fig. 9C)**, and decreased cytokine IL-6 levels **(Fig. 9D)** in comparison to vehicle-treated mice.

To assess the therapeutic potential of ABC294640 in *PA*-induced lung inflammation, we injected mice intraperitoneally with ABC294640 6 h post intratracheal *PA* challenge and observed its effect in reducing the lung inflammation. We noted decreased migration of neutrophils into the alveolar space in ABC294640 mice after *PA* infection **(Fig. 10A)**. On examining the BALF, we detected lower levels of cell counts (**Fig. 10B**), protein concentration **(Fig. 10C)**, and H_2O_2 **(Fig. 10D)**, indicating reduced vascular leakage and decreased levels of pro-inflammatory cytokines IL-6 **(Fig. 10E)** and TNF-α (**Fig. 10F**). These data suggest the critical role of SphK2 and SphK2 generated S1P in the nucleus, in regulating *PA*-induced inflammation in the lung.

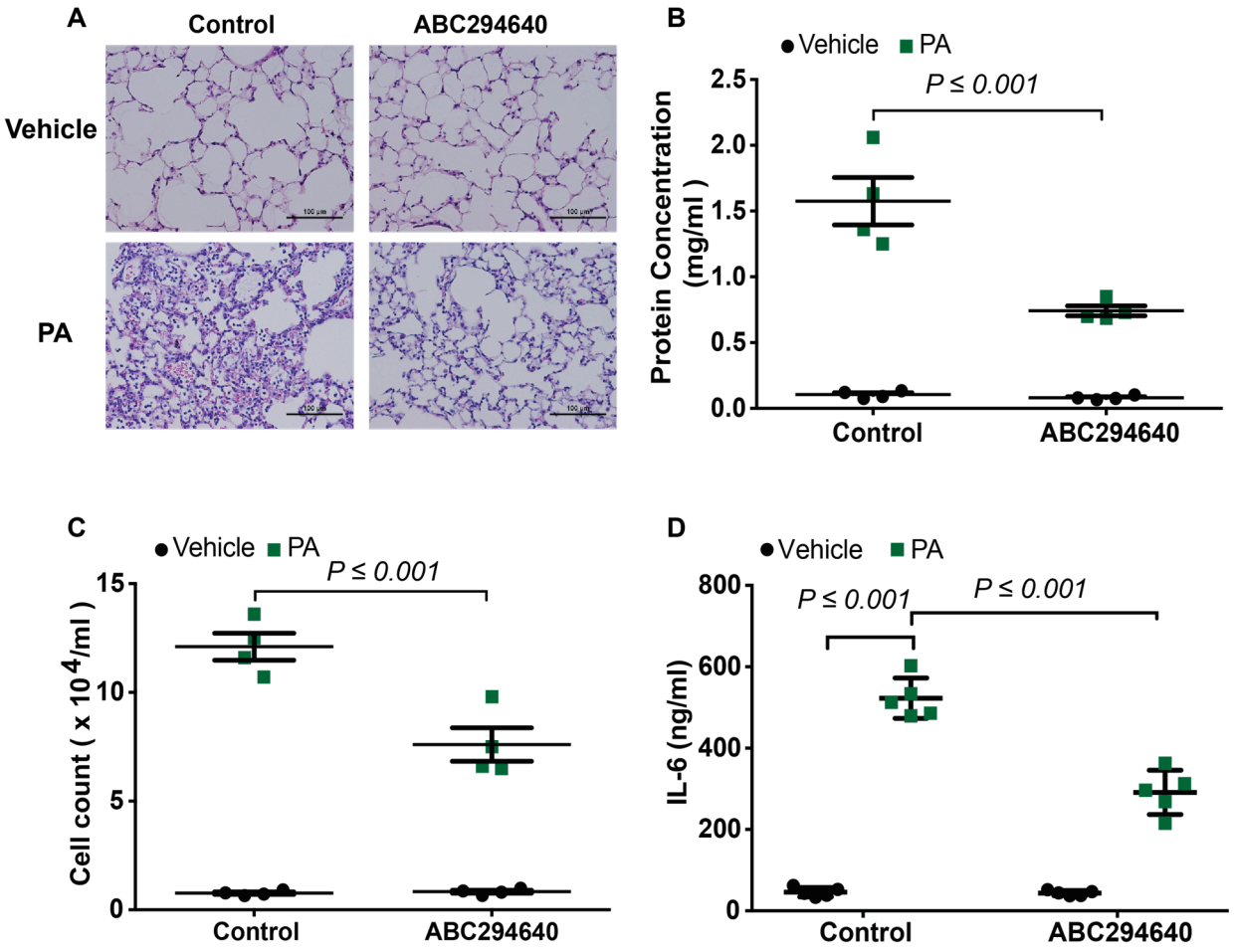

Fig. 9: Administration of SphK2 inhibitor ABC294640 at the time of *PA* infection ameliorates lung inflammation and injury. C57BL/6J mice were challenged intratracheally with sterile PBS (n=10 animals) or *PA*103 (1 x 10^6 CFU/animal) (n=10 animals). Immediately, five mice from each group received intraperitoneally (ip) the SphK2 inhibitor ABC294640 (10 mg/Kg body weight) dissolved in DMSO; control group also received equal volume of DMSO (1 µl in 100 µl). All animals were sacrificed at the end of 24 h post-infection of *PA*, BAL fluid was collected and lung tissues were removed and frozen in liquid N_2. **(A)** Representative Hematoxylin-Eosin staining of lung sections from control, *PA*, ABC294640 and ABC294640 + *PA* treated animals. Scale bars, 100 µm. **(B)** Total protein levels in BAL fluid, **(C)** Total infiltrated cells in BAL fluid, and **(D)** Concentration of IL-6 in BAL fluid

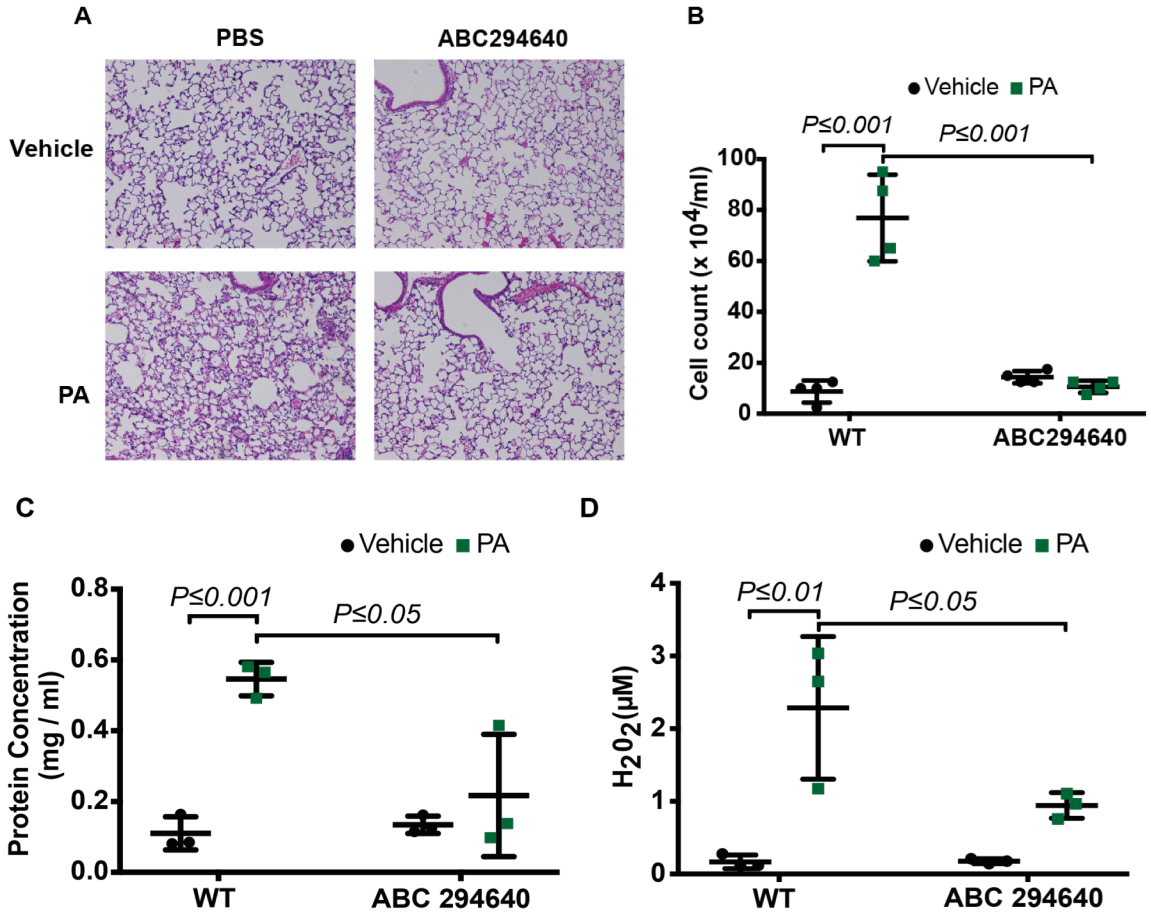

Fig. 10: Inhibition of SphK2 with ABC294640 post-infection ameliorates *PA*-induced inflammatory lung injury. C57BL/6J mice were challenged intratracheally with sterile PBS (n=10 animals) or *PA*103 (1 x 10^7 CFU/ animal) (n=10 animals) as outlined in Fig. 1. After 6 h of *PA* instillation, five mice from each group received intraperitoneally (i.p) the SphK2 inhibitor ABC294640 (10 mg/Kg body weight) dissolved in DMSO; control group also received equal volume of DMSO (1 µl in 100 µl). All animals were sacrificed at the end of 24 h post-infection of *PA*. Animals were sacrificed, BAL fluid was collected and lung tissues were removed and frozen in liquid N_2. **(A)** Representative Hematoxylin-Eosin staining of lung sections from control, *PA*, ABC294640 and ABC294640 + *PA* treated animals. Scale bars, 100 µm. **(B)** Total infiltrated cells in BAL fluid, **(C)** Total protein levels in BAL fluid, and **(D)** Concentration of H_2O_2 in BAL fluids. Data are means ± SD from one experiment.

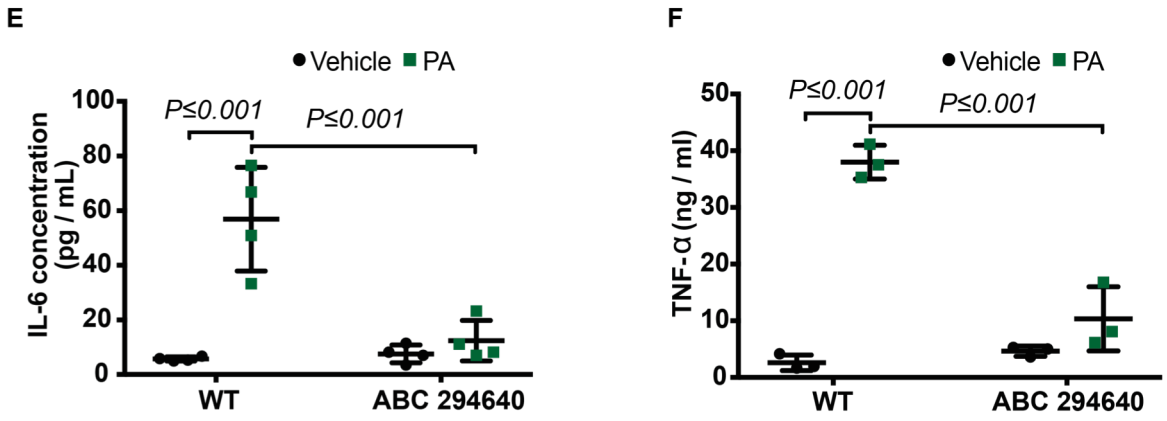

Fig. 10: Inhibition of SphK2 with ABC294640 blocks *PA*-induced cytokines secretion. C57BL/6J mice were challenged intratracheally with sterile PBS (n=10 animals) or *PA*103 (n=10 animals) as outlined in **Fig. 9**. After 6 h of *PA* instillation, five mice from each group received intraperitoneally (i.p) the SphK2 inhibitor, ABC294640 (10 mg/Kg body weight), dissolved in DMSO; control group also received equal volume of DMSO (1 μl in 100 μl). All animals were sacrificed at the end of 24 h post-infection of *PA*. Animals were sacrificed, BAL fluid was collected and lung tissues were removed and frozen in liquid N_2. (**E**) Concentration of IL-6 and, (**F**) TNF-α in BAL fluid. Data are means $\pm$ SD from one experiment.

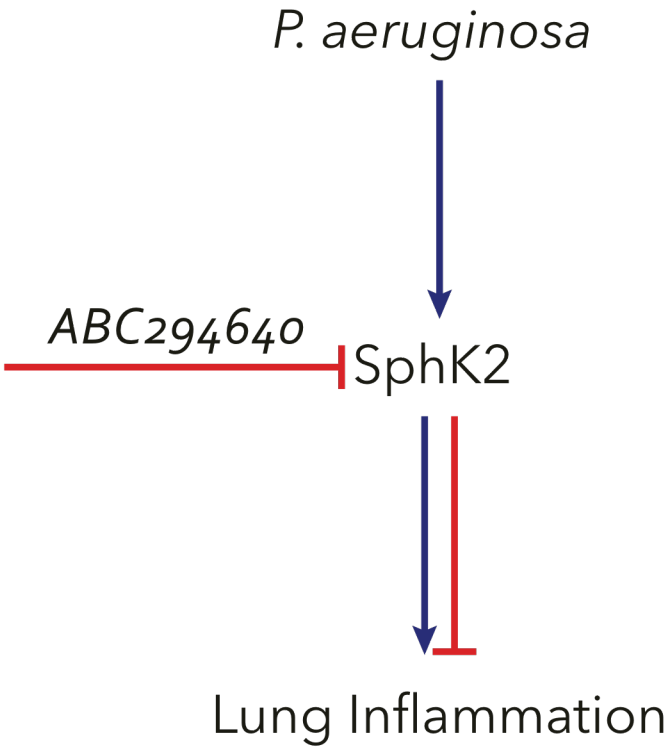

Fig. 11 Schematic diagram showing blocking SphK2 with SphK2 inhibitor ABC294640 attenuates *PA*-induced lung inflammation.

4.1.5 *PA* induces post translational modification of SphK2 and nuclear localization in mouse lung and *in vitro* in mouse lung epithelial cells

Since we observed that SphK2 deletion or inhibition resulted in amelioration of *PA*-induced lung inflammation, we suspected that SphK2 is post-translationally modified by phosphorylation and activated after *PA* infection. We stained the mouse lung sections with anti-SphK2 and p-SphK2 antibodies (Thr614) and we detected increased phospho-SphK2 staining after *PA*-infection **(Fig. 12A)**. Western blotting analysis of cell lysates from mouse lung tissues also showed increase phosphorylation of SphK2 after *PA* challenge **(Fig. 12B)**. Co-staining of lung tissues with nuclear marker DAPI and epithelial cell marker, surfactant protein C (SP-C) divulged p-SphK2 localization in the nucleus **(Fig. 12C)**. On quantification of nuclear p-SphK2 staining of lung specimens, we found that it is significantly enriched in alveolar Type II cells (AT-II) in comparison to bronchial epithelial cells **(Fig. 12D)**. We then investigated the nuclear localization and phosphorylation status of SphK2 in AT II and human HBEpCs. Alveolar Type II cells were isolated from WT C57BL mice and were treated with heat-killed *PA* for 2h. The cells were then fixed and stained with p-SphK2, SP-C and DAPI. Immuno-fluorescence staining showed elevated phosphorylation of SphK2 in the nucleus of AT II cells after *PA* treatment **(Fig. 12E & F)**. Also, HBEpCs after *PA* challenge showed similar results with increased SphK2 phosphorylation and nuclear localization **(Fig. 12G & H)**. We also repeated the same experiments in mouse lung epithelial (MLE-12) line and observed *PA*-induce phosphorylation of SphK2 in a time dependent manner **(Fig. 12I & J)**. Isolation of the cytoplasmic and nuclear fractions from MLE-12 cells by sucrose density gradient separation after *PA* challenge, and subsequent Western blotting of cell lysates confirmed *PA*-induced SphK2 phosphorylation in the nucleus. **(Fig. 12K)**. To further investigate if *PA*-induced phosphorylation of SphK2 affects it enzymatic active, we isolated the nuclei from MLE-

12 post-*PA*-challenge and subjected it to SphK activity assay in the presence or absence of sphingosine, dihydrosphingosine and FTY720, all of which are substrates for SphK2 using with [γ-^{32}P] ATP. Lipids were then extracted following termination of the reaction and subjected to thin layer chromatography and autoradiography. As anticipated, quantification of the phosphorylated products by scintillation counting showed increased [^{32}P] products formed in nuclei isolated after *PA* infection **(Fig 12L)**, suggesting activation of SphK2 in response to *PA* infection and subsequent generation of nuclear S1P, dihydro S1P or FTY-720P. To further confirm the generation of S1P in the nucleus after *PA* challenge, we isolated cytoplasm and nuclei fractions from MLE-12 cells subjected to vehicle or *PA* challenge, extracted the lipids and analyzed for sphingoid bases by LC-MS/MS. Significant elevation of nuclear S1P levels after *PA* treatment was observed **(Fig. 13C)** but the levels of sphingosine, ceramides and dihydro-sphingoid bases remained largely unaltered both in the cytoplasm and nuclear fractions of vehicle and *PA* treated MLE-12 cells **(Fig 13A, B, D, E & F)**. The above results show nuclear localization of SphK2, its activation by phosphorylation and subsequent generation of S1P in response to *PA* infection in the lung.

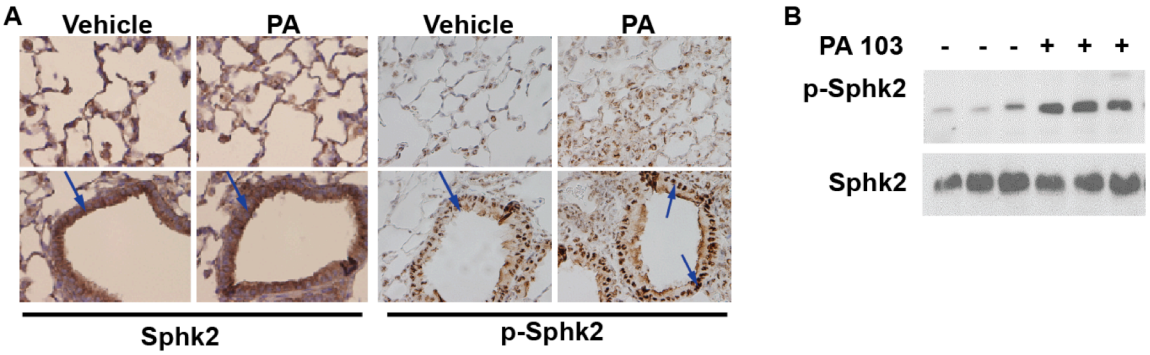

Fig. 12 A & B: *PA* stimulates SphK2 phosphorylation and nuclear localization in lung epithelium. (**A**) Paraffin embedded lung tissues from wild type and *PA*-infected mice were immunostained with SphK2 and p-SphK2 (threonine 614) antibodies, scale bars 100 μm. Arrows indicate staining for SphK2 or p-SphK2 in airway epithelium. (**B**) Total lung tissue lysates from vehicle and *PA*103 instilled animals were analyzed for SphK2 and p-SphK2 (serine578) by Western blotting. The figure shown is a representative blot from five independent experiments.

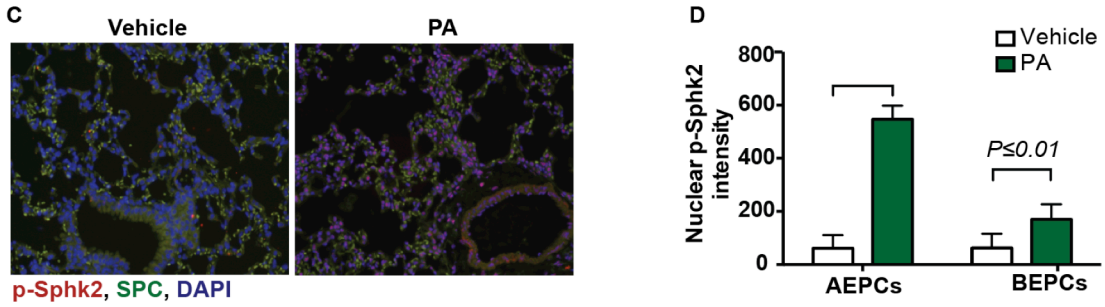

Fig. 12 C & D: ***PA*** **stimulates SphK2 phosphorylation and nuclear localization in lung alveolar epithelium**. Co-immunostaining of p-SphK2 and epithelial marker, SP-C in lung specimens from control and *PA*-challenged mouse lungs, scale bars 100 μm **(C)** and quantification of the co-immunostaining of p-SphK2 and SP-C in alveolar AT II and airway bronchial epithelial cells **(D)**.

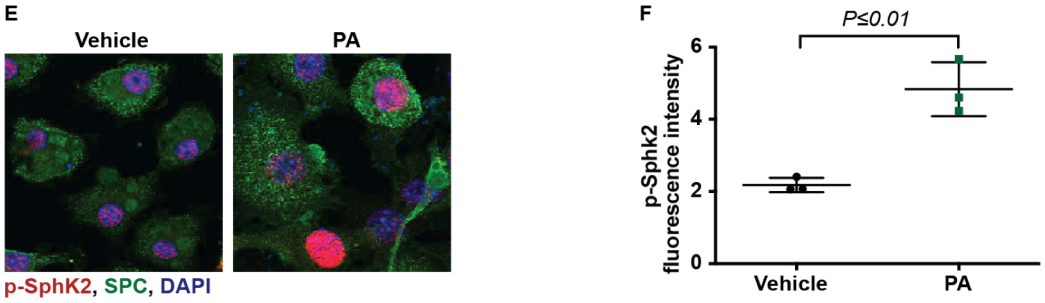

Fig. 12 E & F: *PA* stimulates SphK2 phosphorylation and nuclear localization in alveolar epithelial cells. Primary alveolar epithelial cells isolated from control and *PA* challenged mouse lung were co-immunostained for p-SphK2 and SP-C, scale bars 100 μm . **(E)** Shown is a representative co-immunostained image (five areas per slide; four slides per group) that was quantified by ImageJ software **(F)**.

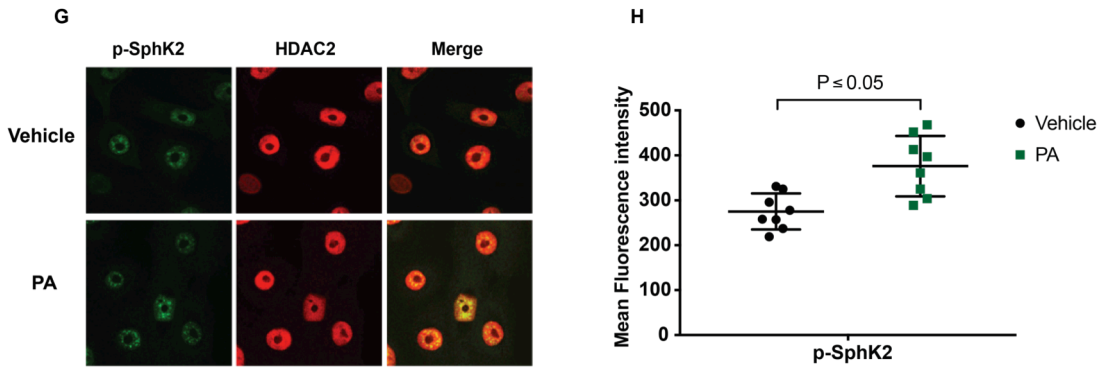

Fig. 12 G & H: *PA* infection stimulates nuclear SphK2 phosphorylation in primary human bronchial epithelial cells. Primary HBEpCs grown on glass slide chambers were challenged with vehicle of heat-inactivated *PA*103 (1 x 10^8 CFU/ml) for 3 h. The cells were fixed, immunostained for p-SphK2 (red) and DAPI (nuclear staining, blue) and merged **(G)**. Shown is a representative image form 4 independent experiments, scale bars 10 μm. Quantification of co-stained images of p-SphK2 and DAPI was performed (five areas per slide; four slides per group) using ImageJ software **(H)**.

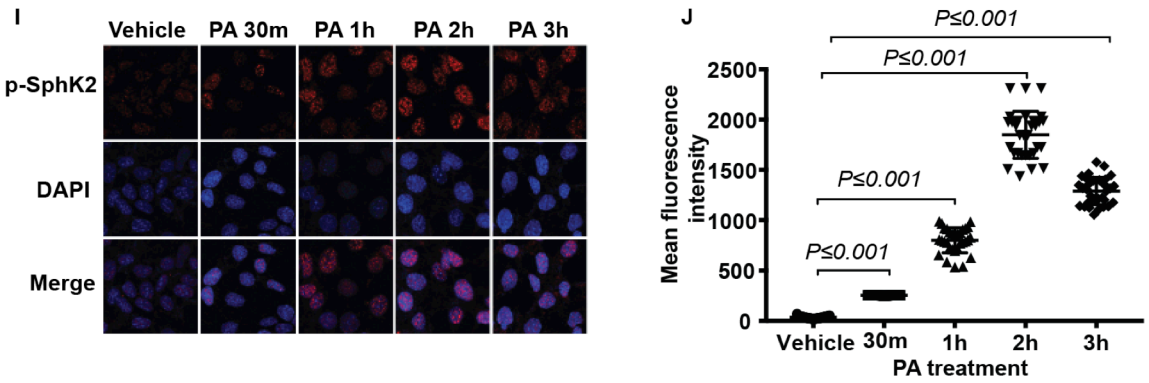

Fig. 12 I & J: *PA* stimulates SphK2 phosphorylation and nuclear localization in MLE-12 cells. MLE-12 epithelial cells grown on glass slide chambers were challenged with vehicle or heat-inactivated *PA*103 (1 x 10^8 CFU/ml) for varying time periods. The slide chambers were fixed, immunostained for p-SphK2 (threonine614) and nuclear staining with DAPI and merged**(I)**. Shown is a representative image form 4 independent experiments, scale bars 10 μm. Quantification of co-stained images of p-SphK2 and DAPI was performed (five areas per slide; four slides per group) using ImageJ software **(J)**.

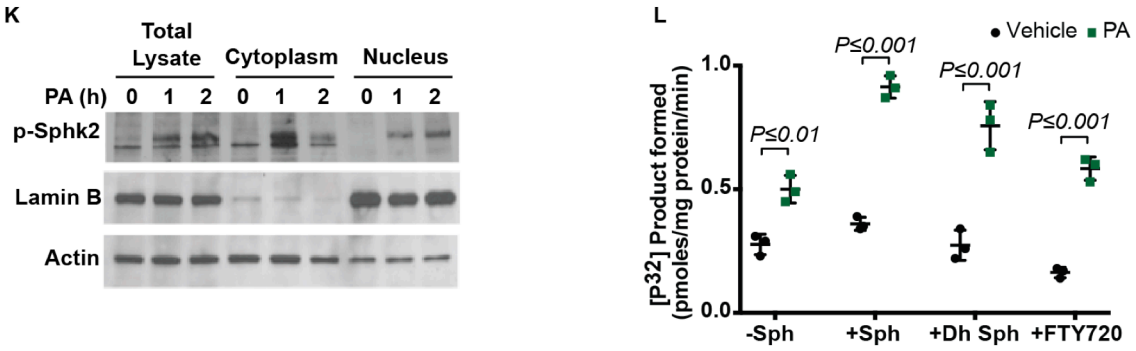

Fig. 12 K & L: *PA* stimulates SphK2 phosphorylation and activation in MLE-12 nuclei.) Immunoassay of total lysate, cytoplasm and nuclear fractions isolated from control and heat-inactivated *PA*103 (1 x 10^8 CFU/ml) MLE-12 cells for 0, 1 and 2 h as outlined in METHODS. The purity of nuclear fraction was assessed by immunostaining for Lamin B (nuclear marker) and lactate dehydrogenase (LDH) (cytoplasm marker) **(K)**. Mouse lung alveolar epithelial (MLE-12) cells in 100-mm dishes were treated with vehicle or heat-inactivated Pseudomonas aeruginosa (1 x 10^8 CFU/ml) for 2 h followed by isolation of nuclear fraction as outlined in METHODS. The nuclear fractions (40 μg protein) were subjected to sphingosine kinase activity assay in Hepes buffer (pH 7.4) containing 10 mM $MgCl_2$, and 1 mM DTT in the absence or presence of 1μM sphingosine (Sph), dihydro Sph or FTY720 in the presence of 0.1% fatty acid BSA and 10 μM [γ-^{32}P]ATP (Specific activity 10,000 dpm/pmol) in a final volume of 100 μl for 30 min at 37^0C. The reaction was terminated by the addition of 0.8 ml of 1 N HCl followed by 1 ml of methanol and 1 ml chloroform to extract the lipids. The lower chloroform layer was subjected to thin-layer chromatography, and auto-radiography and radioactivity associated in S1P, DH S1P or FTY720-P was quantified by scintillation counting as described under Materials and Methods. Values are means $\pm$ SEM of three independent experiments and expressed as pmoles of product formed/mg protein/min **(L)**.

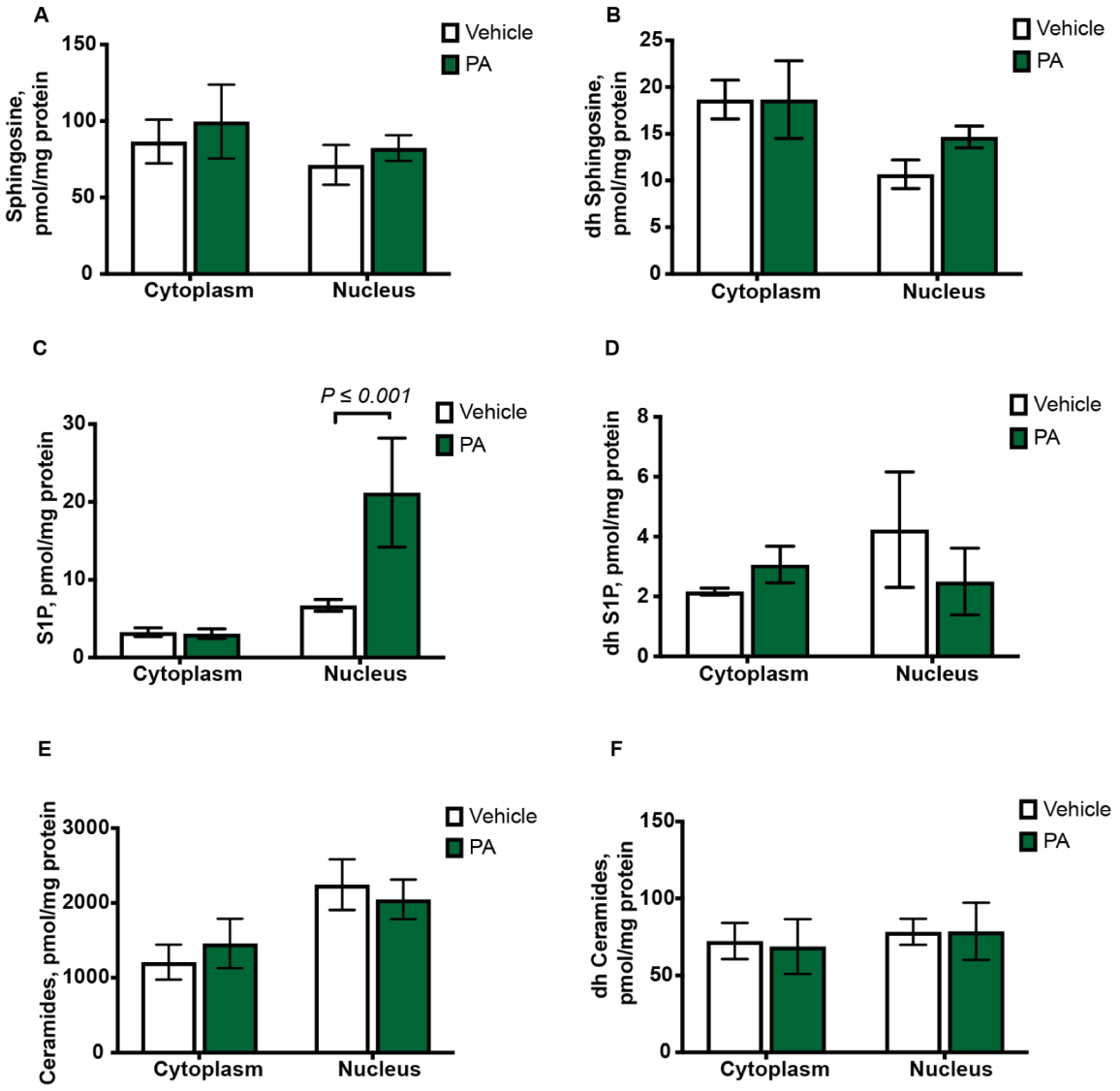

Fig. 13: Sphingoid bases levels in cytoplasm and nuclear fractions of alveolar epithelial cells. MLE-12 cells in 100-mm dishes (~90% confluence) were treated with vehicle or heat-inactivated *PA* (1 X 10^8 CFU/ml) for 3 h. Cells were trypsinized and cytoplasm and nuclear fractions were isolated by sucrose density gradient centrifugation as described in METHODS. Lipids were extracted from the cytoplasm and nuclear fractions according to Bligh & Dyer extraction procedure as described in METHODS (). (**A,B**) sphingosine (Sph), and DH Sph, (**C,D**) S1P and DH S1P and (**E,F)** ceramide (Cer) and DH Cer levels in the cytoplasm and nuclear fractions was determined by LC-MS/MS and quantified. Values are means $\pm$ SD of two independent experiments in triplicate. $^{***}P<0.001$ significantly different from cells challenged with vehicle.

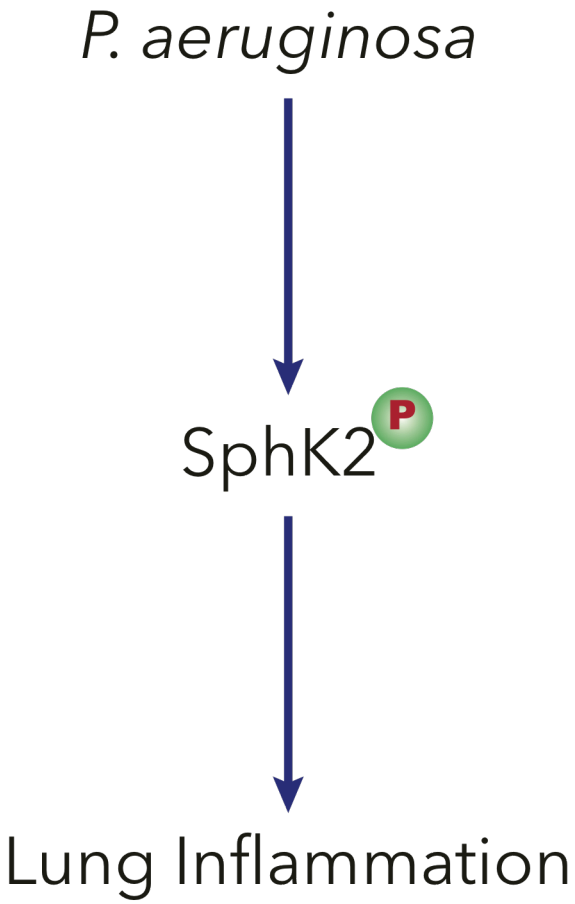

Fig. 14: Schematic diagram showing the role of *PA*-induced phosphorylation of SphK2 in lung inflammation.

5. RESULTS II

5.1. Hypothesis: Sphingosine kinase 2 generated nuclear S1P epigenetically regulates pro-inflammatory cytokine secretion.

5.1.1. Deletion or inhibition of SphK2 reduces *PA*-mediated H3 and H4 histone acetylation and IL-6 secretion:

An earlier study has demonstrated that SphK2 derived S1P to directly bind to HDACs and inhibit its activity in cancer cells(Hait et al. 2009). As *PA*-induced lung inflammation was significantly attenuated in *Sphk2*$^{-/-}$ mice than in their wild type and *Sphk1*$^{-/-}$ counterparts, we next investigated if *PA* enhanced chromatin remodeling *in vivo* in mouse lung and *in vitro* in alveolar epithelial cells. Infection of mouse lung with *PA* increased H3K9 and H4K8 histone acetylation in mouse lungs, which was reduced in SphK2, but not SphK1, knockout mice **(Fig. 15A)**. Similarly, blocking SphK2 activity with a specific inhibitor, ABC294640, *in vivo* in mouse lung attenuated H3K9 and H4K8 histone acetylation without affecting the total expression of H3 and H4 histones **(Fig. 15B)**. *In vitro*, pre-treatment of alveolar epithelial MLE-12 cells with SphK2 inhibitor, ABC294640 attenuated H3K9 and H4K8 histone acetylation **(Fig. 15C);** however, inhibition of SphK1 activity with a specific inhibitor, PF543, had no significant effect on *PA*-mediated H3K9 or H4K8 histone acetylation **(Fig. 15C)**. As accumulation of H3 and H4 acetylated histones is a balance between HATs and HDAC activities, we next measured HDAC activity in epithelial cells after challenge with heat-inactivated *PA*. As shown in **Fig. 15D**, *PA* challenge inhibited total HDAC activity in epithelial cell lysates, which accounts in part for the enhanced H3 and H4 acetylation. To further demonstrate that *PA* inhibits nuclear HDACs and to study the effect of inhibiting the SphKs , MLE-12 cells were pretreated with PF543 and ABC294640, then challenged with *PA*, then isolated the cytoplasm and nuclear fractions and analyzed for HDAC activity. Results

showed that there was no significant change in the cytoplasmic HDAC activity **(Fig. 15E)** after *PA* infection, whereas a decrease of nuclear HDAC activity was observed after *PA* treatment in control cells, which was reversed by blocking SphK2 with ABC294640 **(Fig. 15F)**. This suggests that SphK2 plays a consequential role in blocking HDAC activity after *PA* challenge. Having demonstrated the requirement of SphK2 in *PA*-induced histone acetylation of H3 and H4 histones, next we examined the role of SphK2 and SphK1 in IL-6 secretion in alveolar epithelial cells. In MLE-12 cells, heat-inactivated *PA* stimulated IL-6 secretion (~3 fold) compared to vehicle challenged cells and inhibition of SphK2, but not SphK1, activity inhibited *PA*-mediated IL-6 secretion **(Fig. 15G)**.

To further examine whether *PA* can modulate histone acetylation pattern at IL-6 promoter, ChIP assays were performed. ChIP assays using anti-acetyl histone H3K9 followed by real-time quantitative PCR analysis showed that *PA* significantly increased H3K9 histone acetylation at NF-κB site on IL-6 promoter in 3 h, which was blocked by SphK2 inhibitor ABC294640 and not SphK1 inhibitor PF543 **(Fig. 15H).** Collectively, these results show for the first time a role for SphK2 and SphK2 phosphorylation in *PA*-mediated enhanced H3 and H4 acetylation *in vivo* in lung tissue and *in vitro* in lung epithelial cells. Further, the results suggest regulation of chromatin modifications in IL-6 promoter by *PA*-mediated SphK2 activation in alveolar epithelial cells.

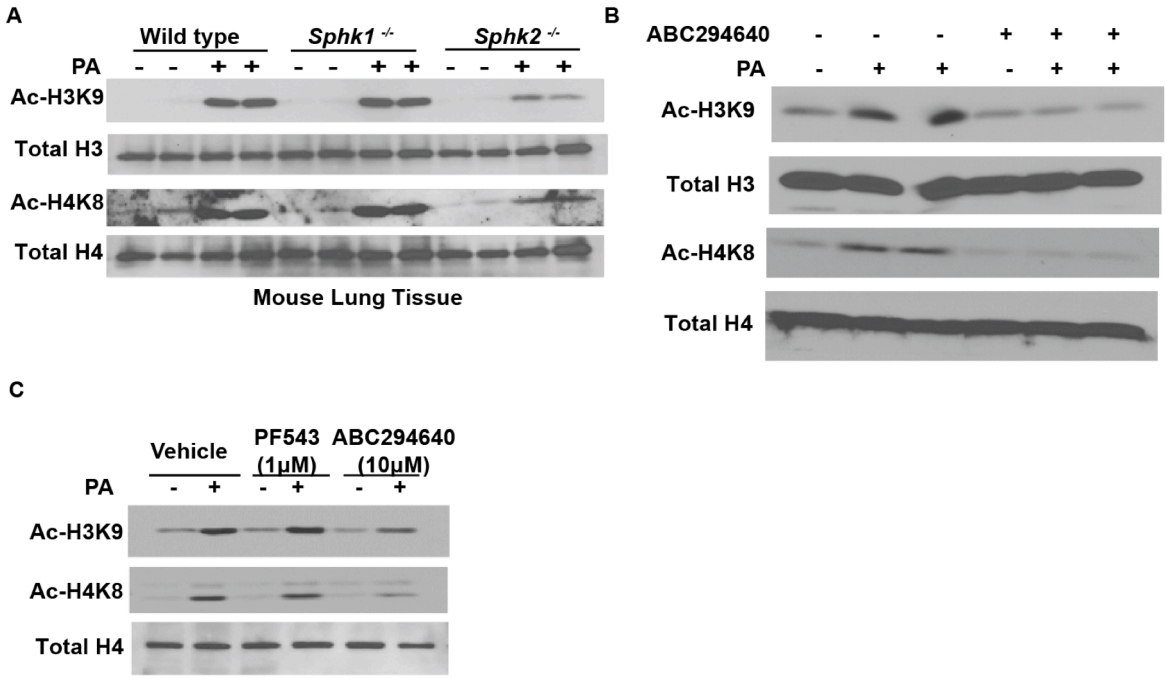

Fig. 15: SphK2 is essential for *PA*-induced H3 and H4 histone acetylation and IL-6 secretion. (A) Lung tissues from the experiments described in **Fig. 2** were analyzed for histone acetylation. Lung tissue lysates (30 μg proteins) were subjected to immunoblot analysis using acetylated H3K9, acetylated H4K8, and total H3 and H4 histones. Shown is a representative Western blot from 5 lung tissue lysates. **(B)** Lung tissues lysates (30 μg proteins) from control, *PA*, ABC294640, ABC294640 + *PA* challenged mice, as described in **Fig. 3**, were analyzed by immunoblotting using acetylated H3K9, acetylated H4K8, and total H3 and H4 histones. Shown is a representative blot from 5 lung tissue lysates subjected to immunoblotting. **(C)** MLE-12 cells were pretreated with vehicle or vehicle containing a SphK1 inhibitor, PF543 (1 μM), or SphK2 inhibitor, ABC294640 (10 μM), for 1 h prior to challenge with heat-inactivated *PA* (1 x 10^8 CFU/ml) for 2 h. Cell lysates (20 μg proteins) were subjected to immunoblotting and immunostaining with acetylated H3K9, acetylated H4K8 and total H4 antibodies. Shown is a representative blot of three independent experiments in triplicate.

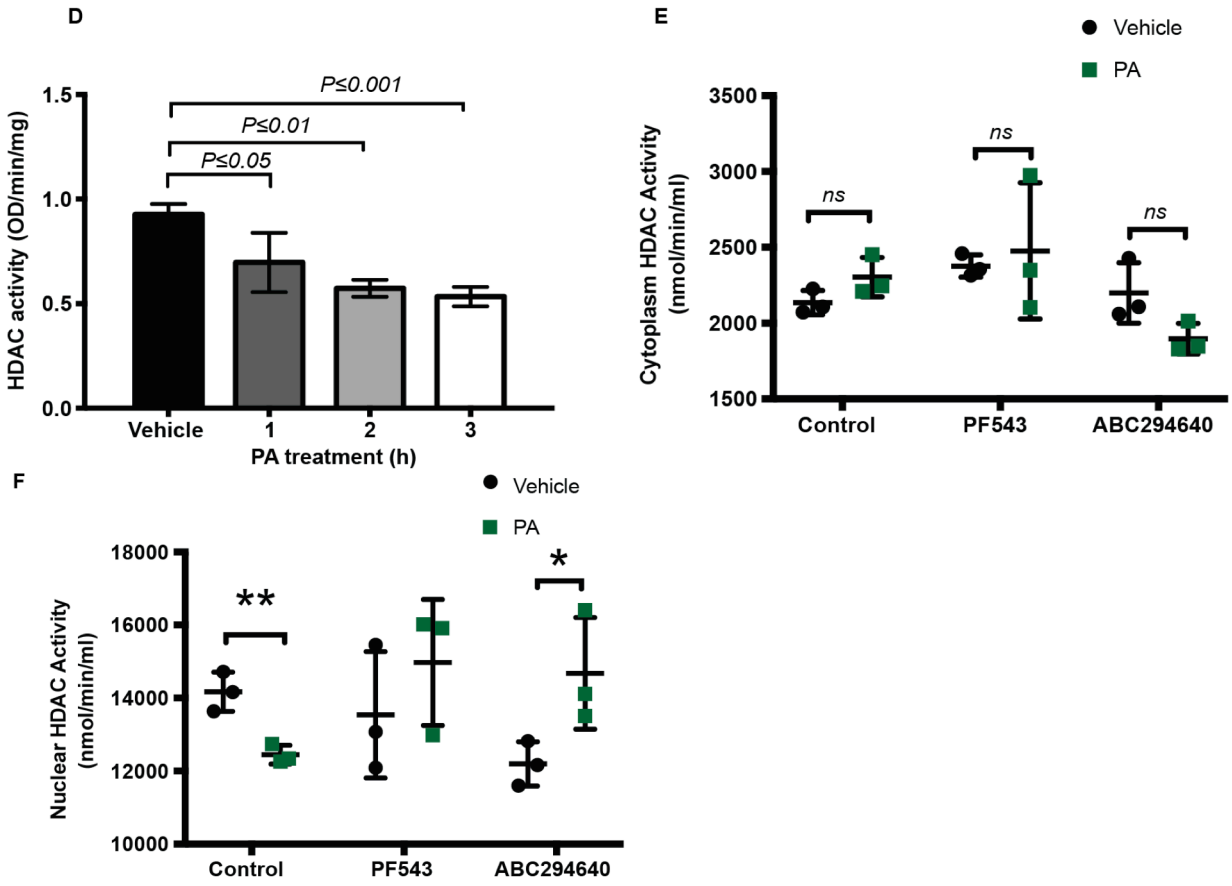

Fig. 15: *PA*-induced HDAC activity reduction is modulated by SphK2 inhibition. (**D**), Primary AT II cells were treated with heat-inactivated *PA* (1 x 10^8 CFU/ml) for 1-3 h and cell lysates were analyzed for HDAC activity using a commercial kit as outlined in METHODS. Values are means ± SD of three experiments in triplicate and normalized to total protein per min. (**E, F**), MLE-12 cells grown in 100-mm dishes (~90% confluence) were pretreated with SphK1 inhibitor PF543 (1 μM) or SphK2 inhibitor, ABC294640 (10 μM), for 1 h prior to challenge with heat-inactivated *PA* (1 x 10^8 CFU/ml) for 3 h. Cytoplasm and nuclear fractions were isolated as outlined in METHODS and total HDAC activity was determined using a commercial kit. Data are means ± SD from two independent experiments in triplicate.

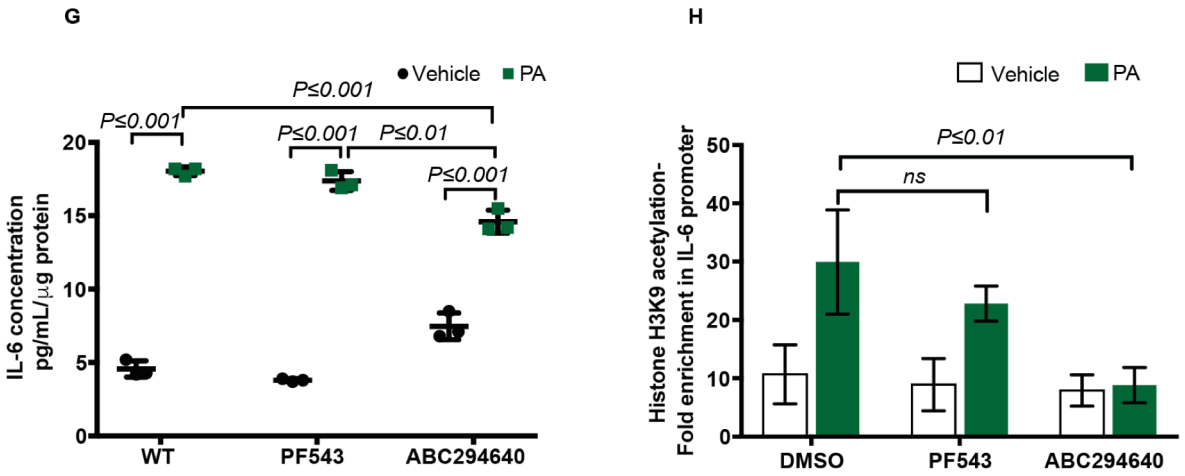

Fig. 15: SphK2 inhibition blocks IL-6 secretion and Acetylated Histone H3K9 enrichment on IL-6 promoter. MLE-12 cells were pretreated with vehicle or vehicle containing a SphK1 inhibitor, PF543 (1 μM) or SphK2 inhibitor, ABC294640 (10 μM) for 1 h prior to challenge with heat-inactivated *PA* (1 x 10^8 CFU/ml) for 2 h. Media were analyzed for IL-6 levels **(G)** using a commercial ELISA as described in METHODS. ChIP assays were performed in cell lysates using anti-acetyl histone H3K9 followed by real-time quantitative PCR **(H)**. Analysis showed that *PA* significantly increased H3K9 histone acetylation at NF-κB sites on IL-6 promoter in 3 h, which was blocked by SphK2 inhibitor ABC294640 and not SphK1 inhibitor PF543. Data are means ± SD from three independent experiments in triplicate.

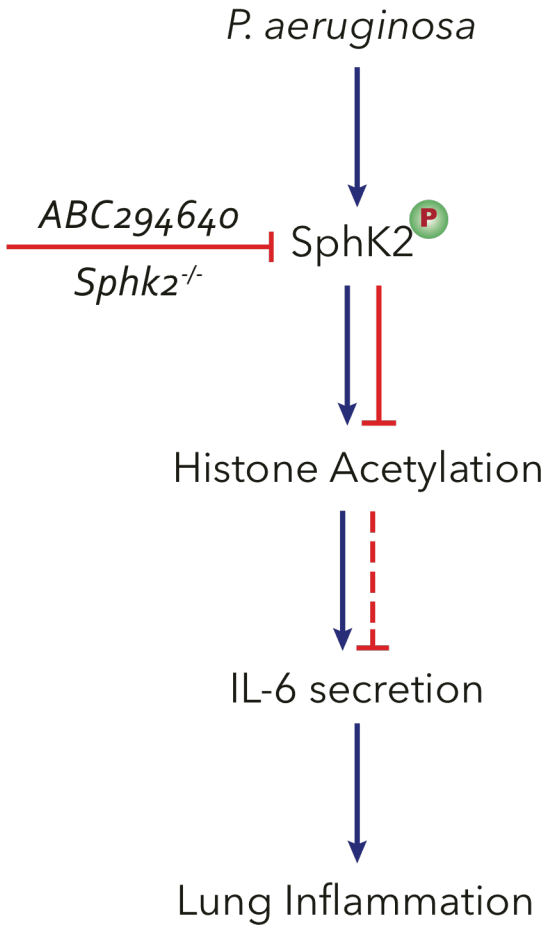

Fig. 16: Schematic diagram showing *PA*-induced Histone acetylation and IL-6 secretion was blocked by inhibiting Sphk2 activity with ABC294640.

5.1.2. Activation of PKC δ is essential for *PA*-induced SphK2 phosphorylation, H3 and H4 histone acetylation and IL-6 secretion

Earlier studies have demonstrated a role for ERK1/2 in agonist-mediated phosphorylation and activation of SphK1 and SphK2 in mammalian cells, however, inhibition of ERK1/2 phosphorylation with PD98059 and U0126, specific inhibitors of MEK1/2 had no effect on *PA*-mediated IL-6 secretion **(Fig. 17A & B)**. Therefore, we interrogated the involvement of PKC isoforms in *PA*-mediated SphK2 phosphorylation, H3 and H4 histone acetylation and IL-6 secretion in alveolar epithelial cells. Mouse and human alveolar and airway epithelial cells express most of the PKC isoforms and *PA* challenge of MLE-12 cells enhanced PKC total activity **(Fig. 17C)**. Pre-treatment of MLE-12 cells with pan PKC inhibitor, bisindolylmaleimide, blocked *PA*-induced SphK2 phosphorylation and histone acetylation **(Fig. 17D)**. To determine the role of PKC isoform(s) in *PA*-mediated SphK2 phosphorylation, and H3K9/H4K8 histone acetylation and IL-6 secretion, MLE-12 cells were infected with dominant negative (DN) PKC α, δ, ε, and ζ isoforms prior to *PA* challenge. Among the PKC isoforms, DN PKC α had no effect on IL-6 secretion while DN PKC δ, ε, and ζ attenuated *PA*-induced IL-6 secretion. However, *PA*-induced inhibition of IL-6 secretion by DN PKC δ was more pronounced compared to DN PKC ε and ζ isoforms **(Fig. 17E)**. Further, DN PKC δ, in a time-dependent manner, significantly attenuated *PA* mediated IL-6 secretion **(Fig. 17F)**. To further substantiate the role of PKC δ in effecting IL-6 secretion, we isolated the mRNA levels from vehicle and *PA* challenged MLE-12 cells with and without DN PKC δ infection at multiple time points (0,1,3,6,9,12 & 24 h) and quantitated the mRNA levels of IL-6 and TNF-α using specific primers using real time PCR. Results showed DN PKC δ affects the mRNA expression of IL-6 and TNF-α at all time points, and not at 3h post *PA* challenge **(Fig. 17 G & H)**. To further verify PKC δ role in phosphorylating SphK2 after *PA* infection, we stained MLE -12 cells for p-

SphK2 after *PA* infection and observed a time dependent increase of SphK2 phosphorylation in the nucleus; *PA*-induced SphK2 phosphorylation was blocked by DN PKC δ **(Fig. 17I & J)**. The involvement of PKC δ was further confirmed by down-regulation of the protein expression with siRNA, which reduced SphK2 phosphorylation and acetylation of H3K9 and H4K8 in MLE-12 cells challenged with *PA* compared to control cells **(Fig. 17K)**. Next, ChIP assays were performed to determine if inhibition of PKC δ would modulate *PA*-mediated H3K9 histone acetylation at NF-κB site on IL-6 promoter. Real-time quantitative PCR analysis showed that *PA* significantly increased H3K9 histone acetylation at NF-κB site on IL-6 promoter, which was blocked by over-expression of DN PKC δ in MLE-12 cells **(Fig. 17L)**. Furthermore, pre-treatment of MLE-12 cells with SphK2 inhibitor ABC294640 or adenoviral DN PKC δ attenuated *PA*-induced increase in nuclear S1P levels **(Fig. 17M)**. Collectively, these results show a key role for *PA*-mediated PKC δ activation in phosphorylation and nuclear localization SphK2 and H3K9 acetylation in IL-6 promoter for secretion of the pro-inflammatory cytokine.

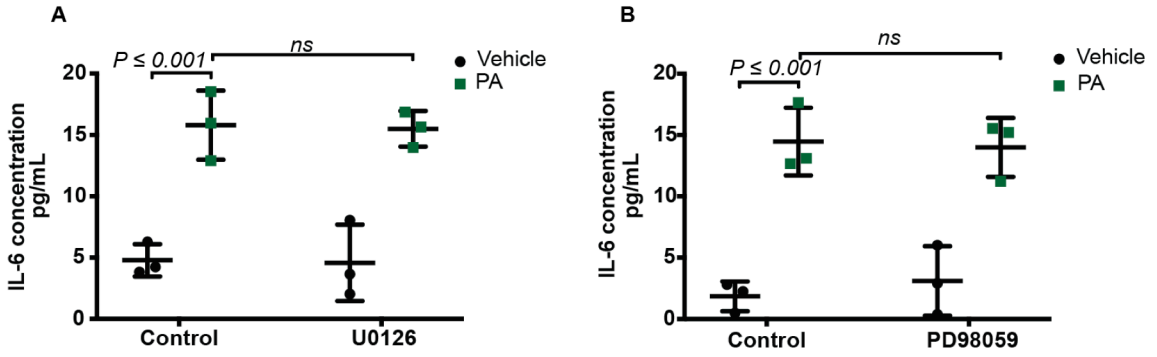

Fig. 17: *PA*-induced SphK2 phosphorylation and IL-6 secretion is not mediated by ERK1/2. MLE-12 cells grown on 35-mm dishes (~90% confluence) were pre-treated with U0126 (5 μM) (**A**) or PD98059 (5 μM) (**B**) for 1 h prior to exposure to vehicle or heat-inactivated *PA* (1 X 10^8 CFU/ml) for 3 h, and IL-6 level in medium was quantified by ELISA as described in METHODS. Data are means ± SD of two independent experiments in triplicate

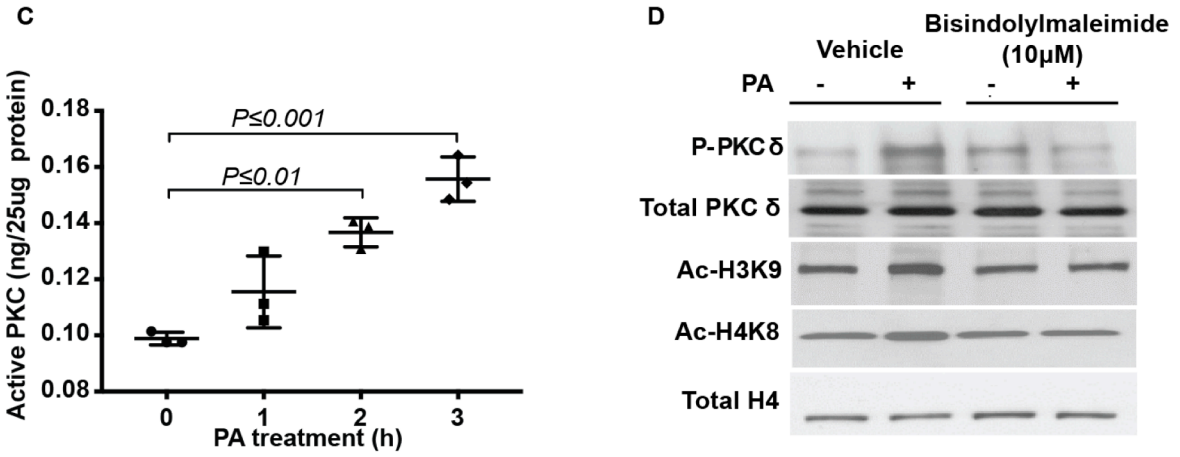

Fig. 17: PKC δ activation regulates *PA*-induced SphK2 phosphorylation, histone acetylation and IL-6 secretion in MLE-12 cells: (**C**), MLE-12 cells were exposed to heat-inactivated *PA*103 (1 x 10^8 CFU/ml) for 1-3 h and total PKC activity in cell lysates was determined using a commercial PKC activity kit. Values are means ± SD from three independent experiments in triplicate. (**D**) MLE-12 cells were pre-treated with a PKC inhibitor, bisindolylmaleimide (10 μM) for 1 h prior to challenge with heat-inactivated *PA* (1 x 10^8 CFU/ml) and cells were incubated for 2 h. Cell lysates (30 μg proteins) were analyzed by Western blot for p-PKCδ, total PKCδ, acetylated H3K9 and H4K8 and total H4 histone using specific antibodies. Shown is a representative blot of three independent experiments in triplicate.

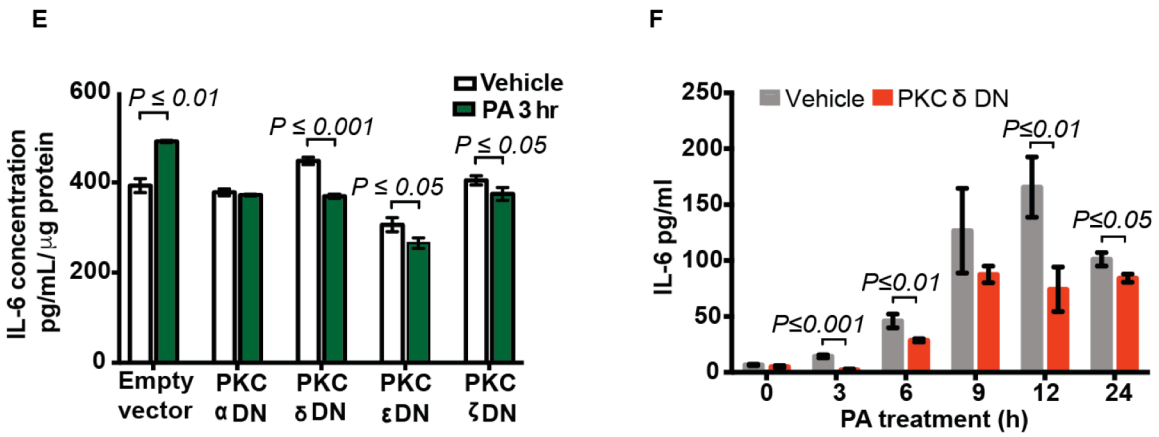

Fig. 17: Inhibition of PKC δ reduces secretion of IL-6. (**E**), MLE-12 cells grown on 100-mm dishes (~60% confluence) were infected with adenoviral vector control or dominant negative (DN) adenoviral PKC α, δ, ε, ζ vectors (25 MOI) for 24 h prior to exposure to vehicle or heat-inactivated *PA* (1 X 10^8 CFU/ml) for 3 h and IL-6 level was determined in the medium by ELISA as described in METHODS. Data are means $\pm$ SD of triplicate determination. (**F**), MLE-12 cells grown on 100-mm dishes (~60% confluence) were infected with adenoviral vector control or dominant negative (DN) adenoviral PKC δ, vector (25 MOI) for 24 h prior to exposure to vehicle or heat-inactivated *PA* (1 X 10^8 CFU/ml) for 0, 3, 6, 9, 12 and 24 h and IL-6 level was determined in the medium by ELISA as described in METHODS. Data are means $\pm$ SD of triplicate determination.

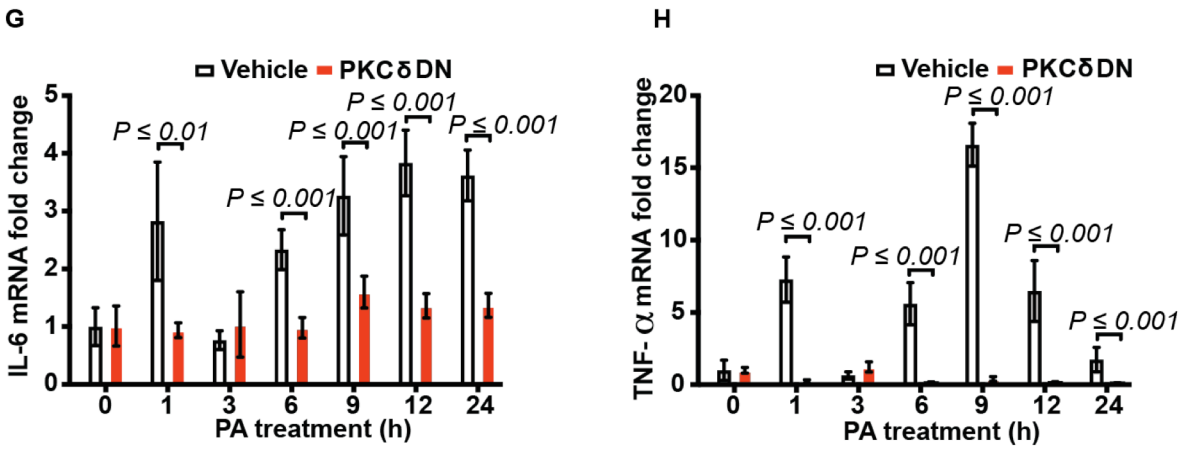

Fig. 17: Inhibition of PKC δ reduces mRNA expression of IL-6 and TNF-α. MLE-12 cells grown on 100-mm dishes (~60% confluence) were infected with adenoviral vector control or DN adenoviral PKC δ vectors (25 MOI) for 24 h prior to exposure to vehicle or heat-inactivated *PA* (1 X 10^8 CFU/ml) for 1, 3, 6,9,12 and 24 h. RNA was isolated and IL-6 (**G**) and TNF-α (**H**) mRNA levels were quantified by real-time RT-PCR and data were normalized to β-actin. Data are means ±of one independent experiment in triplicate.

-

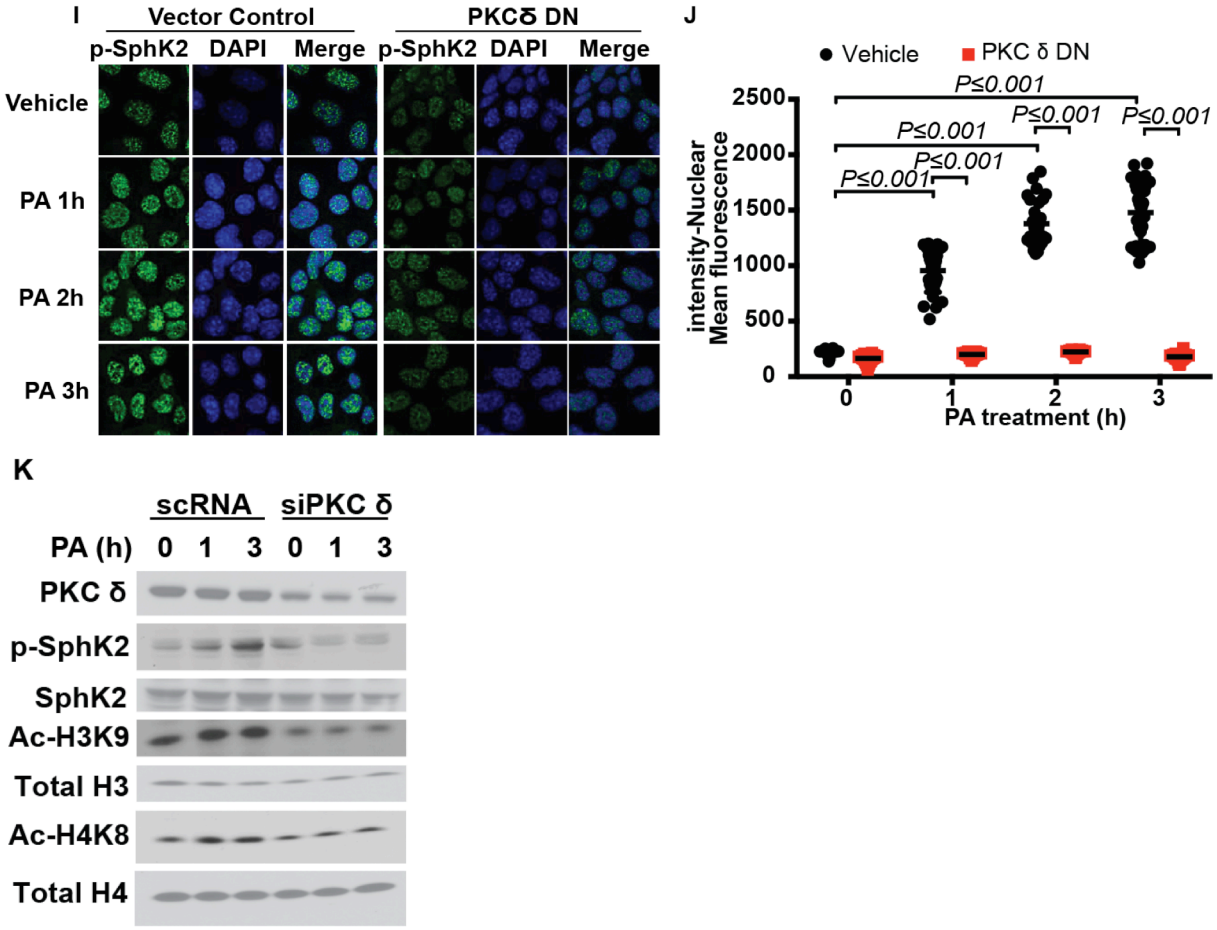

Fig. 17: PKC δ activation regulates *PA*-induced SphK2 phosphorylation in MLE-12 cells and histone acetylation in HBEPC. (**I**), MLE-12 cells grown to ~60% confluence on slide chambers were infected with DN PKC δ (25 MOI) for 24 h prior to *PA* challenge for 1-3 h. Cell were fixed, stained with p-SphK2 antibody and phosphorylation of SphK2 and its nuclear localization was quantified by confocal microscopy. Shown is a representative confocal image (five areas per slide and four independent slides for each experiment) and (**J**), quantification of nuclear p-SphK2 localization by Image J. (**K**), Primary human bronchial epithelial cells (~60% confluence) were transfected with scrambled or PKC δ siRNA (50 nM) for 48 h prior to heat-inactivated *PA* (1 x 10^8 CFU/ml) challenge for 1 and 3 h. Cell lysates (20 μg proteins) were Western blotted and immunobloted with anti-acetylated H3 and H4, PKC δ, p-SphK2, SphK2 and total H3 and H4 antibodies. Shown is a representative Western blot from three independent experiments in triplicate.

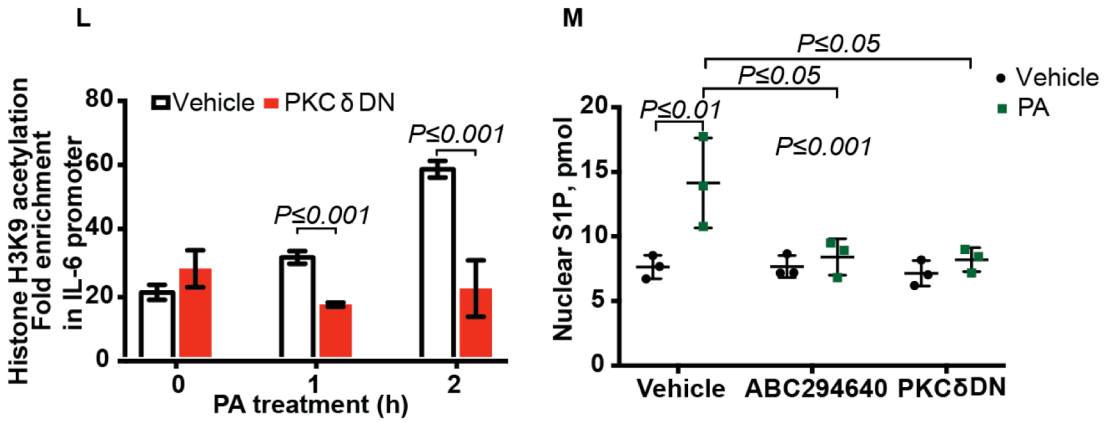

Fig. 17: PKC δ activation enriches histone H3K9 acetylation on IL-6 promoter and nuclear S1P production in MLE-12 cells. (**L**), MLE-12 cells grown on 100-mm dishes (~60% confluence) were transfected with scrambled or PKC δ siRNA (50 nM) for 48 h prior to heat-inactivated *PA* (1 x 10^8 CFU/ml) challenge for 1 and 2 h. ChIP assays were performed using anti-acetyl histone H3K9 followed by real-time quantitative PCR. Analysis showed that *PA* significantly increased H3K9 histone acetylation at NF-κB sites on IL-6 promoter in 1 and 2 h, which was blocked by DN PKC δ adenovirus. Data are means ± SD from three independent experiments in triplicate. (**M**), Primary human bronchial epithelial cells (HBEpCs) in 100-mm dishes (~60% confluence) were infected with control or DN PKC δ adenoviral vector (25 MOI) for 48 h or cells were pre-treated with ABC294640, a SphK2 inhibitor for 1 h prior to heat-inactivated *PA* challenge (1 x 10^8 CFU/ml). Nuclei were isolated by sucrose density gradient and nuclear fractions were extracted with $CHCl_3$:CH_3OH (1:1) followed by phase separation using Bligh & Dyer extraction as outlined in METHODS. S1P level in the nuclear fraction was determined by LC-MS/MS and quantified. Values are means ± SD of two independent experiments in triplicate.

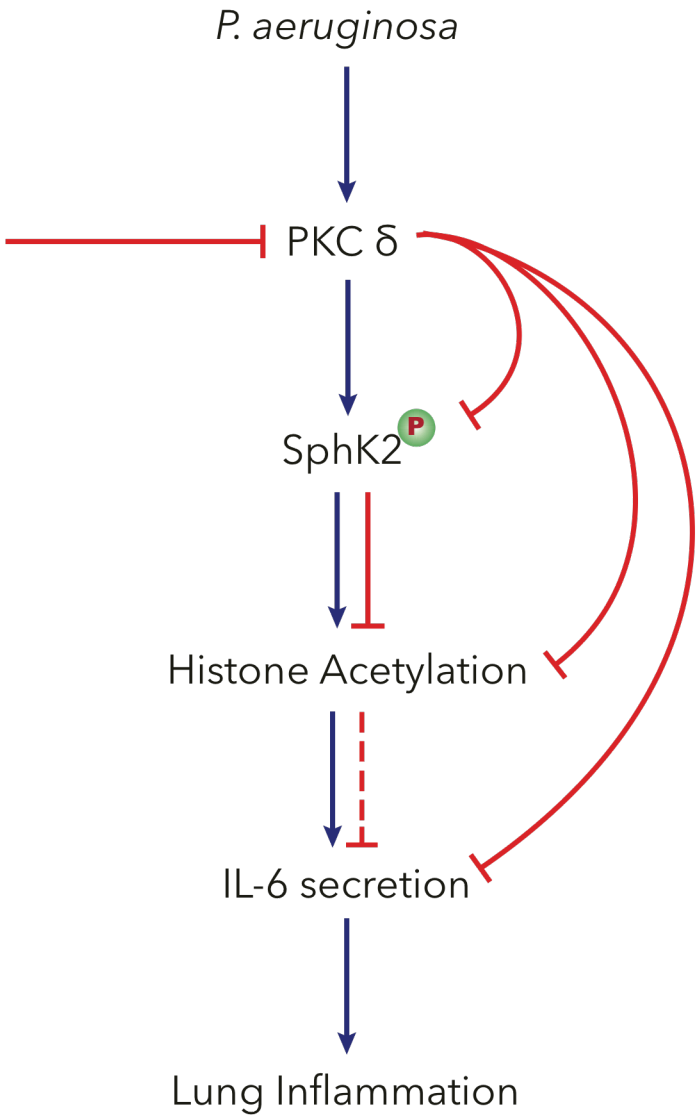

Fig. 18: Schematic diagram showing blocking PKC δ, attenuates *PA*-induced SphK2 phosphorylation and downstream signaling.

5.1.3 *PA* enhances association of SphK2 with HDAC1/2 and S1P generation in the nucleus.

Having established PKC δ dependent nuclear localization of p-SphK2 in response to *PA* in lung epithelial cells, next we determined potential association between SphK2/p-SphK2 and HDAC1/2 in the nucleus. MLE-12 cells were infected with myc-tagged adenoviral SphK2 WT construct for 24 h prior to treatment with heat inactivated *PA* for 1-3h, cell lysates were immuno-precipitated with anti-myc antibody and Western blotted. As shown in **Fig. 19A**, *PA* enhanced association of SphK2 with HDAC1/2 and also with RbAp46/48, a component of Sin3 and NuRD co-repressors. Similarly, *PA* increased co-immunoprecipitation of SphK2/p-SphK2 and p-PKC δ with HDAC1 and HDAC2 **(Fig. 19B & C)**. Next, we co-immuno stained p-SphK2 and HDAC1 in MLE-12 cells after *PA* challenge and used confocal microscopy to visualize the co-localization. We created Z-stack images and analyzed the co-localization coefficients using coloc2 in Image J software. Co-stained MLE-12 Immunohistochemical localization also revealed enhanced association between p-SphK2 with HDAC1 after *PA* challenge of MLE-12 cells **(Fig. 19D & E)**.

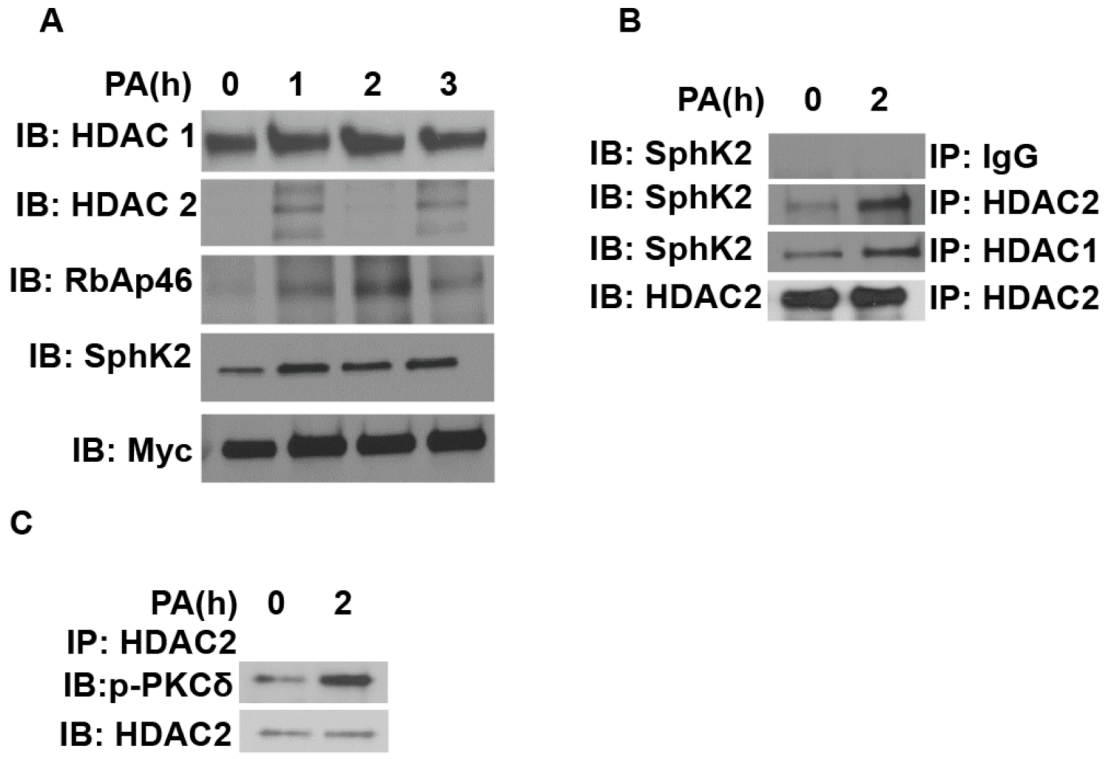

Fig. 19: *PA* enhances association of SphK2 with HDAC1/2 in the nucleus. (A) MLE-12 grown on 100-mm dishes (~70% confluence) were infected with myc-tagged SphK2 WT adenoviral construct (25 MOI) for 25 h prior to exposure to heat-inactivated *PA* (1 x 10^8 CFU/ml) for 1,2 and 3 h. At the end of the incubation period, cells wells trypsinized and nuclei were isolated as described in METHODS, and nuclear extracts (1 mg protein) were subjected to immunoprecipitation with anti-myc antibody and immunoprecipitates were analyzed for HDAC1, HDAC2, RBAP46, total SphK2 and myc by Western blotting. Shown is a representative blot from three independent experiments. **(B),** MLE-12 grown on 100-mm dishes (~90% confluence) were challenged with heat-inactivated *PA* (1 x 10^8 CFU/ml) for 2 h and at the end of the incubation period cells wells trypsinized and nuclei were isolated as described in METHODS. Nuclear extracts (1 mg protein) were subjected to immunoprecipitation with anti-HDAC1 and anti-HDAC2 antibodies and immunoprecipitates were analyzed for HDAC1, HDAC2, and total SphK2 by Western blotting. **(C),** Same as **(B)** and nuclear extracts (1 mg protein) were subjected to immunoprecipitation with anti-HDAC2 antibody and immunoprecipitate was analyzed for HDAC2, and p-PKC δ (S299) by Western blotting.

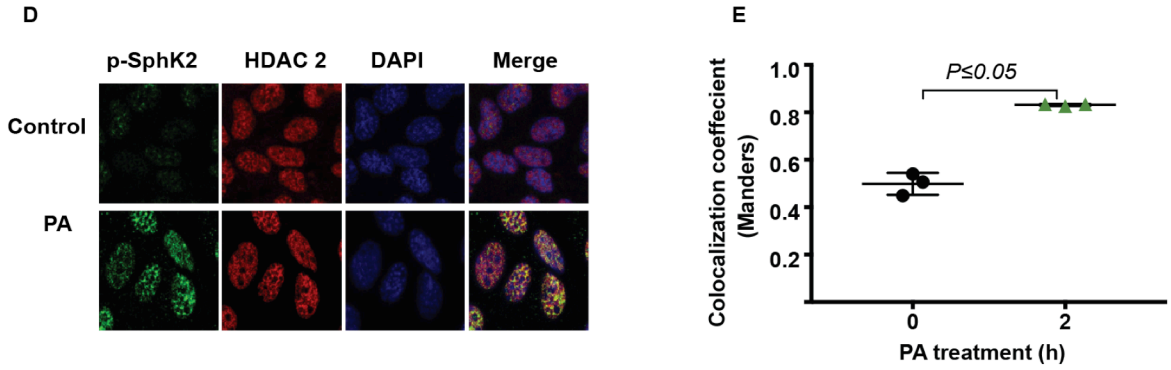

Fig. 19: *PA* enhances association of SphK2 with HDAC 2. (**D & E**), MLE-12 cells grown on slide chambers (~90% confluence) and were challenged with heat-inactivated *PA* (1 x 10^8 CFU/ml) for 2 h. Cells were fixed and co-immunostained with anti-p-SphK2 and anti-HDAC1 antibodies and co-localization of p-SphK2 and HDCA1 was visualized by confocal microscopy. Shown is a representative micrograph from three independent experiments and co-localization was quantified by Image J using Coloc2 (five areas per slide; three z-stack of 40 images per group).

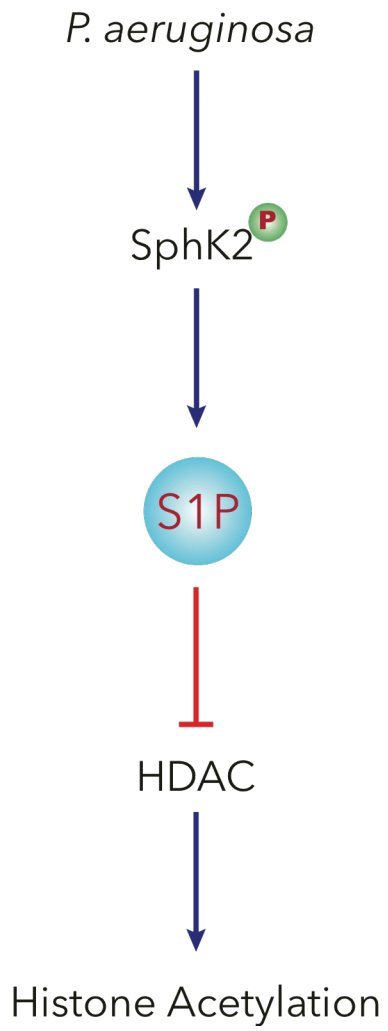

Fig. 20: Schematic diagram showing SphK2-mediated S1P blocks HDAC activity in the nucleus after *PA*-infection.

5.1.4 *PA*-mediated nuclear SphK2/S1P signaling stimulates nuclear ROS production and oxidation of HDACs.

Earlier studies have shown that exogenous S1P signals via $S1P_1$ and stimulates NOX2 and NOX4 and superoxide production in endothelial cells (Fu et al. 2013). Further, ROS generated in the nucleus of myocytes was shown to oxidize cysteine residues on HDAC4 resulting in modulation of HDAC4 activity (Matsushima et al. 2012). Therefore, to further define the mechanism(s) of nuclear regulation of HDAC1/2 by SphK2/S1P signaling axis, we expressed p-Hyper, a mammalian expression vector encoding fluorescent hydrogen peroxide sensor, targeting to the nucleus, cytoplasm or mitochondria of epithelial cells and monitored the generation of ROS after *PA* challenge by confocal microscopy. *PA* stimulated ROS generation in the cytoplasm, mitochondria and nucleus of MLE-12 cells **(Fig. 21A-C)** but inhibition of SphK2 with ABC294640 attenuated only the nuclear and not the cytoplasmic- or mitochondria-derived ROS **(Fig. 21 A-C)**. Having established the effect of SphK2 on nuclear ROS generation, we further investigated the oxidative modification of HDAC1/2 by determining the oxidation of carbonyl groups in HDAC1/2 using Oxyblot protein oxidation detection kit. As shown in **Fig. 21D**, exposure of MLE-12 cells to *PA* increased oxidation of carbonyl groups in HDAC1/2. Further, pre-treatment of MLE-12 cells with DN PKC δ or SphK2 inhibitor ABC294640 significantly reduced oxidation of carbonyl groups in HDAC2 **(Fig. 21E)**. Additionally, scavenging *PA*-induced ROS with N-acetylcysteine (NAC) also drastically reduced oxidation of carbonyl groups in HDAC2 (**Fig. 21F**). These results show that *PA*-induced nuclear ROS generation mediated by nuclear PKC δ/SphK2/S1P signaling axis modulates HDAC activity by oxidation of carbonyl groups in HDAC1/2.

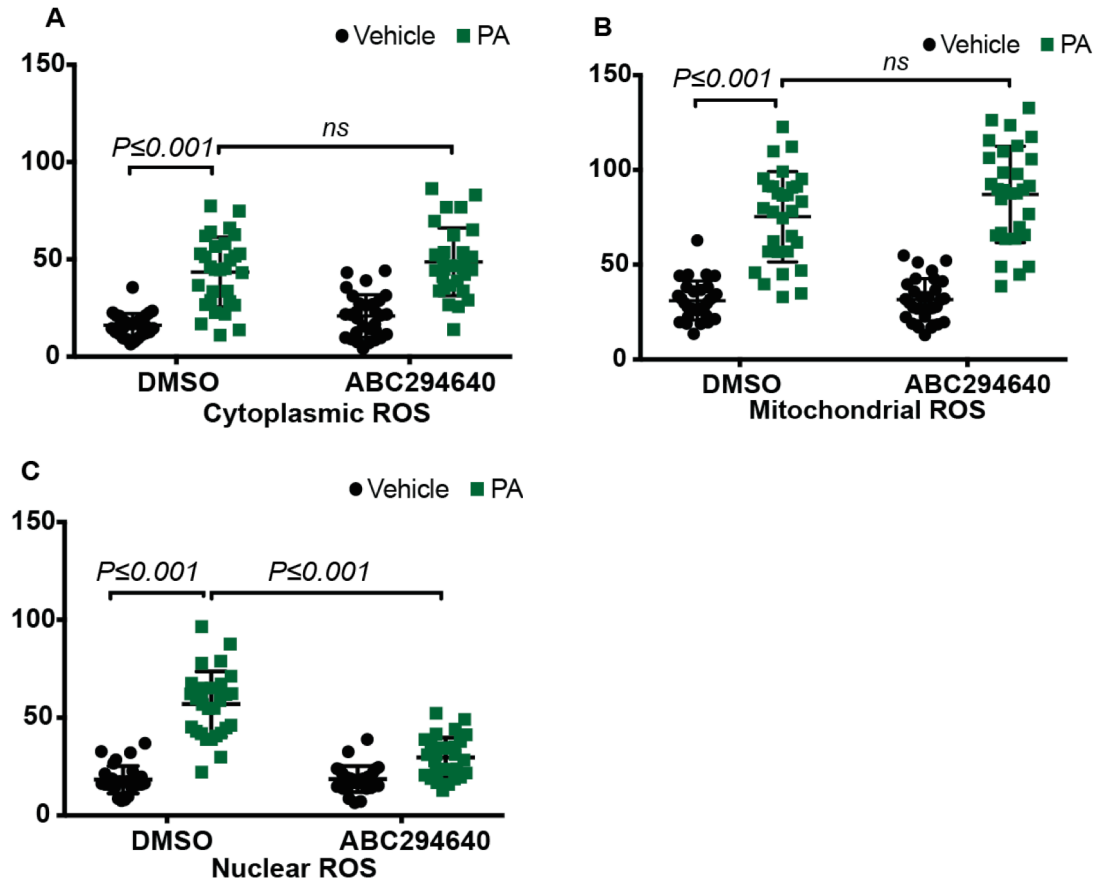

Fig. 21: *PA*-mediated nuclear SphK2/S1P signaling stimulates ROS production in the nucleus. **(A-C)** MLE-12 cells were grown on glass bottom 35-mm dishes (~60% confluence) were transfected with scrambled or p-Hyper (cytoplasm) **(A),** p-Hyper mitochondria **(B)** or p-Hyper nuclear **(C)** (3 μg cDNA) for 24 h prior to exposure to heat-inactivated *PA* (1 x 10^8 CFU/ml) for 3 h. Cells were washed with phenol red free basal DMEM medium and fluorescence of p-Hyper- cytosol, p-Hyper-mitochondria or p-Hyper-nuclear in living cells was measured by confocal microscopy as outlined in METHODS. Shown is a representative confocal image (Twenty areas per slide; four slides per group) and the fluorescence intensity was quantified by ImageJ software.

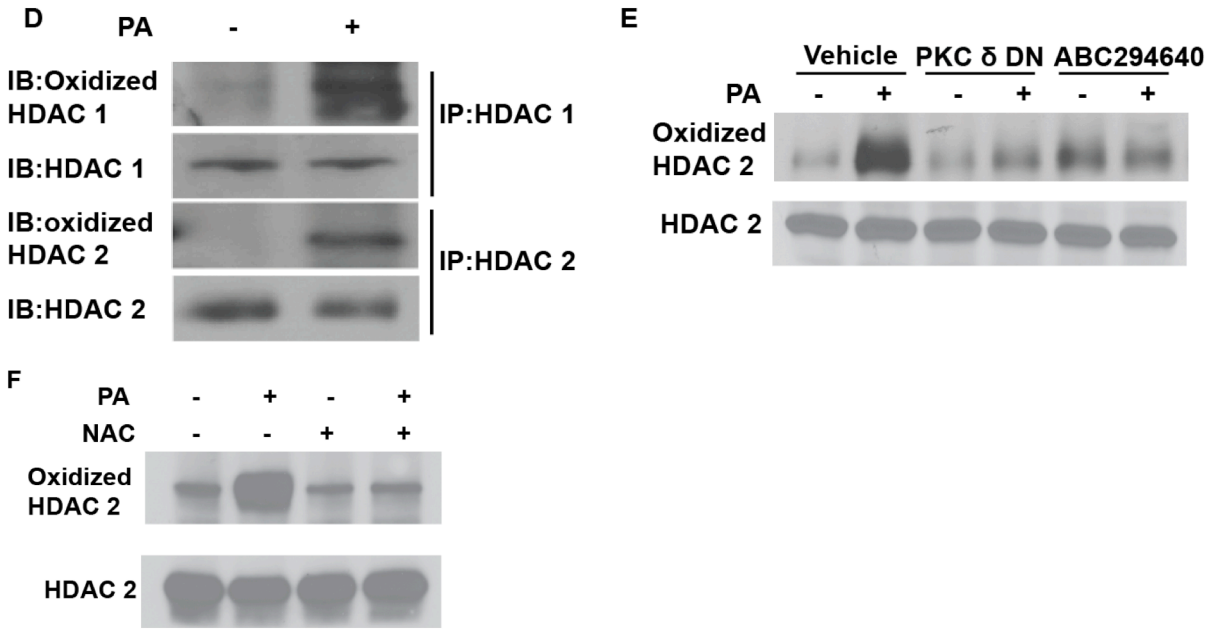

Fig. 21: *PA*-mediated nuclear SphK2/S1P signaling stimulates oxidation of HDACs. (**D**), MLE-12 cells grown in 100-mm dishes were exposed to vehicle or heat-inactivated *PA* (1 x 10^8 CFU/ml) for 3 h, cells trypsinized, and nuclei were isolated as outlined in METHODS. The nuclei were sonicated, and lysates (1 mg protein) subjected to immunoprecipitation with anti-IgG, anti-HDAC1 or anti-HDAC2 antibodies. The immunoprecipitates were subjected to OxyBlot protein oxidation detection (EMD Millipore kit) of carbonyl groups introduced into HDAC1 and HDAC2 by oxidation reaction of H_2O_2 generated in the nucleus by *PA*. Shown is a representative OxyBlot of three independent experiments in triplicate. (**E**), MLE-12 cells grown in 100-mm dishes (~60% confluence) were infected with DN PKC δ adenoviral construct (25 MOI) for 24 h or pre-treated with SphK2 inhibitor, ABC294640 (10 μM) for 1 h prior to exposure to heat-inactivated *PA* (1 x 10^8 CFU/ml) for 3 h. Nuclei were isolated as described above, subjected to HDAC2 immunoprecipitation (1 mg protein), and immunoprecipitates analyzed by OxyBlot protein oxidation kit as per the manufacturer's instruction. Shown is an immunoblot from three independent experiments in triplicate after OxyBlot analysis. (**F**), MLE-12 cells grown in 10-mm dishes (~90% confluence) were pretreated with vehicle or N-acetylcysteine (1 mM) for 1 h prior to *PA* (1 x 10^8 CFU/ml) challenge for 3 h. Nuclei were isolated and subjected to HDAC2 immunoprecipitation and OxyBlot protein oxidation detection as outlined in METHODS. Shown is a representative OxyBlot immunoblot from three independent experiments in triplicate.

5.1.5 *PA*-mediates nuclear ROS production and oxidation of HDACs by stimulating NOX4 in the nucleus.

An earlier study has shown activation of NOX proteins in response to *PA* infection in lung endothelium and has delineated the role of NOX4 in regulating lung inflammation (Fu et al. 2013). So, to further elucidate the molecular mechanism by which nuclear ROS is generated in response to *PA* infection, we first investigated if NOX4 is expressed in the nuclear fractions after *PA* infection in MLE-12 cells. We isolated the cytoplasmic and a nuclear fraction from MLE-12 cells after *PA* infection and immunoblotted them for NOX2 and NOX4. We observed NOX4 isoform expressed in the nuclear fractions after *PA* infection **(Fig. 22A)**; however, no NOX2 was expressed in the nucleus. To test whether *PA*-induced ROS generation is NOX4 or NOX 2 dependent, we silenced NOX4 or NOX2 expression by transfecting cells with NOX4 siRNA or NOX2 siRNA for 72 h, followed by expression of nuclear p-Hyper and then challenged MLE-12 cells with *PA*. Analysis of fluorescence intensity of the Nuclear p-Hyper by confocal microscopy showed *PA*-induced nuclear ROS generation was blocked only when NOX4 expression was downregulated **(Fig 22. C, D, E)**. However, downregulation of NOX2 with siNOX2 had no effect on nuclear ROS generation by *PA* **(Fig. 22 F- H)**.

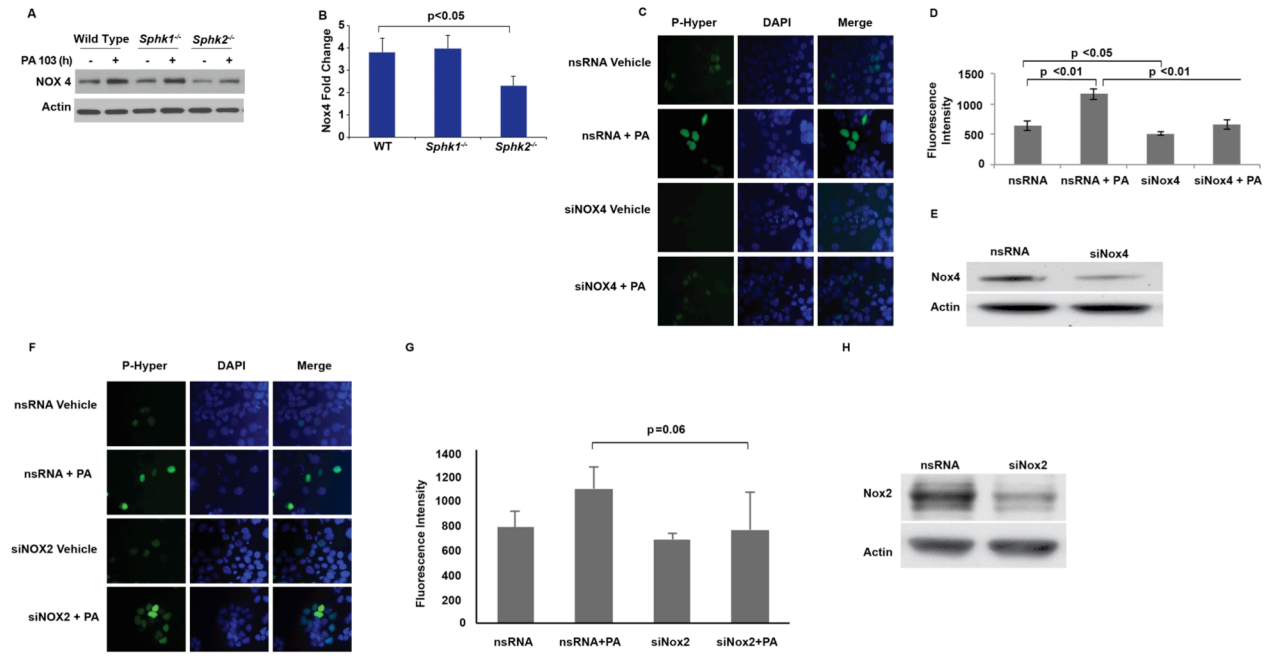

Figure 22: SphK2, but not SphK1, deletion modulates NOX4 expression and NOX4-dependent nuclear ROS generation. (**A**) C57BL/6J, *Sphk1*$^{-/-}$ and *Sphk2*$^{-/-}$ mice were challenged intratracheally with sterile PBS or *PA*103 (1 x 10^6 CFU/animal) in a total volume of 50 µl for 24 h. Animals were sacrificed, bronchoalveolar (BAL) fluid was collected, centrifuged and analyzed. Lungs were removed and frozen in liquid N_2 immediately. Total lysates were lung tissues were subjected to SDS-PAGE and immunostained with anti NOX4 and anti-actin antibodies. Shown is a representative blot from three independent experiments (n=3 per group). (**B**) Quantification of NOX4 from (**A**) was carried out by Image J and normalized to total actin. Genetic deletion of sphK2, but not SphK1, reduced *PA*-induced Nox4 expression. **NOX4 siRNA attenuates *PA*-induced nuclear ROS generation.** (**C**), MLE-12 cells grown in glass bottom dishes to ~60% confluence were transfected with scrambled or NOX4 siRNA (50 nM) for 48 h; cells were transfected with p-Hyper nuclear (3 µg cDNA) for 24 h using Gene Silencer (Genlantis, CA) prior to heat-inactivated *PA* challenge (1 x 10^8 CFU/ml) for 3 h. ROS-dependent p-Hyper fluorescence was measured in a confocal microscope and fluorescence intensity was quantified (**D**) using Image J. as per the manufacturer's instruction. Silencing of NOX4 by siRNA was verified by Western blotting of cell lysates as depicted in (**E**). **NOX2 siRNA has no effect on *PA*-induced nuclear ROS generation. (F),** MLE-12 cells grown in glass bottom dishes to ~60% confluence were transfected with scrambled or NOX2 siRNA (50 nM) for 48 h; cells were transfected with p-Hyper nuclear (3 µg cDNA) for 24 h using Gene Silencer (Genlantis, CA) prior to heat-inactivated *PA* challenge (1 x 10^8 CFU/ml) for 3 h. ROS-dependent p-Hyper fluorescence was measured in a confocal microscope and fluorescence intensity was quantified (**G**) using Image J. as per the manufacturer's instruction. (**H**), Silencing of Nox2 by siRNA was verified by Western blotting.

In MLE-12 cells, inhibition of SphK2 with ABC294640 attenuated *PA*-induced nuclear ROS as determined by p-Hyper nuclear transfection (**Fig 23. A & B**). Similarly, down-regulation of PKC δ with DN-PKC δ also blocked *PA*-mediated nuclear ROS production (**Fig. 23C**).

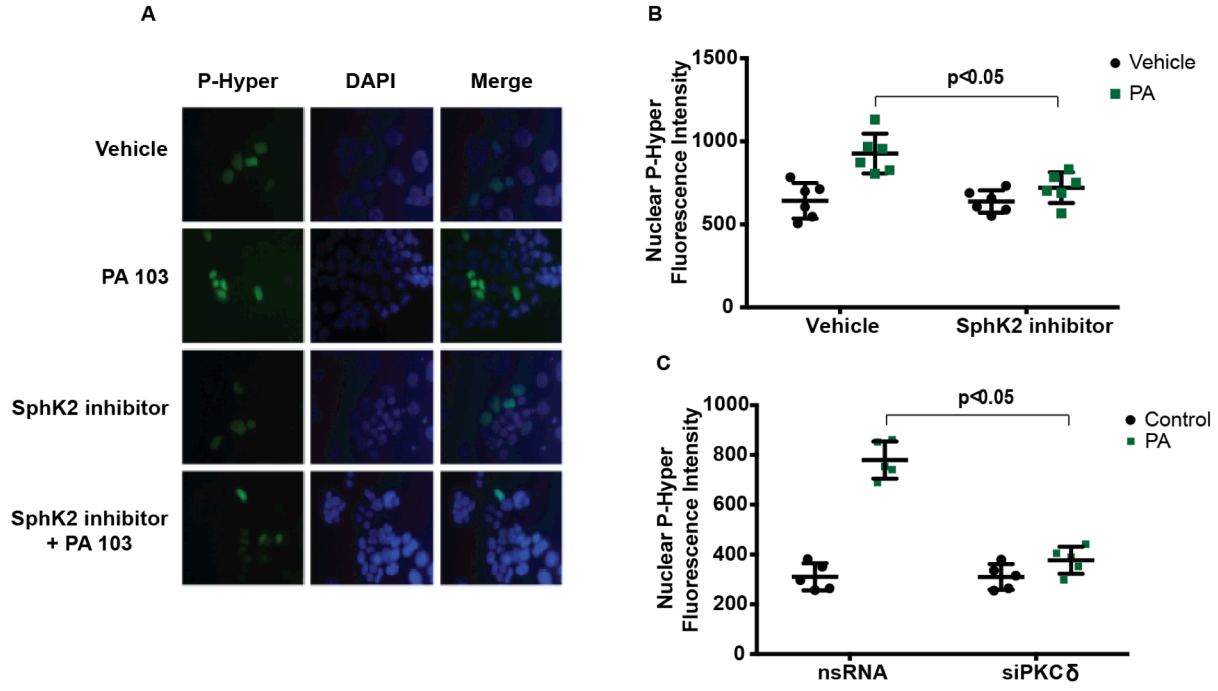

Figure 23: Inhibition of SphK2 with ABC294640 or PKC δ with DN PKC δ attenuated *PA*-induced nuclear ROS production. (**A**), MLE-12 cells grown in glass bottom dishes to ~60% confluence were transfected with p-Hyper nuclear (3 μg cDNA) for 24 h using Gene Silencer (Genlantis, CA); pretreated with SphK2 inhibitor, ABC 294640 (10 μM) for 1 h prior to challenge with heat-inactivated *PA* challenge (1 x 10^8 CFU/ml) for 3 h. ROS-dependent p-Hyper fluorescence was measured in a confocal microscope and fluorescence intensity was quantified (**B**) using Image J. as per the manufacturer's instruction. (**C**), MLE-12 cells grown in glass bottom dishes to ~60% confluence were infected with adenovirus vector control or DN PKC δ adenoviral construct (50 MOI for 48 h), cells were transfected with p-Hyper nuclear (3 μg cDNA) for 24 h using Gene Silencer (Genlantis, CA) prior to heat-inactivated *PA* challenge (1 x 10^8 CFU/ml) for 3 h. ROS-dependent p-Hyper fluorescence was measured in a confocal microscope and fluorescence intensity was quantified (**C**). Inhibition of SphK2 or PKC δ attenuated *PA*-induced nuclear ROS production.

To further corroborate that nuclear ROS generated by *PA* is NOX 4 dependent, we transfected C57BL/6 mice with NOX4 siRNA or NOX2 siRNA (5mg/kg body weight) for 72 h, lung lysate were immunoblotted to see changes in Histone acetylation patterns. *PA* challenge of lung tissues showed enhanced H3 and H4 acetylation, which was blocked by NOX 4 and not NOX 2 siRNA. NOX 4 siRNA also reduced staining of NOX4 in lung epithelium **(Fig. 24 A, B)**. In addition, we also carried out the experiment in MLE-12 cells and found similar results where NOX4 siRNA blocked *PA*-induced histone acetylation **(Fig. 24C)**. To further define the role of NOX 4 in *PA*-induced histone acetylation, we isolated nuclear fractions from primary HBEpCs cells that were transfected with scrambled, NOX4 or NOX 2 siRNA and were immunoprecipitated with HDAC2 antibody. The immuno-precipitates were subjected to protein oxidation detection Assay. *PA* infection caused significant oxidation of HDAC2 that was attenuated by NOX 4 siRNA but not by NOX2 siRNA **(Fig 24 D).** Collectively, these results suggest that Nuclear ROS generated in response to *PA* is NOX 4 and not NOX 2 dependent; Upstream regulators PKC δ and SphK2 regulate NOX4 generated ROS modifies HDAC2 function by oxidation which enhances histone acetylation.

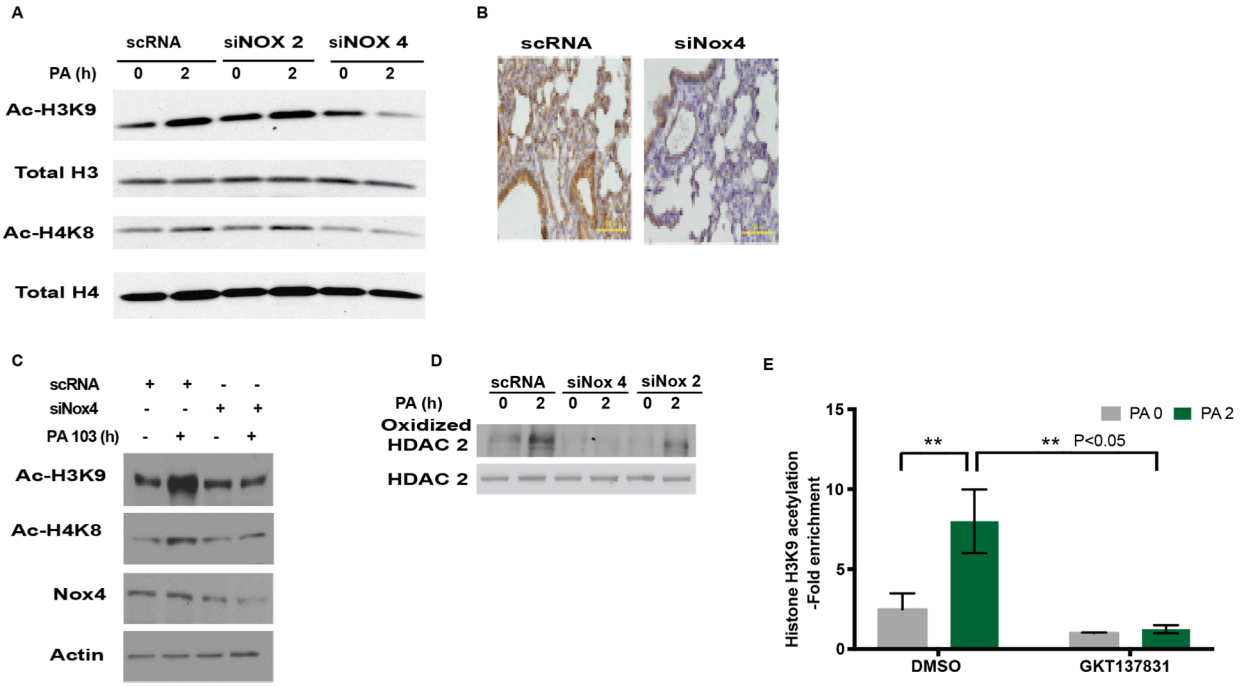

Figure 24: Downregulation of NOX4, but not NOX2, with siRNA attenuated *PA*-induced H3 and H4 histone acetylation *in vivo* and *in vitro* as well as oxidation of HDAC2. (A), C57BL/6J mice were challenged intratracheally with naked NOX4 or NOX2 shRNA (1 μM) or sterile PBS for 72 h prior to challenge with *PA*103 (1 x 10^6 CFU/animal) in a total volume of 50 μl for 24 h. Animals were sacrificed, lungs were removed and frozen in liquid N_2 immediately. Total lysates were lung tissues were subjected to SDS-PAGE and immunostained with anti-acetylated H3 and H4 histone and total H3 and H4 histone antibodies. Shown is a representative Western blot from five lung lysates. (**B**), Paraffin embedded lung tissues from (**A**) were immunostained for NOX4 and shown is a representative immunohistochemistry slide showing reduced immunostaining for NOX4 in shRNA instilled lungs. (**C**), MLE-12 cells grown to ~60% confluence in 35-mm dishes were transfected with scrambled or NOX4 siRNA (50 nM) for 48 h prior to challenge with *PA* (1 x 10^8 CFU/ml) for 3 h. Cell lysates (30 μg proteins) were subjected to SDS-PAGE and immunostained with anti-NOX4, and anti-acetylated H3 and H4 antibodies. Shown is a representative immunoblot of three independent experiments. (**D**), MLE-12 cells grown to ~60% confluence in 100-mm dishes were transfected with scrambled, NOX4 siRNA or NOX2 siRNA (50 nM) for 48 h prior to challenge with *PA* (1 x 10^8 CFU/ml) for 3 h. Cells were trypsinized and nuclei were isolated as described in METHODS. Nuclear extracts (1 mg protein) were subjected to immunoprecipitation with anti-HDAC2 antibody and immunoprecipitates were analyzed for oxidation of carbonyl groups by OxyBlot protein oxidation detection as outlined in METHODS. Shown is a representative OxyBlot immunoblot from three independent experiments in triplicate. (**E**), MLE-12 cells grown in 100-mm dishes (~90% confluence) were pre-treated with NOX4/NOX1 inhibitor, GKT137831 (10 μM) for 1 h prior to heat-inactivated *PA* (1 x 10^8 CFU/ml) challenge for 1 and 2 h. ChIP assays were performed using anti-acetyl histone H3K9 followed by real-time quantitative PCR. Analysis showed that *PA* significantly increased H3K9 histone acetylation at NF-κB sites on IL-6 promoter in 3 h, which was blocked by GKT137831. Data are means ±SD from three independent experiments in triplicate.

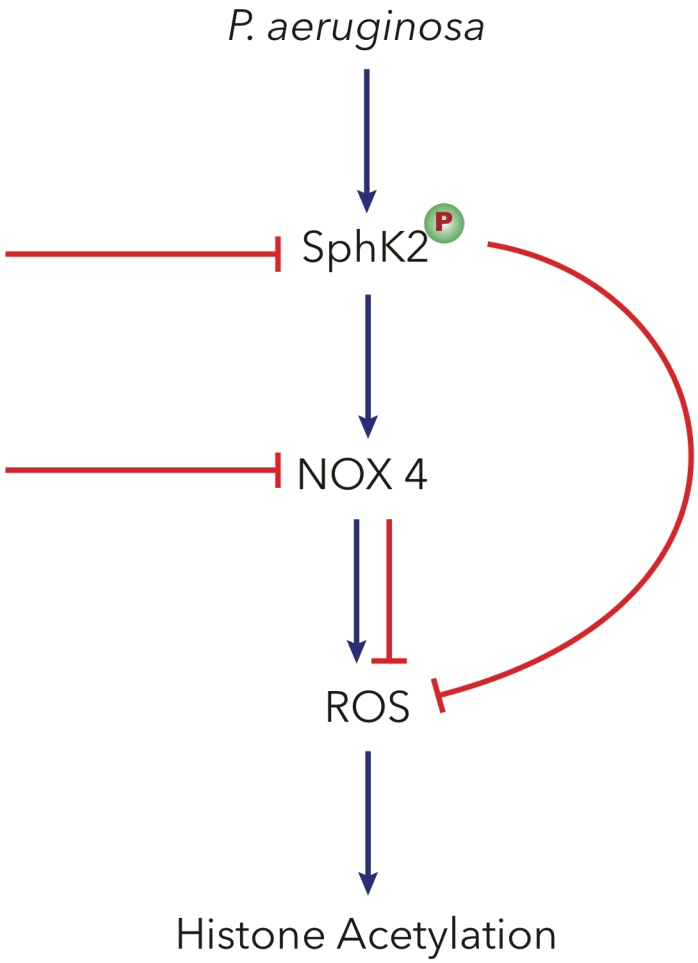

Fig. 25: Schematic diagram showing PA-induced histone acetylation is regulated by SphK2/S1P signaling to stimulate NOX4 dependent ROS generation in the nucleus.

5.1.6 Nuclear co-localization of SphK2 in Cystic fibrosis lung specimens

Cystic fibrosis (CF) patients are plagued with chronic *PA* lung infections, a hallmark of the disease. Changes in sphingolipids levels have been reported in lung tissues and BALF from CF patients and animal models of CF(Aureli et al. 2016) , however, the role of S1P and S1P metabolizing enzymes in CF pathophysiology is unclear. Immunostaining of normal and CF lung tissue specimens with anti-phospho SphK2 antibody (Thr 578) revealed extensive nuclear staining of p-SphK2 in airway and alveolar epithelial cells in CF specimens compared to normal **(Fig. 26)**. On the other hand, normal lungs showed localized p-SphK2 nuclear expression in airway and vascular wall cells, and expression in alveolar septal cells was also less prominent that found in CF samples and more localized staining in endothelial and smooth muscle cells of pulmonary artery. These results in CF lung specimens supported the paradigm in animal and cell culture models that *PA* infection impacts host SphK2 nuclear localization and inflammatory responses.

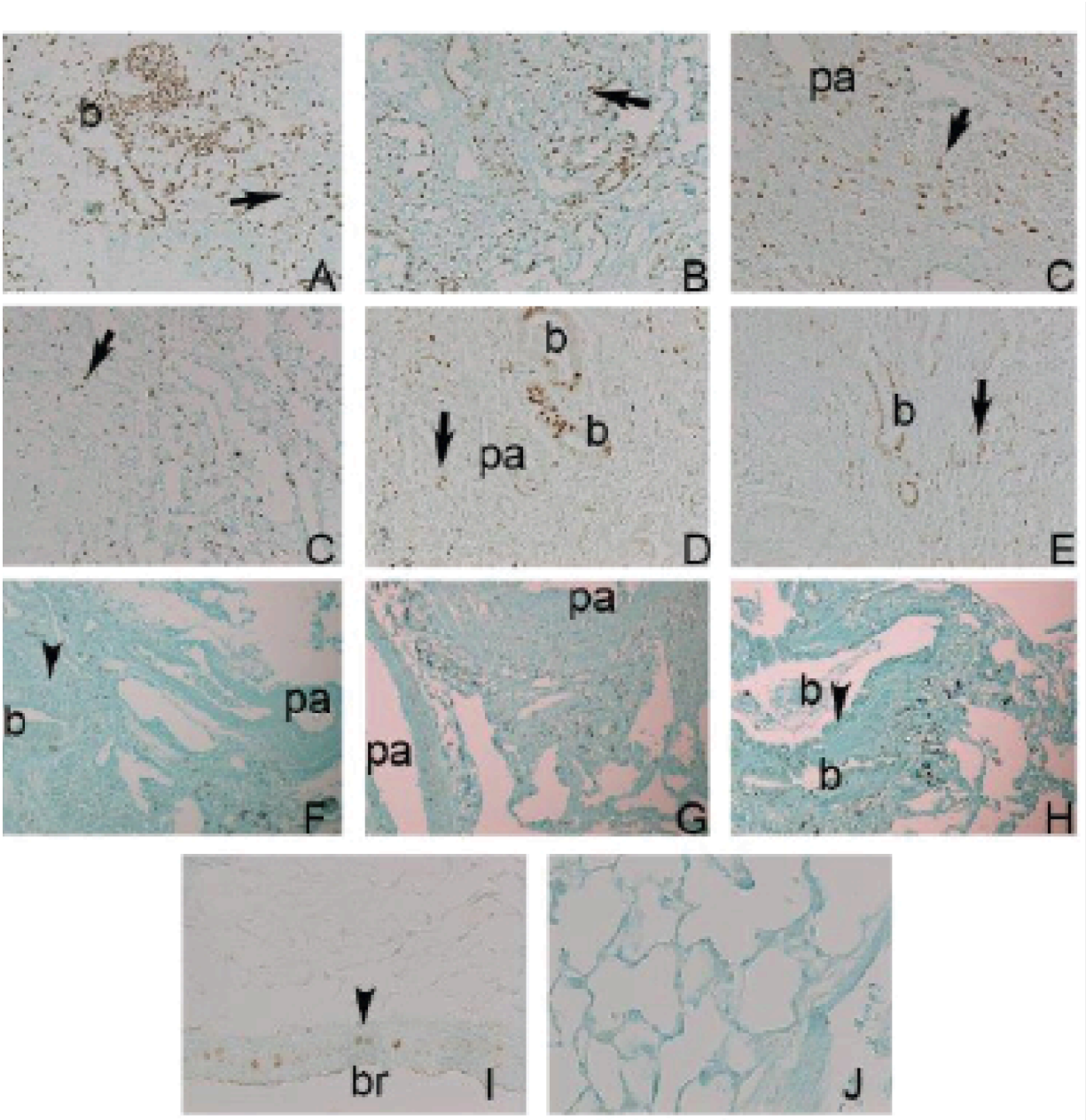

Fig. 26: Nuclear localization of p-SphK2 in cystic fibrosis lung specimens. (**A-E**) Representative fields of six explanted cystic fibrosis lungs showing extensive nuclear SPK-2 staining in airway cells (**B**) and alveolar cells (arrows). There was more localized staining in endothelial and smooth muscle cells of pulmonary arteries (*PA*). (**F-G**) On the other hand, normal lungs (n=6) showed localized SphK2 nuclear expression in airway (**B**) (arrowheads) and vascular wall cells. Expression in alveolar septal cells was also less prominent that that found in CF samples (**G**). Positive (**I**) and knockout negative (**J**) control mouse lungs (Magnification bar= 100 μm)

6. DISCUSSION

Pseudomonas aeruginosa is a common multi-drug resistant, opportunistic, nosocomial pathogen. It is the single most common cause of ventilator-associated pneumonia (Tsay et al. 2016), and is also associated with increased morbidity and mortality. Multi-drug resistance and recurrence makes *PA* infection life threatening, which can lead to rapid lung destruction. Studies have shown elevated levels of IL-6 and TNF-α levels in TLR-4 mediated immune response after *PA* infection (Song et al. 2017). IL-6 has also been shown to be secreted by primary lung epithelial cells in response to various external stimuli (Mattoli, Marini, and Fasoli 1992; Stadnyk 1994),(Yokoyama et al. 1995),(Broide et al. 1992) and elevated IL-6 levels observed in various lung infections contribute to various immuno-modulatory functions (Dienz and Rincon 2009). This pleotropic nature of the immuno-regulatory response suggests a greater role of IL-6 in contributing to lung infection where the epithelium is compromised. IL-6 secretion and its regulation by NF-kB in response to various external stimuli have been well studied; however, the role of sphingolipids in regulating IL-6 secretion and lung inflammation by bacterial infection is not well understood.

Sphingolipids and its metabolites have been implicated for normal cell functions and in the pathogenesis of human diseases including pulmonary disorders (Natarajan et al. 2013),(Ebenezer, Fu, and Natarajan 2016). Among the sphingolipid metabolites, ceramide plays an important role in bacterial lung inflammation, COPD (Lea et al. 2016; Scarpa et al. 2013), and CF (Grassmé et al. 2014; Ziobro et al. 2013). *PA* infection of the lung stimulates acid sphingomyelinase to generate ceramide from sphingomyelin. Previous studies have demonstrated that SphK1/S1P signaling axis contributes to the development of several lung pathologies such as pulmonary fibrosis (Huang et al. 2013; Huang et al. 2015), pulmonary artery hypertension (Chen et al. 2014), and bronchopulmonary dysplasia (Harijith

et al. 2013). In these studies, genetic deletion or inhibition of SphK1, but not SphK2, conferred protection against development of the lung inflammation and injury. In the current study, we have described for the first time a novel role for *PA* mediated activation of SphK2 and generation of nuclear S1P in pulmonary inflammatory injury. S1P is a naturally occurring bioactive sphingolipid that mediates many of the cellular responses via ligation to five G-protein coupled receptors, $S1P_{1-5}$, which are expressed on the plasma membrane of cells (Rivera, Proia, and Olivera 2008). S1P is biosynthesized in mammalian cells by phosphorylation of Sph, catalyzed by SphKs 1 & 2 (Neubauer and Pitson 2013; Gault, Obeid, and Hannun 2010), and catabolized by SPPs and S1P lyase (Neubauer and Pitson 2013). Although both isoforms of SphK catalyze S1P formation from Sph, the sub-cellular localization and expression vary in different cells that dictate spatio-temporal S1P production and function. Two functional nuclear export signal sequences (NES) direct SphK1 localization to the cytosol (Inagaki et al. 2003); in contrast, SphK2 has nuclear import and export sequences, and is found predominantly in the nucleus in many cell types(N. Igarashi et al. 2003). Exposure of mouse lungs to *PA* enhanced ceramide, S1P, and sphingosine levels in lung tissue and BAL fluids at different time points of exposure **(Fig. 5 A-F).** While pathological increase of ceramide levels in the lung after *PA* infection was shown to be associated with apoptosis and cytokine responses, S1P was effective in clearing the mycobacterial burden in a mouse model of Mycobacterium tuberculosis infection (Garg et al. 2004). *PA* infection enhanced nuclear localization of p-SphK2 in alveolar and bronchial epithelial cells and endothelial cells of the mouse lung **(Fig. 12 A-F)**. Lungs of CF patients are chronically infected with *PA* and our current observation of predominant nuclear localization of SphK2 in alveolar and bronchial epithelial cells in CF lung specimens suggest a potential role of nuclear SphK2 in lung inflammation associated with CF (**Fig. 26**). Furthermore, deletion of *Sphk2* increased survival of mice compared to *Sphk1* knock out and

WT animals after PA treatment. There was no variability in the bacterial colony formation after 6 & 24 hours between *Sphk1*$^{-/-}$, *Sphk2*$^{-/-}$ and WT mice (**Fig**. **7K&L**). This probably could be attributed to regulation of the parameters such as phagocytosis and bacterial multiplication influenced by the disease state and other bacterial clearance mechanisms involved in suppression of inflammation as noted in *Sphk2*$^{-/-}$ mice after PA infection. Since the inflammation following *PA* infection is only partially reduced and not completely blocked in *Sphk2*$^{-/-}$ mice, which can explain their extended survival compared to SphK1 and WT mice, even after 72 hours.

A salient feature of this study is the ability of *PA* to induce phosphorylation of the host SphK2 and generate S1P in a spatio-temporal manner in the nucleus of alveolar epithelial cells (**Fig**. **12E**). S1P levels in plasma (0.1 – 1.0 μM) are much higher compared to tissues and interstitial fluids (< 0.1 μM) (Olivera, Allende, and Proia 2013). However, under basal condition, S1P levels are very low in nuclear preparations from lung epithelial (~10 pmoles/mg protein) and breast cancer cell line MCF-7 (~2 pmoles) (Hait et al. 2009) compared to other sphingoid bases. Exposure of mouse embryonic fibroblasts to FTY720, an analog of sphingosine, elevated FTY720-P levels both in the cytoplasm and nuclear fractions (Gardner, Riley, Showker, Voss, Sachs, Maddox, and Gelineau-van Waes 2016a); however, it is unclear if FTY720-P was generated in the nucleus. An important step in generation of nuclear S1P by SphK2 is its phosphorylation and localization in the nucleus in response to a stimulus. Infection of mouse lung or lung epithelial cells with *PA* induced SphK2 phosphorylation and its nuclear localization. Inhibition of SphK2 activity with ABC294640, a specific SphK2 inhibitor, reduced S1P accumulation in the nucleus. SphK2 is localized in the cytoplasm as well as in nucleus of many cell types; however, in MLE-12 cells, SphK2 was predominantly localized in the nucleus, as visualized by immunostaining of the cells (**Fig 12 I&J**). Recent evidences suggest that elevated nuclear S1P and S1P

analogs are linked to increased risk for neural tube defects (Gardner, Riley, Showker, Voss, Sachs, Maddox, and Gelineau-van Waes 2016a; Gardner, Riley, Showker, Voss, Sachs, Maddox, and Gelineau-van Waes 2016b) and neurodegeneration in neuron models of Huntington disease (Moruno-Manchon et al. 2017). Inhibition of SphK2 activity by ABC294640 attenuated *PA*-induced nuclear S1P accumulation and IL-6 generation in lung epithelial cells, thus demonstrating a role of nuclear S1P in bacterial lung inflammation (**Fig 10 E&F)**. Our study has provided ample evidence that SphK2 plays a decisive role in regulating bacterial inflammation in the lung epithelium that makes it a viable therapeutic target. Importantly, the highly selective SphK2 inhibitor, ABC294640 has been shown from previous therapeutic studies that it does not impede immune functions and exhibits low toxicity (Beljanski, Knaak, and Smith 2010; Maines et al. 2010), which makes it an attractive therapeutic tool for the treatment of bacterial lung inflammation. Our study also reinforces the pivotal role of nuclear S1P metabolism in regulating the host immune response and offers an attractive therapeutic option.

Both SphK1 and SphK2 are phosphorylated at Ser/Thr residues by ERK1/2 (Pitson et al. 2003) and PKC (Serrano-Sanchez, Tanfin, and Leiber 2008). *PA* infection of lung epithelial cells stimulated phosphorylation of PKC δ, ε, and ζ and blocked PKC δ activity with DN PKC δ or knockdown of PKC δ with a siRNA attenuated SphK2 phosphorylation in the nucleus and S1P production, suggesting an important role for this PKC isoform in nuclear S1P accumulation after bacterial infection of epithelial cells (**Fig. 17 C-M**). Further, the phosphorylated PKC δ co-localized with SphK2/p-SphK2 in the nucleus of the epithelial cells after *PA* treatment (**Fig. 17 J & K**). . Inhibition of PKC δ or SphK2 attenuated *PA*-induced nuclear S1P accumulation and IL-6 generation in lung epithelial cells, thus demonstrating a role of nuclear S1P in bacterial lung inflammation (**Fig 17 L & M)**.

Acetylation of lysine residues in histones is an epigenetic mark of active gene expression. The interplay between HATs and HDACs, along with other chromatin remodeling factors, tightly regulates gene expression. HDAC 1 and HDAC 2 are the core catalytic components of multi-protein repressor complexes, Sin3 and NuRD that regulate the chromatin structure in response to external stimuli. Previously, PMA induced SphK2 localization with nuclear HDACs 1 & 2 in breast cancer MCF-7 cell line was shown to inhibit HDAC activity through nuclear S1P (Hait et al. 2009). Increased acetylation of histone proteins H3 and H4 on the promoters of pro-inflammatory genes plays a key role in cigarette smoke and lipopolysaccharide-induced lung inflammation (Yao et al. 2010; Borgas et al. 2016); however, signaling mechanisms that regulate chromatin remodeling have not been extensively studied. Altered histone patterns affect chromatin structure and regulation of transcription, and HDACs by removing acetyl marks on histones, silence gene expression. Abundant evidence exists that blocking HDACs by trichostatin A (TSA) heightens NF-κB driven inflammatory gene expression (Ito, Barnes, and Adcock 2000; Ashburner, Westerheide, and Baldwin 2001) (Chen Lf et al. 2001) (Zhong et al. 2002). However, inhibiting HDACs can also affect the function of transcription factors by reversible acetylation, thereby suppressing the expression of genes (M. S. Kim et al. 2001; Nair et al. 2001; Tong, Yin, and Giardina 2004). Also, the consequence of HDAC inhibition on inflammatory cytokines varies by cell type and their response to various stimuli. TSA blocked LPS-induced nitric oxide synthase (NOS 2) in murine macrophages (Yu, Zhang, and Kone 2002) but increased NOS2 expression in microglial cells (Suuronen et al. 2005). Interestingly, HDAC inhibition can differentially affect gene expression in the same cells; HDAC inhibition by TSA increased LPS-stimulated IL-8 but repressed IL-12 levels in BEAS-2B cells (Iwata et al. 2002). While *in vitro* and *in vivo* studies indicate that HDAC inhibitors could be anti-inflammatory by regulating non-histone proteins, they have not been successful in many

clinical trials because of cytotoxicity and the lack of efficacy in treating inflammation (Drummond et al. 2005) (Moradei et al. 2005). Due to non-selective nature of HDAC inhibitors and their multifarious effects on inflammatory gene expression in response to different stimuli, there is a pressing need for selective targeting of HDACs with small molecule inhibitors to modulate inflammation and injury in human diseases. It is intriguing to note in our studies that activated SphK2 regulates the acetylation of lysine 9 in histone H3 and lysine 8 in histone H4, markers of active transcription, in mouse lung and epithelial cells. Changes in histone acetylation patterns also translated to increased gene and protein expression of the inflammatory cytokines IL-6 & TNF-α. Furthermore, we demonstrated *PA*-induced enrichment of Acetyl H3K9 in the IL-6 promoter, which was blocked by SphK2 inhibition (**Fig. 15 G&H)**. We also noted that the activation of PKC δ was paramount in downstream histone acetylation and inflammatory cytokine generation. Also, *PA*-induced PKC δ activation was crucial in the enrichment of histone H3K9 acetylation in the IL-6 promoter region (**Fig.17L**). The critical role played by PKC δ in modulating the epigenetic landscape during a bacterial infection through SphK2 is a novel finding from our studies and opens up selective therapeutic options to target both PKC δ and SphK2 to ameliorate bacterial lung injury.

While it has been reported earlier about the interaction between HDAC and SphK2 and the nuclear S1P inhibiting the HDAC activity in PMA induced cancer cells (Hait et al. 2009), our study for the first time has shown such an interaction occurs during a bacterial infection in the lung. We observed that SphK2/p-SphK2 to be an integral component of the nuclear HDAC repressor complex and blocking SphK2 activity or PKC δ dependent phosphorylation in the nucleus inhibited *PA*-induced H3 and H4 histone acetylation (**Fig. 19 A-E**). We also observed a significant increase in the interaction between HDAC1/2 and p-SphK2 after *PA* treatment and this interaction was crucial in regulating the spatio-

temporal generation of S1P in the nucleus. While the mechanism by which S1P generated in the nucleus regulated HDAC activity is still being investigated, molecular modeling of S1P binding into the active site of HDAC1 homologue from Aquifex aeolicus showed that S1P was docked tightly in the pocket with the highly conserved Arg27 with a predicted binding energy that was comparable to the binding energy of HDAC inhibitor, suberoylanilide hydroxamic acid (SAHA) (Hait et al. 2009). Additionally, *in vitro* competitive binding studies with [^{32}P] S1P showed total displacement of the bound S1P by HDAC inhibitors SAHA and Trichostatin A as well as by unlabeled S1P (Hait et al. 2009). These results suggested that binding of S1P, similar to HDAC inhibitors, directly inhibited HDAC activity. However, binding of S1P generated in the nucleus to HDAC1/2 has not been demonstrated in cells stimulated with an agonist that activate nuclear SphK2.

Another novel finding here is the potential regulation of HDAC1/2 activity by SphK2/S1P signaling via nuclear ROS generation in epithelial cells. Inhibition of SphK2 or knockdown of PKC δ reduced nuclear, but not cytoplasmic or mitochondrial ROS in alveolar epithelial cells **(Fig. 21 A-C)** and histone acetylation **(Fig. 24 A-E**). Our results also showed that *PA* challenge enhanced oxidation/carbonylation of HDAC1 & 2 in alveolar epithelial cells that was blocked by N-acetylcysteine and inhibition of SphK2, or PKC δ **(Fig. 21 D-F)**. Earlier, we have demonstrated that *PA* stimulated NOX2 dependent ROS in mouse lungs and human lung ECs (Fu et al. 2013) and hyperoxia-induced ROS generation in endothelial cells was regulated by S1P (Harijith et al. 2016). Further, several studies have shown that the HDAC activity is regulated by post-translational modifications such as phosphorylation, oxidation, carbonylation, nitration, nitrosylation, acetylation, and SuMoylation (Arana et al. 2013; Colombo et al. 2002). Cigarette smoke-induced oxidative stress stimulated oxidation/carbonylation modification of HDAC2 with decreased HDAC2 level and activity (Ito et al. 2005; Yao and Rahman 2012) while

phenylephrine and pressure overload of cardiac myocytes increased NOX4 dependent cysteine oxidation of HDAC4 and nuclear exit of HDAC4 resulting in cardiac hypertrophy (Matsushima et al. 2012).

Our previous study identified the role of NOX4 in *PA*-induced lung inflammation in endothelium. Here we have extended those findings to delineate the role of NOX4 as a key modulator of epigenetic landscape of inflammatory cytokines. While NOX protein participation in the host defense against bacteria is well documented, the mechanism by which it regulates inflammation remains still unclear. A previous research study has linked the metabolic action of NOX4 to inflammasome activation and pharmacologic inhibition of NOX4/NOX1 by GKT137831 or VAS-2870 attenuated NLRP3 inflammasome activation(Moon et al. 2016) . Here, we show a novel role for NOX 4 in the nucleus, where the ROS generated in response to *PA* infection can act in a spatio-temporal manner to modulate HDAC activity. ROS has been shown to covalently modify two conserved cysteine residues, 261 and 273 leading to diminished HDAC activity and changes in histone acetylation patterns (Doyle and Fitzpatrick 2010). Our data suggest a mechanism by which the SphK2 generated nuclear S1P in turn activates the NOX4 to produce ROS (predominantly H_2O_2) to modify HDACs that regulate the inflammatory cytokine secretion. This mechanism of action of NOX4 mediated nuclear ROS could play a crucial role in orchestrating the inflammatory response in the host by aberrant modification of proteins that regulate the inflammatory signaling.

S1P generated in the nucleus after *PA* infection does not accumulate and could be hydrolysed by SPPs and S1P lyase. Our preliminary studies have identified S1P lyase as a component of epithelial nuclear fraction and *PA* infection of MLE-12 cells enhanced accumulation of *Δ2*-hexadecenal in the nucleus as quantified by LC-MS/MS. *Δ2*-hexadecenal is a long-chain fatty aldehyde, which is very reactive and

can form adducts with nuclear proteins and phosphatidylethanolamine. It is postulated that *Δ2*-hexadecenal reacts with HDACs and modulates its activity, which can be tested both *in vivo* and *in vitro*. Thus, S1P generated in the nucleus via PKCδ►p-SphK2►NOX4►ROS►oxidative modification of HDAC1/2 serves as an epigenetic co-regulator in chromatin remodeling and increased transcription of inflammatory cytokines that regulate lung inflammation and injury.

In summary, our findings collectively support a novel role for nuclear SphK2/S1P signaling for *PA*-mediated ROS generation and pro-inflammatory cytokines secretion by modulation of HDAC1/2 activity via oxidation/carbonylation modification by NOX4 generated ROS. Our results also show the significance of PKC δ activation by *PA* in SphK2 phosphorylation and S1P generation in the nucleus of the epithelium. The clinical significance of our findings is supported by nuclear localization of p-SphK2 in alveolar and bronchial epithelial cells of lung specimens from CF patients chronically infected with *PA*. Further studies are necessary to determine if blocking SphK2 in genetically engineered $Cftr^{\Delta 508}$ KO mice will have a beneficial effect in *PA*-mediated airway inflammation. The anti-inflammatory effect of inhibition of NOX4, PKC δ and SphK2 described here would suggest that targeting NOX4, PKC δ and SphK2 might be a potentially useful therapeutic strategy in ameliorating bacterial lung inflammatory injury.

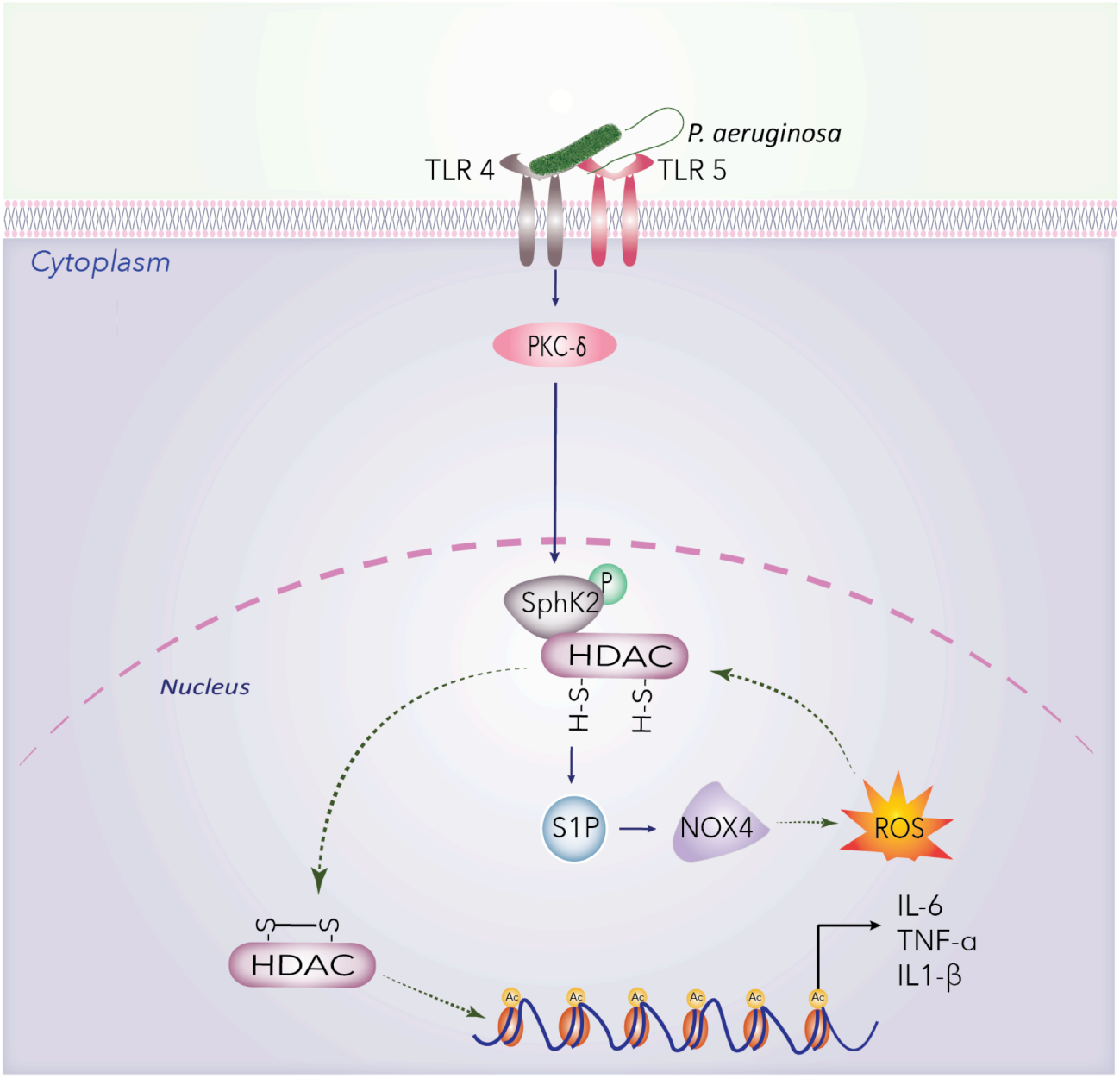

Fig. 27: Proposed model for the role of nuclear SphK2/S1P signaling axis in the epigenetic regulation of *PA*-induced lung inflammation. *P. aeruginosa* infection activates SphK2 through PKC-δ, which generates nuclear S1P. NOX4 is activated by nuclear S1P, which produces ROS. NOX4-generated ROS, which oxidatively modifies HDAC1/2 in the nucleus. Oxidative modification of HADC1/2 inhibits HDAC activity, which enhances histone acetylation, leading to increased expression of pro-inflammatory cytokines such as IL-6 and TNF-α in *PA*-induced bacterial inflammation of the lung. Blocking PKC δ, SphK2 or NOX4 attenuates *PA*-induced lung inflammatory injury.

CITED LITERATURE

Aitken, R J, H M Fisher, N Fulton, E Gomez, W Knox, B Lewis, and S Irvine. 1997. "Reactive Oxygen Species Generation by Human Spermatozoa Is Induced by Exogenous NADPH and Inhibited by the Flavoprotein Inhibitors Diphenylene Iodonium and Quinacrine.." *Molecular Reproduction and Development* 47 (4): 468–82. doi:10.1002/(SICI)1098-2795(199708)47:4<468::AID-MRD14>3.0.CO;2-S.

Alemany, Regina, Chris J van Koppen, Kerstin Danneberg, Michael Ter Braak, and Dagmar Meyer zu Heringdorf. 2007. "Regulation and Functional Roles of Sphingosine Kinases.." *Naunyn-Schmiedeberg's Archives of Pharmacology* 374 (5-6). Springer-Verlag: 413–28. doi:10.1007/s00210-007-0132-3.

Alfred H Merrill, Jr. 2002. "De Novo Sphingolipid Biosynthesis: a Necessary, but Dangerous, Pathway." *The Journal of Biological Chemistry* 277 (29). American Society for Biochemistry and Molecular Biology: 25843–46. doi:10.1074/jbc.R200009200.

Alvarez, Sergio E, Kuzhuvelil B Harikumar, Nitai C Hait, Jeremy Allegood, Graham M Strub, Eugene Y Kim, Michael Maceyka, et al. 2010. "Sphingosine-1-Phosphate Is a Missing Cofactor for the E3 Ubiquitin Ligase TRAF2." *Nature* 465 (7301): 1084–88. doi:10.1038/nature09128.

Amiel, Eyal, Rustin R Lovewell, George A O'Toole, Deborah A Hogan, and Brent Berwin. 2010. "Pseudomonas Aeruginosa Evasion of Phagocytosis Is Mediated by Loss of Swimming Motility and Is Independent of Flagellum Expression.." *Infection and Immunity* 78 (7): 2937–

45. doi:10.1128/IAI.00144-10.

Arana, Lide, Marta Ordoñez, Alberto Ouro, Io-Guané Rivera, Patricia Gangoiti, Miguel Trueba, and Antonio Gomez-Muñoz. 2013. "Ceramide 1-Phosphate Induces Macrophage Chemoattractant Protein-1 Release: Involvement in Ceramide 1-Phosphate-Stimulated Cell Migration." *American Journal of Physiology - Endocrinology and Metabolism* 304 (11). American Physiological Society: E1213–26. doi:10.1152/ajpendo.00480.2012.

Armstrong, Lynne, Andrew R L Medford, Kay M Uppington, John Robertson, Ian R Witherden, Teresa D Tetley, and Ann B Millar. 2004. "Expression of Functional Toll-Like Receptor-2 and -4 on Alveolar Epithelial Cells.." *American Journal of Respiratory Cell and Molecular Biology* 31 (2): 241–45. doi:10.1165/rcmb.2004-0078OC.

Ashburner, B P, S D Westerheide, and A S Baldwin. 2001. "The P65 (RelA) Subunit of NF-kappaB Interacts with the Histone Deacetylase (HDAC) Corepressors HDAC1 and HDAC2 to Negatively Regulate Gene Expression.." *Molecular and Cellular Biology* 21 (20): 7065–77. doi:10.1128/MCB.21.20.7065-7077.2001.

Aureli, Massimo, Domitilla Schiumarini, Nicoletta Loberto, Rosaria Bassi, Anna Tamanini, Giulia Mancini, Matteo Tironi, et al. 2016. "Unravelling the Role of Sphingolipids in Cystic Fibrosis Lung Disease.." *Chemistry and Physics of Lipids* 200 (October): 94–103. doi:10.1016/j.chemphyslip.2016.08.002.

Barkauskas, Christina E, Michael J Cronce, Craig R Rackley, Emily J Bowie, Douglas R Keene, Barry R Stripp, Scott H Randell, Paul W Noble, and Brigid L M Hogan. 2013. "Type 2

Alveolar Cells Are Stem Cells in Adult Lung.." *Journal of Clinical Investigation* 123 (7): 3025–36. doi:10.1172/JCI68782.

Barnes, P J, and M Karin. 1997. "Nuclear Factor-kappaB: a Pivotal Transcription Factor in Chronic Inflammatory Diseases.." Edited by Franklin H Epstein. *New England Journal of Medicine* 336 (15): 1066–71. doi:10.1056/NEJM199704103361506.

Barnes, Peter J. 2008. "Immunology of Asthma and Chronic Obstructive Pulmonary Disease." *Nature Reviews Immunology* 8 (3). Nature Publishing Group: 183–92. doi:10.1038/nri2254.

Barros, S P, and S Offenbacher. 2009. "Epigenetics: Connecting Environment and Genotype to Phenotype and Disease.." *Journal of Dental Research* 88 (5): 400–408. doi:10.1177/0022034509335868.

Bayarsaihan, D. 2010. "Epigenetic Mechanisms in Inflammation." *Journal of Dental Research* 90 (1): 9–17. doi:10.1177/0022034510378683.

Bedard, Karen, and Karl-Heinz Krause. 2007. "The NOX Family of ROS-Generating NADPH Oxidases: Physiology and Pathophysiology.." *Physiological Reviews* 87 (1): 245–313. doi:10.1152/physrev.00044.2005.

Beljanski, Vladimir, Christian Knaak, and Charles D Smith. 2010. "A Novel Sphingosine Kinase Inhibitor Induces Autophagy in Tumor Cells.." *Journal of Pharmacology and Experimental Therapeutics* 333 (2): 454–64. doi:10.1124/jpet.109.163337.

Berdyshev, Evgeny V, Irina A Gorshkova, Peter Usatyuk, Yutong Zhao, Bahman Saatian, Walter Hubbard, and Viswanathan Natarajan. 2006. "De Novo Biosynthesis of

Dihydrosphingosine-1-Phosphate by Sphingosine Kinase 1 in Mammalian Cells.." *Cellular Signalling* 18 (10): 1779–92. doi:10.1016/j.cellsig.2006.01.018.

Berger, M. 1991. "Inflammation in the Lung in Cystic Fibrosis. a Vicious Cycle That Does More Harm Than Good?." *Clinical Reviews in Allergy* 9 (1-2): 119–42.

BLIGH, E G, and W J DYER. 1959. "A Rapid Method of Total Lipid Extraction and Purification.." *Canadian Journal of Biochemistry and Physiology* 37 (8): 911–17. doi:10.1139/o59-099.

Borgas, Diana, Eboni Chambers, Julie Newton, Junsuk Ko, Stephanie Rivera, Sharon Rounds, and Qing Lu. 2016. "Cigarette Smoke Disrupted Lung Endothelial Barrier Integrity and Increased Susceptibility to Acute Lung Injury via Histone Deacetylase 6.." *American Journal of Respiratory Cell and Molecular Biology* 54 (5): 683–96. doi:10.1165/rcmb.2015-0149OC.

Broide, D H, M Lotz, A J Cuomo, D A Coburn, E C Federman, and S I Wasserman. 1992. "Cytokines in Symptomatic Asthma Airways.." *The Journal of Allergy and Clinical Immunology* 89 (5): 958–67.

Campos, Eric I, and Danny Reinberg. 2009. "Histones: Annotating Chromatin.." *Annual Review of Genetics* 43 (1): 559–99. doi:10.1146/annurev.genet.032608.103928.

Chalfant, Charles E, and Sarah Spiegel. 2005. "Sphingosine 1-Phosphate and Ceramide 1-Phosphate: Expanding Roles in Cell Signaling." *Journal of Cell Science* 118 (20). The Company of Biologists Ltd: 4605–12. doi:10.1242/jcs.02637.

Chaube, S K, P V Prasad, S C Thakur, and T G Shrivastav. 2005. "Hydrogen Peroxide

Modulates Meiotic Cell Cycle and Induces Morphological Features Characteristic of Apoptosis in Rat Oocytes Cultured in Vitro.." *Apoptosis* 10 (4): 863–74. doi:10.1007/s10495-005-0367-8.

Chen Lf, W Fischle, E Verdin, and W C Greene. 2001. "Duration of Nuclear NF-kappaB Action Regulated by Reversible Acetylation.." *Science* 293 (5535): 1653–57. doi:10.1126/science.1062374.

Chen, Jiwang, Haiyang Tang, Justin R Sysol, Liliana Moreno-Vinasco, Krystyna M Shioura, Tianji Chen, Irina Gorshkova, et al. 2014. "The Sphingosine Kinase 1/Sphingosine-1-Phosphate Pathway in Pulmonary Arterial Hypertension." *American Journal of Respiratory and Critical Care Medicine*, October. American Thoracic Society. doi:10.1164/rccm.201401-0121OC.

Cheng, Xiaodong, and Robert M Blumenthal. 2010. "Coordinated Chromatin Control: Structural and Functional Linkage of DNA and Histone Methylation.." *Biochemistry* 49 (14): 2999–3008. doi:10.1021/bi100213t.

Chi, Hongbo. 2011. "Sphingosine-1-Phosphate and Immune Regulation: Trafficking and Beyond." *Trends in Pharmacological Sciences* 32 (1): 16–24. doi:10.1016/j.tips.2010.11.002.

Choi, Yong Seok, and Sunjoo Jeong. 2005. "PI3-Kinase and PDK-1 Regulate HDAC1-Mediated Transcriptional Repression of Transcription Factor NF-kappaB.." *Molecules and Cells* 20 (2): 241–46.

Colombo, Riccardo, Roberto Boggio, Christian Seiser, Giulio F Draetta, and Susanna Chiocca.

2002. “The Adenovirus Protein Gam1 Interferes with Sumoylation of Histone Deacetylase 1..” *EMBO Reports* 3 (11): 1062–68. doi:10.1093/embo-reports/kvf213.

de Ruijter, Annemieke J M, Albert H van Gennip, Huib N Caron, Stephan Kemp, and Andre B P van Kuilenburg. 2003. “Histone Deacetylases (HDACs): Characterization of the Classical HDAC Family..” *Biochemical Journal* 370 (Pt 3). Portland Press Ltd: 737–49. doi:10.1042/BJ20021321.

Delcuve, G P, D H Khan, and J R Davie. 2012. “Roles of Histone Deacetylases in Epigenetic Regulation: Emerging Paradigms From Studies with Inhibitors.” *Clin Epigenetics*.

Dempsey, Edward C, Carlyne D Cool, and Cassana M Littler. 2007. “Lung Disease and PKCs..” *Pharmacological Research* 55 (6): 545–59. doi:10.1016/j.phrs.2007.04.010.

Deng, Wu-Guo, Ying Zhu, and Kenneth K Wu. 2004. “Role of P300 and PCAF in Regulating Cyclooxygenase-2 Promoter Activation by Inflammatory Mediators..” *Blood* 103 (6): 2135–42. doi:10.1182/blood-2003-09-3131.

Dienz, Oliver, and Mercedes Rincon. 2009. “The Effects of IL-6 on CD4 T Cell Responses..” *Clinical Immunology (Orlando, Fla.)* 130 (1): 27–33. doi:10.1016/j.clim.2008.08.018.

Dong, Xianjun, and Zhiping Weng. 2013. “The Correlation Between Histone Modifications and Gene Expression..” *Epigenomics* 5 (2): 113–16. doi:10.2217/epi.13.13.

Doyle, Kelly, and F A Fitzpatrick. 2010. “Redox Signaling, Alkylation (Carbonylation) of Conserved Cysteines Inactivates Class I Histone Deacetylases 1, 2, and 3 and Antagonizes Their Transcriptional Repressor Function..” *Journal of Biological Chemistry* 285 (23): 17417–

24. doi:10.1074/jbc.M109.089250.

Driscoll, James A, Steven L Brody, and Marin H Kollef. 2007. "The Epidemiology, Pathogenesis and Treatment of Pseudomonas Aeruginosa Infections." *Drugs* 67 (3). Springer International Publishing: 351–68. doi:10.2165/00003495-200767030-00003.

Drummond, Daryl C, Charles O Noble, Dmitri B Kirpotin, Zexiong Guo, Gary K Scott, and Christopher C Benz. 2005. "Clinical Development of Histone Deacetylase Inhibitors as Anticancer Agents.." *Annual Review of Pharmacology and Toxicology* 45 (1): 495–528. doi:10.1146/annurev.pharmtox.45.120403.095825.

Ebenezer, David L, Panfeng Fu, and Viswanathan Natarajan. 2016. "Targeting Sphingosine-1-Phosphate Signaling in Lung Diseases.." *Pharmacology & Therapeutics* 168 (December): 143–57. doi:10.1016/j.pharmthera.2016.09.008.

Elborn, J S, S M Cordon, D Parker, F M Delamere, and D J Shale. 1993. "The Host Inflammatory Response Prior to Death in Patients with Cystic Fibrosis and Chronic Pseudomonas Aeruginosa Infection.." *Respiratory Medicine* 87 (8): 603–7.

Elsharkawy, Ahmed M, Fiona Oakley, Feng Lin, Graham Packham, Derek A Mann, and Jelena Mann. 2010. "The NF-kappaB P50:P50:HDAC-1 Repressor Complex Orchestrates Transcriptional Inhibition of Multiple Pro-Inflammatory Genes.." *Journal of Hepatology* 53 (3): 519–27. doi:10.1016/j.jhep.2010.03.025.

Epelman, Slava, Danuta Stack, Chris Bell, Erica Wong, Graham G Neely, Stephan Krutzik, Kensuke Miyake, et al. 2004. "Different Domains of Pseudomonas Aeruginosa Exoenzyme

S Activate Distinct TLRs.." *Journal of Immunology (Baltimore, Md. : 1950)* 173 (3): 2031–40.

Ferreira, Julio Cesar Batista, Patricia Chakur Brum, and Daria Mochly-Rosen. 2011. "βIIPKC and εPKC Isozymes as Potential Pharmacological Targets in Cardiac Hypertrophy and Heart Failure.." *Journal of Molecular and Cellular Cardiology* 51 (4): 479–84. doi:10.1016/j.yjmcc.2010.10.020.

Fischer, Horst. 2009. "Mechanisms and Function of DUOX in Epithelia of the Lung.." *Antioxidants & Redox Signaling* 11 (10): 2453–65. doi:10.1089/ars.2009.2558.

Foster, Simmie L, Diana C Hargreaves, and Ruslan Medzhitov. 2007. "Gene-Specific Control of Inflammation by TLR-Induced Chromatin Modifications.." *Nature* 447 (7147): 972–78. doi:10.1038/nature05836.

Fu, Panfeng, Vijay Mohan, Syed Mansoor, Chinnaswamy Tiruppathi, Ruxana T Sadikot, and Viswanathan Natarajan. 2013. "Role of Nicotinamide Adenine Dinucleotide Phosphate–Reduced Oxidase Proteins in Pseudomonas Aeruginosa–Induced Lung Inflammation and Permeability." *American Journal of Respiratory Cell and Molecular Biology*, April. American Thoracic Society. doi:10.1165/rcmb.2012-0242OC.

Fuchs, Jörg, Dmitri Demidov, Andreas Houben, and Ingo Schubert. 2006. "Chromosomal Histone Modification Patterns--From Conservation to Diversity.." *Trends in Plant Science* 11 (4): 199–208. doi:10.1016/j.tplants.2006.02.008.

Garcia, J G, F Liu, A D Verin, A Birukova, M A Dechert, W T Gerthoffer, J R Bamberg, and D English. 2001. "Sphingosine 1-Phosphate Promotes Endothelial Cell Barrier Integrity by

Edg-Dependent Cytoskeletal Rearrangement.." *Journal of Clinical Investigation* 108 (5). American Society for Clinical Investigation: 689–701. doi:10.1172/JCI12450.

Gardner, Nicole M, Ronald T Riley, Jency L Showker, Kenneth A Voss, Andrew J Sachs, Joyce R Maddox, and Janee B Gelineau-van Waes. 2016a. "Elevated Nuclear and Cytoplasmic FTY720-Phosphate in Mouse Embryonic Fibroblasts Suggests the Potential for Multiple Mechanisms in FTY720-Induced Neural Tube Defects.." *Toxicological Sciences : an Official Journal of the Society of Toxicology* 150 (1): 161–68. doi:10.1093/toxsci/kfv321.

Gardner, Nicole M, Ronald T Riley, Jency L Showker, Kenneth A Voss, Andrew J Sachs, Joyce R Maddox, and Janee B Gelineau-van Waes. 2016b. "Elevated Nuclear Sphingoid Base-1-Phosphates and Decreased Histone Deacetylase Activity After Fumonisin B1 Treatment in Mouse Embryonic Fibroblasts.." *Toxicology and Applied Pharmacology* 298 (May): 56–65. doi:10.1016/j.taap.2016.02.018.

Garg, Sanjay K, Elisabetta Volpe, Graziana Palmieri, Maurizio Mattei, Domenico Galati, Angelo Martino, Maria S Piccioni, et al. 2004. "Sphingosine 1-Phosphate Induces Antimicrobial Activity Both in Vitro and in Vivo.." *The Journal of Infectious Diseases* 189 (11): 2129–38. doi:10.1086/386286.

Gault, Christopher R, Lina M Obeid, and Yusuf A Hannun. 2010. "An Overview of Sphingolipid Metabolism: From Synthesis to Breakdown." In *Sphingolipids as Signaling and Regulatory Molecules*, 688:1–23. Advances in Experimental Medicine and Biology. New York, NY: Springer, New York, NY. doi:10.1007/978-1-4419-6741-1_1.

Gilchrist, Mark, Vesteinn Thorsson, Bin Li, Alistair G Rust, Martin Korb, Jared C Roach, Kathleen Kennedy, Tsonwin Hai, Hamid Bolouri, and Alan Aderem. 2006. "Systems Biology Approaches Identify ATF3 as a Negative Regulator of Toll-Like Receptor 4.." *Nature* 441 (7090): 173–78. doi:10.1038/nature04768.

Grassmé, Heike, Alexander Carpinteiro, Michael J Edwards, Erich Gulbins, and Katrin Anne Becker. 2014. "Regulation of the Inflammasome by Ceramide in Cystic Fibrosis Lungs.." *Cellular Physiology and Biochemistry* 34 (1): 45–55. doi:10.1159/000362983.

Gregoretti, Ivan V, Yun-Mi Lee, and Holly V Goodson. 2004. "Molecular Evolution of the Histone Deacetylase Family: Functional Implications of Phylogenetic Analysis.." *Journal of Molecular Biology* 338 (1): 17–31. doi:10.1016/j.jmb.2004.02.006.

Hait, Nitai C, Jeremy Allegood, Michael Maceyka, Graham M Strub, Kuzhuvelil B Harikumar, Sandeep K Singh, Cheng Luo, et al. 2009. "Regulation of Histone Acetylation in the Nucleus by Sphingosine-1-Phosphate." *Science Signaling* 325 (5945). AAAS: 1254–pe1. doi:10.1126/science.1176709.

Hajjar, Adeline M, Robert K Ernst, Jeff H Tsai, Christopher B Wilson, and Samuel I Miller. 2002. "Human Toll-Like Receptor 4 Recognizes Host-Specific LPS Modifications.." *Nature Immunology* 3 (4): 354–59. doi:10.1038/ni777.

Harijith, Anantha, Srikanth Pendyala, David L Ebenezer, Alison W Ha, Panfeng Fu, Yue-Ting Wang, Ke Ma, et al. 2016. "Hyperoxia-Induced P47phox Activation and ROS Generation Is Mediated Through S1P Transporter Spns2, and S1P/S1P1&Amp;2 Signaling Axis in Lung

Endothelium." *American Journal of Physiology - Lung Cellular and Molecular Physiology* 311 (2). American Physiological Society: L337–51. doi:10.1152/ajplung.00447.2015.

Harijith, Anantha, Srikanth Pendyala, Narsa M Reddy, Tao Bai, Peter V Usatyuk, Evgeny Berdyshev, Irina Gorshkova, et al. 2013. "Sphingosine Kinase 1 Deficiency Confers Protection Against Hyperoxia-Induced Bronchopulmonary Dysplasia in a Murine Model: Role of S1P Signaling and Nox Proteins.." *The American Journal of Pathology* 183 (4): 1169–82. doi:10.1016/j.ajpath.2013.06.018.

Hayashi, F, K D Smith, A Ozinsky, T R Hawn, E C Yi, D R Goodlett, J K Eng, S Akira, D M Underhill, and A Aderem. 2001. "The Innate Immune Response to Bacterial Flagellin Is Mediated by Toll-Like Receptor 5.." *Nature* 410 (6832): 1099–1103. doi:10.1038/35074106.

Hla, Timothy. 2001. "Sphingosine 1-Phosphate Receptors." *Prostaglandins & Other Lipid Mediators* 64 (1-4): 135–42. doi:10.1016/S0090-6980(01)00109-5.

Huang, Long Shuang, Evgeny Berdyshev, Biji Mathew, Panfeng Fu, Irina A Gorshkova, Donghong He, Wenli Ma, et al. 2013. "Targeting Sphingosine Kinase 1 Attenuates Bleomycin-Induced Pulmonary Fibrosis." *FASEB Journal : Official Publication of the Federation of American Societies for Experimental Biology* 27 (4). Federation of American Societies for Experimental Biology: 1749–60. doi:10.1096/fj.12-219634.

Huang, Long Shuang, Evgeny V Berdyshev, John T Tran, Lishi Xie, Jiwang Chen, David L Ebenezer, Biji Mathew, et al. 2015. "Sphingosine-1-Phosphate Lyase Is an Endogenous Suppressor of Pulmonary Fibrosis: Role of S1P Signalling and Autophagy.." *Thorax* 70 (12):

1138–48. doi:10.1136/thoraxjnl-2014-206684.

Igarashi, Nobuaki, Taro Okada, Shun Hayashi, Toshitada Fujita, Saleem Jahangeer, and Shun-ichi Nakamura. 2003. "Sphingosine Kinase 2 Is a Nuclear Protein and Inhibits DNA Synthesis." *The Journal of Biological Chemistry* 278 (47). American Society for Biochemistry and Molecular Biology: 46832–39. doi:10.1074/jbc.M306577200.

Inagaki, Yuichi, Pei-Yun Li, Atsushi Wada, Susumu Mitsutake, and Yasuyuki Igarashi. 2003. "Identification of Functional Nuclear Export Sequences in Human Sphingosine Kinase 1.." *Biochemical and Biophysical Research Communications* 311 (1): 168–73.

Ito, K, P J Barnes, and I M Adcock. 2000. "Glucocorticoid Receptor Recruitment of Histone Deacetylase 2 Inhibits Interleukin-1beta-Induced Histone H4 Acetylation on Lysines 8 and 12.." *Molecular and Cellular Biology* 20 (18). American Society for Microbiology (ASM): 6891–6903.

Ito, Kazuhiro, Misako Ito, W Mark Elliott, Borja Cosio, Gaetano Caramori, Onn Min Kon, Adam Barczyk, et al. 2005. "Decreased Histone Deacetylase Activity in Chronic Obstructive Pulmonary Disease.." *New England Journal of Medicine* 352 (19): 1967–76. doi:10.1056/NEJMoa041892.

Iwata, Kyoko, Katsuyuki Tomita, Hiroyuki Sano, Yoshihiro Fujii, Akira Yamasaki, and Eiji Shimizu. 2002. "Trichostatin a, a Histone Deacetylase Inhibitor, Down-Regulates Interleukin-12 Transcription in SV-40-Transformed Lung Epithelial Cells.." *Cellular Immunology* 218 (1-2): 26–33.

Kawahara, Atsuo, Tsuyoshi Nishi, Yu Hisano, Hajime Fukui, Akihito Yamaguchi, and Naoki Mochizuki. 2009. "The Sphingolipid Transporter Spns2 Functions in Migration of Zebrafish Myocardial Precursors.." *Science* 323 (5913). American Association for the Advancement of Science: 524–27. doi:10.1126/science.1167449.

Kiernan, Rosemary, Vanessa Brès, Raymond W M Ng, Marie-Pierre Coudart, Selma El Messaoudi, Claude Sardet, Dong-Yan Jin, Stephane Emiliani, and Monsef Benkirane. 2003. "Post-Activation Turn-Off of NF-Kappa B-Dependent Transcription Is Regulated by Acetylation of P65.." *The Journal of Biological Chemistry* 278 (4): 2758–66. doi:10.1074/jbc.M209572200.

Kim, M S, H J Kwon, Y M Lee, J H Baek, J E Jang, S W Lee, E J Moon, et al. 2001. "Histone Deacetylases Induce Angiogenesis by Negative Regulation of Tumor Suppressor Genes.." *Nature Medicine* 7 (4): 437–43. doi:10.1038/86507.

Kim, Roger H, Kazuaki Takabe, Sheldon Milstien, and Sarah Spiegel. 2009. "Export and Functions of Sphingosine-1-Phosphate.." *Biochimica Et Biophysica Acta* 1791 (7): 692–96. doi:10.1016/j.bbalip.2009.02.011.

Kobayashi, Naoki, Nobuyoshi Kobayashi, Akihito Yamaguchi, and Tsuyoshi Nishi. 2009. "Characterization of the ATP-Dependent Sphingosine 1-Phosphate Transporter in Rat Erythrocytes.." *The Journal of Biological Chemistry* 284 (32). American Society for Biochemistry and Molecular Biology: 21192–200. doi:10.1074/jbc.M109.006163.

Koyanagi, Tomoyoshi, Kenichiro Noguchi, Akifumi Ootani, Koichi Inagaki, Robert C Robbins,

and Daria Mochly-Rosen. 2007. "Pharmacological Inhibition of Epsilon PKC Suppresses Chronic Inflammation in Murine Cardiac Transplantation Model.." *Journal of Molecular and Cellular Cardiology* 43 (4): 517–22. doi:10.1016/j.yjmcc.2007.06.003.

Lea, Simon R, Hannah J Metcalfe, Jonathan Plumb, Christian Beerli, Chris Poll, Dave Singh, and Katharine H Abbott-Banner. 2016. "Neutral Sphingomyelinase-2, Acid Sphingomyelinase, and Ceramide Levels in COPD Patients Compared to Controls.." *International Journal of Chronic Obstructive Pulmonary Disease* 11: 2139–47. doi:10.2147/COPD.S95578.

Lee, Jen-Fu, Qun Zeng, Harunobu Ozaki, Lichun Wang, Arthur R Hand, Timothy Hla, Eugenia Wang, and Menq-Jer Lee. 2006. "Dual Roles of Tight Junction-Associated Protein, Zonula Occludens-1, in Sphingosine 1-Phosphate-Mediated Endothelial Chemotaxis and Barrier Integrity." *The Journal of Biological Chemistry* 281 (39). American Society for Biochemistry and Molecular Biology: 29190–200. doi:10.1074/jbc.M604310200.

Lee, M J, S Thangada, K P Claffey, N Ancellin, C H Liu, M Kluk, M Volpi, R I Sha'afi, and T Hla. 1999. "Vascular Endothelial Cell Adherens Junction Assembly and Morphogenesis Induced by Sphingosine-1-Phosphate.." *Cell* 99 (3): 301–12.

Lee, Menq-Jer, Shobha Thangada, Ji-Hye Paik, Gopal P Sapkota, Nicolas Ancellin, Sung-Suk Chae, Mingtao Wu, et al. 2001. "Akt-Mediated Phosphorylation of the G Protein-Coupled Receptor EDG-1 Is Required for Endothelial Cell Chemotaxis." *Molecular Cell* 8 (3): 693–704. doi:10.1016/S1097-2765(01)00324-0.

Lee, Min Gyu, Christopher Wynder, Neil Cooch, and Ramin Shiekhattar. 2005. "An Essential Role for CoREST in Nucleosomal Histone 3 Lysine 4 Demethylation.." *Nature* 437 (7057): 432–35. doi:10.1038/nature04021.

Levkau, Bodo. 2008. "Sphingosine-1-Phosphate in the Regulation of Vascular Tone: a Finely Tuned Integration System of S1P Sources, Receptors, and Vascular Responsiveness.." *Circulation Research* 103 (3). Lippincott Williams & Wilkins: 231–33. doi:10.1161/CIRCRESAHA.108.181610.

Liu, Hong, Rachelle E Toman, Sravan K Goparaju, Michael Maceyka, Victor E Nava, Heidi Sankala, Shawn G Payne, et al. 2003. "Sphingosine Kinase Type 2 Is a Putative BH3-Only Protein That Induces Apoptosis.." *The Journal of Biological Chemistry* 278 (41). American Society for Biochemistry and Molecular Biology: 40330–36. doi:10.1074/jbc.M304455200.

Lu, Jun, Haijing Sun, Xiuli Wang, Chunyan Liu, Xin Xu, Fen Li, and Baiqu Huang. 2005. "Interleukin-12 P40 Promoter Activity Is Regulated by the Reversible Acetylation Mediated by HDAC1 and P300.." *Cytokine* 31 (1): 46–51. doi:10.1016/j.cyto.2005.03.001.

Maines, Lynn W, Leo R Fitzpatrick, Cecelia L Green, Yan Zhuang, and Charles D Smith. 2010. "Efficacy of a Novel Sphingosine Kinase Inhibitor in Experimental Crohn's Disease.." *Inflammopharmacology* 18 (2): 73–85. doi:10.1007/s10787-010-0032-x.

Marks, P, R A Rifkind, V M Richon, R Breslow, T Miller, and W K Kelly. 2001. "Histone Deacetylases and Cancer: Causes and Therapies.." *Nature Reviews Cancer* 1 (3): 194–202. doi:10.1038/35106079.

Martin, Francis J, and Alice S Prince. 2008. "TLR2 Regulates Gap Junction Intercellular Communication in Airway Cells.." *Journal of Immunology (Baltimore, Md. : 1950)* 180 (7). NIH Public Access: 4986–93.

Matsushima, Shouji, Junya Kuroda, Tetsuro Ago, Peiyong Zhai, Ji Yeon Park, Lai-Hua Xie, Bin Tian, and Junichi Sadoshima. 2012. "Increased Oxidative Stress in the Nucleus Caused by Nox4 Mediates Oxidation of HDAC4 and Cardiac Hypertrophy." *Circulation Research* 112 (4). American Heart Association, Inc.: CIRCRESAHA.112.279760–663. doi:10.1161/CIRCRESAHA.112.279760.

Mattoli, S, M Marini, and A Fasoli. 1992. "Expression of the Potent Inflammatory Cytokines, GM-CSF, IL6, and IL8, in Bronchial Epithelial Cells of Asthmatic Patients.." *Chest* 101 (3 Suppl): 27S–29S.

Maturana, Andrés, Karl-Heinz Krause, and Nicolas Demaurex. 2002. "NOX Family NADPH Oxidases: Do They Have Built-in Proton Channels?." *The Journal of General Physiology* 120 (6). The Rockefeller University Press: 781–86. doi:10.1085/jgp.20028713.

McKenzie, Casey W, Joshua M Klonoski, Taylor Maier, Glenda Trujillo, Peter F Vitiello, Victor C Huber, and Lance Lee. 2013. "Enhanced Response to Pulmonary Streptococcus Pneumoniae Infection Is Associated with Primary Ciliary Dyskinesia in Mice Lacking Pcdp1 and Spef2.." *Cilia* 2 (1): 18. doi:10.1186/2046-2530-2-18.

Medzhitov, Ruslan, and Tiffany Horng. 2009. "Transcriptional Control of the Inflammatory Response.." *Nature Reviews Immunology* 9 (10): 692–703. doi:10.1038/nri2634.

Mehta, Dolly, Maria Konstantoulaki, Gias U Ahmmed, and Asrar B Malik. 2005. "Sphingosine 1-Phosphate-Induced Mobilization of Intracellular Ca2+ Mediates Rac Activation and Adherens Junction Assembly in Endothelial Cells." *The Journal of Biological Chemistry* 280 (17). American Society for Biochemistry and Molecular Biology: 17320–28. doi:10.1074/jbc.M411674200.

Melendez, A J, E Carlos-Dias, M Gosink, J M Allen, and L Takacs. 2000. "Human Sphingosine Kinase: Molecular Cloning, Functional Characterization and Tissue Distribution.." *Gene* 251 (1): 19–26.

Mitra, Poulami, Carole A Oskeritzian, Shawn G Payne, Michael A Beaven, Sheldon Milstien, and Sarah Spiegel. 2006. "Role of ABCC1 in Export of Sphingosine-1-Phosphate From Mast Cells.." *Proceedings of the National Academy of Sciences of the United States of America* 103 (44). National Acad Sciences: 16394–99. doi:10.1073/pnas.0603734103.

Mitsutake, Susumu, Tack-Joong Kim, and Yasuyuki Igarashi. 2006. "Ceramide 1-Phosphate." In *Sphingolipid Biology*, 207–18. Springer Japan. doi:10.1007/4-431-34200-1_15.

Mizugishi, Kiyomi, Tadashi Yamashita, Ana Olivera, Georgina F Miller, Sarah Spiegel, and Richard L Proia. 2005. "Essential Role for Sphingosine Kinases in Neural and Vascular Development." *Molecular and Cellular Biology* 25 (24). American Society for Microbiology: 11113–21. doi:10.1128/MCB.25.24.11113-11121.2005.

Mochly-Rosen, D, and A S Gordon. 1998. "Anchoring Proteins for Protein Kinase C: a Means for Isozyme Selectivity.." *FASEB Journal : Official Publication of the Federation of American*

Societies for Experimental Biology 12 (1): 35–42.

Mochly-Rosen, Daria, Kanad Das, and Kevin V Grimes. 2012. "Protein Kinase C, an Elusive Therapeutic Target?." *Nature Reviews Drug Discovery* 11 (12): 937–57. doi:10.1038/nrd3871.

Monick, Martha M, Timur O Yarovinsky, Linda S Powers, Noah S Butler, A Brent Carter, Gunnar Gudmundsson, and Gary W Hunninghake. 2003. "Respiratory Syncytial Virus Up-Regulates TLR4 and Sensitizes Airway Epithelial Cells to Endotoxin.." *The Journal of Biological Chemistry* 278 (52): 53035–44. doi:10.1074/jbc.M308093200.

Moon, Jong-Seok, Kiichi Nakahira, Kuei-Pin Chung, Gina M DeNicola, Michael Jakun Koo, Maria A Pabón, Kristen T Rooney, et al. 2016. "NOX4-Dependent Fatty Acid Oxidation Promotes NLRP3 Inflammasome Activation in Macrophages.." *Nature Medicine* 22 (9): 1002–12. doi:10.1038/nm.4153.

Moradei, Oscar, Christiane R Maroun, Isabelle Paquin, and Arkadii Vaisburg. 2005. "Histone Deacetylase Inhibitors: Latest Developments, Trends and Prospects.." *Current Medicinal Chemistry. Anti-Cancer Agents* 5 (5): 529–60.

Morrell, Craig N. 2008. "Reactive Oxygen Species: Finding the Right Balance.." *Circulation Research* 103 (6): 571–72. doi:10.1161/CIRCRESAHA.108.184325.

Moruno-Manchon, Jose F, Ndidi-Ese Uzor, Maria P Blasco-Conesa, Sishira Mannuru, Nagireddy Putluri, Erin E Furr-Stimming, and Andrey S Tsvetkov. 2017. "Inhibiting Sphingosine Kinase 2 Mitigates Mutant Huntingtin-Induced Neurodegeneration in Neuron Models of Huntington Disease.." *Human Molecular Genetics* 26 (7): 1305–17.

doi:10.1093/hmg/ddx046.

Nair, A R, L J Boersma, L Schiltz, M A Chaudhry, R J Muschel, and A Chaudry. 2001. "Paradoxical Effects of Trichostatin a: Inhibition of NF-Y-Associated Histone Acetyltransferase Activity, Phosphorylation of hGCN5 and Downregulation of Cyclin a and B1 mRNA.." *Cancer Letters* 166 (1): 55–64.

Natarajan, Viswanathan, Steven M Dudek, Jeffrey R Jacobson, Liliana Moreno-Vinasco, Long Shuang Huang, Taimur Abassi, Biji Mathew, et al. 2013. "Sphingosine-1–Phosphate, FTY720, and Sphingosine-1–Phosphate Receptors in the Pathobiology of Acute Lung Injury." *American Journal of Respiratory Cell and Molecular Biology*, July. American Thoracic Society. doi:10.1165/rcmb.2012-0411TR.

Neubauer, Heidi A, and Stuart M Pitson. 2013. "Roles, Regulation and Inhibitors of Sphingosine Kinase 2.." *The FEBS Journal* 280 (21): 5317–36. doi:10.1111/febs.12314.

Nusinzon, Inna, and Curt M Horvath. 2006. "Positive and Negative Regulation of the Innate Antiviral Response and Beta Interferon Gene Expression by Deacetylation.." *Molecular and Cellular Biology* 26 (8): 3106–13. doi:10.1128/MCB.26.8.3106-3113.2006.

Oliver, A, and A Mena. 2010. "Bacterial Hypermutation in Cystic Fibrosis, Not Only for Antibiotic Resistance.." *Clinical Microbiology and Infection : the Official Publication of the European Society of Clinical Microbiology and Infectious Diseases* 16 (7): 798–808. doi:10.1111/j.1469-0691.2010.03250.x.

Olivera, Ana, Maria Laura Allende, and Richard L Proia. 2013. "Shaping the Landscape:

Metabolic Regulation of S1P Gradients." *Biochimica Et Biophysica Acta (BBA) - Molecular and Cell Biology of Lipids* 1831 (1): 193–202. doi:10.1016/j.bbalip.2012.06.007.

Olivera, Ana, Takafumi Kohama, Lisa Edsall, Victor Nava, Olivier Cuvillier, Samantha Poulton, and Sarah Spiegel. 1999. "Sphingosine Kinase Expression Increases Intracellular Sphingosine-1-Phosphate and Promotes Cell Growth and Survival." *The Journal of Cell Biology* 147 (3). Rockefeller Univ Press: 545–58. doi:10.1083/jcb.147.3.545.

Osoata, Grace O, Satoshi Yamamura, Misako Ito, Chaitanya Vuppusetty, Ian M Adcock, Peter J Barnes, and Kazuhiro Ito. 2009. "Nitration of Distinct Tyrosine Residues Causes Inactivation of Histone Deacetylase 2.." *Biochemical and Biophysical Research Communications* 384 (3): 366–71. doi:10.1016/j.bbrc.2009.04.128.

Panneer Selvam, Shanmugam, Ryan M De Palma, Joshua J Oaks, Natalia Oleinik, Yuri K Peterson, Robert V Stahelin, Emmanuel Skordalakes, et al. 2015. "Binding of the Sphingolipid S1P to hTERT Stabilizes Telomerase at the Nuclear Periphery by Allosterically Mimicking Protein Phosphorylation.." *Science Signaling* 8 (381). American Association for the Advancement of Science: ra58–ra58. doi:10.1126/scisignal.aaa4998.

Parker, Dane, and Alice Prince. 2011. "Type I Interferon Response to Extracellular Bacteria in the Airway Epithelium.." *Trends in Immunology* 32 (12): 582–88. doi:10.1016/j.it.2011.09.003.

Pendyala, Srikanth, Peter V Usatyuk, Irina A Gorshkova, Joe G N Garcia, and Viswanathan Natarajan. 2009. "Regulation of NADPH Oxidase in Vascular Endothelium: the Role of Phospholipases, Protein Kinases, and Cytoskeletal Proteins.." *Antioxidants & Redox*

Signaling 11 (4): 841–60. doi:10.1089/ars.2008.2231.

Pier, Gerald B. 2007. "Pseudomonas Aeruginosa Lipopolysaccharide: a Major Virulence Factor, Initiator of Inflammation and Target for Effective Immunity.." *International Journal of Medical Microbiology : IJMM* 297 (5): 277–95. doi:10.1016/j.ijmm.2007.03.012.

Pitson, Stuart M, Paul A B Moretti, Julia R Zebol, Helen E Lynn, Pu Xia, Mathew A Vadas, and Binks W Wattenberg. 2003. "Activation of Sphingosine Kinase 1 by ERK1/2-Mediated Phosphorylation.." *The EMBO Journal* 22 (20). EMBO Press: 5491–5500. doi:10.1093/emboj/cdg540.

Richman-Eisenstat, J. 1996. "Cytokine Soup: Making Sense of Inflammation in Cystic Fibrosis.." *Pediatric Pulmonology* 21 (1): 3–5.

Rivera, Juan, Richard L Proia, and Ana Olivera. 2008. "The Alliance of Sphingosine-1-Phosphate and Its Receptors in Immunity.." *Nature Reviews Immunology* 8 (10): 753–63. doi:10.1038/nri2400.

Saba, Julie D, and Timothy Hla. 2004. "Point-Counterpoint of Sphingosine 1-Phosphate Metabolism.." *Circulation Research* 94 (6). Lippincott Williams & Wilkins: 724–34. doi:10.1161/01.RES.0000122383.60368.24.

Sato, Koichi, Enkhzol Malchinkhuu, Yuta Horiuchi, Chihiro Mogi, Hideaki Tomura, Masahiko Tosaka, Yuhei Yoshimoto, Atsushi Kuwabara, and Fumikazu Okajima. 2007. "Critical Role of ABCA1 Transporter in Sphingosine 1-Phosphate Release From Astrocytes.." *Journal of Neurochemistry* 103 (6). Blackwell Publishing Ltd: 2610–19. doi:10.1111/j.1471-

4159.2007.04958.x.

Scarpa, Maria C, Simonetta Baraldo, Emanuela Marian, Graziella Turato, Fiorella Calabrese, Marina Saetta, and Piero Maestrelli. 2013. "Ceramide Expression and Cell Homeostasis in Chronic Obstructive Pulmonary Disease.." *Respiration; International Review of Thoracic Diseases* 85 (4): 342–49. doi:10.1159/000341185.

Serrano-Sanchez, Martin, Zahra Tanfin, and Denis Leiber. 2008. "Signaling Pathways Involved in Sphingosine Kinase Activation and Sphingosine-1-Phosphate Release in Rat Myometrium in Late Pregnancy: Role in the Induction of Cyclooxygenase 2.." *Endocrinology* 149 (9): 4669–79. doi:10.1210/en.2007-1756.

Song, Chao, Hongdong Li, Yunhui Zhang, and Jialin Yu. 2017. "Effects of Pseudomonas Aeruginosa and Streptococcus Mitis Mixed Infection on TLR4-Mediated Immune Response in Acute Pneumonia Mouse Model.." *BMC Microbiology* 17 (1): 82. doi:10.1186/s12866-017-0999-1.

Spiegel, Sarah, and Sheldon Milstien. 2011. "The Outs and the Ins of Sphingosine-1-Phosphate in Immunity." *Nature Reviews Immunology* 11 (6). Nature Publishing Group: 403–15. doi:10.1038/nri2974.

Stadnyk, A W. 1994. "Cytokine Production by Epithelial Cells.." *FASEB Journal : Official Publication of the Federation of American Societies for Experimental Biology* 8 (13): 1041–47.

Stiban, Johnny, Rotem Tidhar, and Anthony H Futerman. 2010. "Ceramide Synthases: Roles in Cell Physiology and Signaling." In *Sphingolipids as Signaling and Regulatory Molecules*,

edited by Charles Chalfant and Maurizio Del Poeta, 60–71. Springer New York. doi:10.1007/978-1-4419-6741-1_4.

Stoffel, Wilhelm. 1970. "Studies on the Biosynthesis and Degradation of Sphingosine Bases." *Chemistry and Physics of Lipids* 5 (1). Elsevier: 139–58. doi:10.1016/0009-3084(70)90014-9.

Suuronen, T, T Nuutinen, J Huuskonen, J Ojala, A Thornell, and A Salminen. 2005. "Anti-Inflammatory Effect of Selective Estrogen Receptor Modulators (SERMs) in Microglial Cells.." *Inflammation Research : Official Journal of the European Histamine Research Society ... [Et Al.]* 54 (5): 194–203. doi:10.1007/s00011-005-1343-z.

Tong, Xin, Lei Yin, and Charles Giardina. 2004. "Butyrate Suppresses Cox-2 Activation in Colon Cancer Cells Through HDAC Inhibition.." *Biochemical and Biophysical Research Communications* 317 (2): 463–71. doi:10.1016/j.bbrc.2004.03.066.

Travassos, Leonardo H, Stephen E Girardin, Dana J Philpott, Didier Blanot, Marie-Anne Nahori, Catherine Werts, and Ivo G Boneca. 2004. "Toll-Like Receptor 2-Dependent Bacterial Sensing Does Not Occur via Peptidoglycan Recognition.." *EMBO Reports* 5 (10): 1000–1006. doi:10.1038/sj.embor.7400248.

Tsay, Tzyy-Bin, Yu-Zhen Jiang, Ching-Mei Hsu, and Lee-Wei Chen. 2016. "Pseudomonas Aeruginosa Colonization Enhances Ventilator-Associated Pneumonia-Induced Lung Injury.." *Respiratory Research* 17 (1): 101. doi:10.1186/s12931-016-0417-5.

Usatyuk, Peter V, Donghong He, Vytas Bindokas, Irina A Gorshkova, Evgeny V Berdyshev, Joe G N Garcia, and Viswanathan Natarajan. 2011. "Photolysis of Caged Sphingosine-1-

Phosphate Induces Barrier Enhancement and Intracellular Activation of Lung Endothelial Cell Signaling Pathways." *American Journal of Physiology - Lung Cellular and Molecular Physiology* 300 (6). American Physiological Society: L840–50. doi:10.1152/ajplung.00404.2010.

Villagra, A, E M Sotomayor, and E Seto. 2010. "Histone Deacetylases and the Immunological Network: Implications in Cancer and Inflammation.." *Oncogene* 29 (2): 157–73. doi:10.1038/onc.2009.334.

Wang, Lichun, and Steven M Dudek. 2009. "Regulation of Vascular Permeability by Sphingosine 1-Phosphate." *Microvascular Research* 77 (1): 39–45. doi:10.1016/j.mvr.2008.09.005.

Weete, John D. 1974. "Sphingolipids." In *Fungal Lipid Biochemistry*, 267–86. Boston, MA: Springer US. doi:10.1007/978-1-4684-2829-2_9.

Whitsett, Jeffrey A, and Theresa Alenghat. 2015. "Respiratory Epithelial Cells Orchestrate Pulmonary Innate Immunity.." *Nature Immunology* 16 (1): 27–35. doi:10.1038/ni.3045.

Williams, Bryan J, Joanne Dehnbostel, and Timothy S Blackwell. 2010. "Pseudomonas Aeruginosa: Host Defence in Lung Diseases.." *Respirology (Carlton, Vic.)* 15 (7): 1037–56. doi:10.1111/j.1440-1843.2010.01819.x.

Wu-Zhang, Alyssa X, and Alexandra C Newton. 2013. "Protein Kinase C Pharmacology: Refining the Toolbox.." *Biochemical Journal* 452 (2): 195–209. doi:10.1042/BJ20130220.

Yang, Xiang-Jiao, and Edward Seto. 2008. "The Rpd3/Hda1 Family of Lysine Deacetylases:

From Bacteria and Yeast to Mice and Men.." *Nature Reviews Molecular Cell Biology* 9 (3): 206–18. doi:10.1038/nrm2346.

Yao, Hongwei, and Irfan Rahman. 2012. "Role of Histone Deacetylase 2 in Epigenetics and Cellular Senescence: Implications in Lung Inflammaging and COPD.." *American Journal of Physiology - Lung Cellular and Molecular Physiology* 303 (7): L557–66. doi:10.1152/ajplung.00175.2012.

Yao, Hongwei, Jae-woong Hwang, Jorge Moscat, Maria T Diaz-Meco, Michael Leitges, Nandini Kishore, Xiong Li, and Irfan Rahman. 2010. "Protein Kinase C Zeta Mediates Cigarette Smoke/Aldehyde- and Lipopolysaccharide-Induced Lung Inflammation and Histone Modifications.." *Journal of Biological Chemistry* 285 (8): 5405–16. doi:10.1074/jbc.M109.041418.

Yokoyama, A, N Kohno, S Fujino, H Hamada, Y Inoue, S Fujioka, S Ishida, and K Hiwada. 1995. "Circulating Interleukin-6 Levels in Patients with Bronchial Asthma.." *American Journal of Respiratory and Critical Care Medicine* 151 (5): 1354–58. doi:10.1164/ajrccm.151.5.7735584.

Yu, Zhiyuan, Wenzheng Zhang, and Bruce C Kone. 2002. "Histone Deacetylases Augment Cytokine Induction of the iNOS Gene.." *Journal of the American Society of Nephrology : JASN* 13 (8): 2009–17.

Zhong, Haihong, Michael J May, Eijiro Jimi, and Sankar Ghosh. 2002. "The Phosphorylation Status of Nuclear NF-Kappa B Determines Its Association with CBP/P300 or HDAC-1.."

Molecular Cell 9 (3): 625–36.

Ziobro, Regan, Brian Henry, Michael J Edwards, Alex B Lentsch, and Erich Gulbins. 2013. "Ceramide Mediates Lung Fibrosis in Cystic Fibrosis.." *Biochemical and Biophysical Research Communications* 434 (4): 705–9. doi:10.1016/j.bbrc.2013.03.032.

VITAE

NAME: David L. Ebenezer

Education:

2011-2017 **Ph.D**, Biochemistry & Molecular Genetics, University of Illinois at Chicago, Illinois, Chicago

2001-2003 **M.Sc**, Microbiology, Madurai Kamaraj University, Madurai, India

1997-2000 **B.Sc**, Microbiology, Madurai Kamaraj University, Madurai, India

Experience:

2010-2011 **Research Technologist**, Section of Hematology/Oncology, University of Chicago, Chicago, IL

2007-2010 **Research Technologist**, Human Immunological monitoring-cGMP facility, University of Chicago, Chicago, IL

2004-2006 **Senior Demonstrator**, Department of Clinical Virology, Christian Medical College, Vellore, India

Honors:

NIH T32 Training program fellowship in Lung Biology and Pathobiology 2013-2014

University of Illinois CCTS-Pre-doctoral education for clinical and translational scientists (PECTS) fellowship 2014-2015

Invited Speaker for ASPET young investigator symposium in Northwestern University, Chicago, June 2015

Experimental Biology Travel Award, 2016, American Society of Biochemistry and Molecular Biology.

Publications:

1. **David L. Ebenezer**, Evgeny V Berdyshev, Irina A. Bronova, Yuru Liu, Chinnaswamy Tiruppathi, Yulia Kumarova, Vidyani Suryadevara, Alison Ha, Anantha Harijith, Rubin Tuder, Viswanathan Natarajan and Panfeng Fu ***(2017)*** *Pseudomonas aeruginosa* infection stimulates nuclear sphingosine kinase 2 mediated S1P generation and epigenetic regulation of lung inflammatory injury *(in preparation)*

2. Panfeng Fu, **David L. Ebenezer**, Alison W. Ha, Vidyani Suryadevara, Anantha Harijith, and Viswanathan Natarajan (***2017***) Nuclear Lipid Mediators: Role of Nuclear Sphingolipids and Sphingosine-1-Phosphate Signaling in Epigenetic Regulation of Inflammation and Gene Expression. Journal of Cellular Biochemistry. 2017 (*under review*)

3. Natarajan V, Ha AW, Dong Y, Reddy NM, **Ebenezer DL**, Kanteti P, Reddy SP, Usha Raj J, Lei Z, Maienschein-Cline M, Arbieva Z, Harijith A (2017) Expression profiling of genes regulated by sphingosine kinase1 signaling in a murine model of hyperoxia induced neonatal bronchopulmonary dysplasia.BMC Genomics. 2017 Aug 29;18(1):664. doi: 10.1186/s12864-017-4048-0

4. Fu P, **Ebenezer DL**, Berdyshev EV, Bronova IA, Shaaya M, Harijith A, Natarajan V (2016). Role of Sphingosine Kinase 1 and S1P Transporter Spns2 in HGF-mediated Lamellipodia Formation in Lung Endothelium.J Biol Chem. 2016 Dec 30;291(53):27187-27203. doi: 10.1074/jbc.M116.758946. PMID: 27864331

5. **Ebenezer DL**, Fu P, Suryadevara V, Zhao Y, Natarajan V (2016). Epigenetic regulation of pro-inflammatory cytokine secretion by sphingosine 1-phosphate (S1P) in acute lung injury: Role of S1P lyase.Adv Biol Regul. 2016 Sep 29. pii: S2212-4926(16)30044-6. doi: 10.1016/j.jbior.2016.09.007.

6. **Ebenezer DL**, Fu P, Natarajan V (2016) Targeting sphingosine-1-phosphate signaling in lung diseases. Pharmacol Ther. 2016 Sep 10. pii: S0163-7258(16)30164-4. doi: 10.1016/j.pharmthera.2016.09.008. Review.

7. Harijith A, Pendyala S, **Ebenezer DL**, Ha AW, Fu P, Wang YT, Ma K, Toth PT, Berdyshev EV, Kanteti P, Natarajan V (2016) Hyperoxia-induced p47phox activation and ROS generation is mediated through S1P transporter Spns2, and S1P/S1P1&2 signaling axis in lung endothelium.Am J Physiol Lung Cell Mol Physiol. 2016 Aug 1;311(2):L337-51. doi: 10.1152/ajplung.00447.2015. Epub 2016 Jun 24.PMID: 27343196

8. Sundaravel S, Duggan R, Bhagat T, **Ebenezer DL**, Liu H, Yu Y, Bartenstein M, Unnikrishnan M, Karmakar S, Liu TC, Torregroza I, Quenon T, Anastasi J, McGraw KL, Pellagatti A, Boultwood J, Yajnik V, Artz A, Le Beau MM, Steidl U, List AF, Evans T, Verma A, Wickrema A.(2015) Reduced DOCK4 expression leads to erythroid dysplasia in myelodysplastic syndromes. Proc Natl Acad Sci U S A. 2015 Nov 17;112(46):E6359-68. doi: 10.1073/pnas.1516394112. Epub 2015 Nov 2. PMID: 26578796

9. Huang LS, Berdyshev EV, Tran JT, Xie L, Chen J, **Ebenezer DL**, Mathew B, Gorshkova I, Zhang W, Reddy SP, Harijith A, Wang G, Feghali-Bostwick C, Noth I, Ma SF, Zhou T, Ma W, Garcia JG, Natarajan V (2015) Sphingosine-1-phosphate lyase is an endogenous suppressor of pulmonary fibrosis: role of S1P signalling and autophagy.Thorax. 2015 Dec;70(12):1138-48. doi: 10.1136/thoraxjnl-2014-206684. Epub 2015 Aug 18.PMID: 26286721 Free Article

10. Harijith A, **Ebenezer DL**, Natarajan V (2014) Reactive oxygen species at the crossroads of inflammasome and inflammation.Front Physiol. 2014 Sep 29;5:352. doi: 10.3389/fphys.2014.00352. eCollection 2014. Review.

11. Usatyuk PV, Burns M, Mohan V, Pendyala S, He D, **Ebenezer DL**, Harijith A, Fu P, Huang LS, Bear

JE, Garcia JG, Natarajan V (2013) Coronin 1B regulates S1P-induced human lung endothelial cell chemotaxis: role of PLD2, protein kinase C and Rac1 signal transduction, PLoS One. 2013 May 8;8(5): e63007.

12. Yu Y, Mo Y, **Ebenezer D**, Bhattacharyya S, Liu H, Sundaravel S, Giricz O, Wontakal S, Cartier J, Caces B, Artz A, Nischal S, Bhagat T, Bathon K, Maqbool S, Gligich O, Suzuki M, Steidl U, Godley L, Skoultchi A, Greally J, Wickrema A, Verma A (2013). High resolution methylome analysis reveals widespread functional hypomethylation during adult human erythropoiesis, J Biol Chem. 29; 288(13): 8805-14.

13. Kannangai R, Sachithanandham J, Kandathil AJ, **Ebenezer DL**, Danda D, Vasuki Z, Thomas N, Vasan SK, Sridharan G.(2010)Immune responses to Epstein-Barr virus in individuals with systemic and organ specific autoimmune disorders.Indian J Med Microbiol. 2010 Apr-Jun;28(2):120-3. doi: 10.4103/0255-0857.62487.PMID: 20404456

14. Kannangai R, Kandathil AJ, **Ebenezer DL**, Mathai E, Prakash AJ, Abraham OC, Sudarsanam TD, Pulimood, SA, Selvakumar R, Job V, Sridharan G (2008). Usefulness of alternate prognostic serum and plasma markers for antiretroviral therapy for human immunodeficiency virus type 1 infection. Clinical Vaccine Immunology, 15 (1): 154-158

15. Kannagai R, Kandathil AJ, **Ebenezer DL**, Nithyanadam G, Samuel P, Abraham OC, Sudarsanam TD, Pulimood SA, Sridharan G (2008). Evidence of lower CD4+ T cell and higher viral load in Asymptomatic HIV-1 infected individuals of India: implications for therapy initiation. Indian Journal of Medical Microbiology, 26(3): 217-221

16. Goyal S, Kannangai R, Abraham AM, **Ebenezer DL**, Sridharan G (2007). Lack of increased frequency of human immunodeficiency virus infection in individuals with dengue-like illness in south India, Indian Journal of Medical Microbiology, 25(3): 300-301